UNIVERSIDADE ESTADUAL PAULISTA
"JÚLIO DE MESQUITA FILHO"
Campus de Botucatu

RECONSTRUCTION OF MOLECULAR NETWORKS INVOLVED IN CYTOKINE-INDUCED MYOTUBES ATROPHY INTEGRATING MICRORNA AND MRNA EXPRESSION

Geysson Javier Fernandez Garcia

BOTUCATU – SP

2013

UNIVERSIDADE ESTADUAL PAULISTA
"JÚLIO DE MESQUITA FILHO"
Campus de Botucatu

UNIVERSIDADE ESTADUAL PAULISTA
"Júlio de Mesquita Filho"

INSTITUTO DE BIOCIÊNCIAS DE BOTUCATU

RECONSTRUCTION OF MOLECULAR NETWORKS INVOLVED IN CYTOKINE-INDUCED MYOTUBES ATROPHY INTEGRATING MICRORNA AND MRNA EXPRESSION

GEYSSON JAVIER FERNANDEZ GARCIA
DR. ROBSON F. CARVALHO

Qualificação apresentada ao Instituto de Biociências de Botucatu, Universidade Estadual Paulista "Júlio de Mesquita Filho" - UNESP, como requisito à obtenção do título de Mestre em Ciências Biológicas – Área de concentração: Genética.

BOTUCATU – SP
2013

FICHA CATALOGRÁFICA ELABORADA PELA SEÇÃO TÉC. AQUIS. TRATAMENTO DA INFORM.
DIVISÃO DE BIBLIOTECA E DOCUMENTAÇÃO - CAMPUS DE BOTUCATU - UNESP
BIBLIOTECÁRIA RESPONSÁVEL: ROSEMEIRE APARECIDA VICENTE - CRB 8/5651

Fernandez Garcia, Geysson Javier.
Reconstruction of molecular networks involved in cytokine-induced myotubes atrophy integrating microRNA and mRNA expression. : data integration analysis in cancer cachexia / Geysson Javier Fernandez Garcia. - Botucatu, 2013

Dissertação (mestrado) - Universidade Estadual Paulista, Instituto de Biociências de Botucatu
Orientador: Robson Francisco Carvalho
Coorientador: Maeli dal Pai Silva
Capes: 20601000

1. Sistema musculoesquelético. 2. Síndrome metabólica. 3. Atrofia muscular. 4. Cachexia.

Palavras-chave: Cachexia; Músculo esquelético; RNAseq; miRNA.

I dedicate this dissertation to my loves:

My parents, my brothers and my girlfriend Luz Ochoa,

For all the love, affection and encouragement.

ACKNOWLEDGEMENTS

To my heaven family, God and Virgin Mary, enable me to achieve another great achievement, to give me all wisdom and patience to complete over this step in my life.

I wish to thank my committee members who were more than generous with their expertise and precious time. A special thanks to Dr. Robson Carvalho, my advisor and friend, for his countless hours of reflecting, reading, encouraging, patience and most of all advices in academic and personal life throughout the entire process.

To Professor Kathleen Marshal and Maeli Dal Pai for the opportunity given to me to make this work in their labs in Belgium and Brazil.

To my parents and siblings, that always gave me so much love and affection and comforting in helping me in difficult times. You were my strength so I never gave up my dream. My Thanks will never be enough for everything you all have done for me.

To my girlfriend Luz Ochoa, for your love, support, caring, understanding, and companionship, for always being by my side. Thank you for understanding my absence. You are my greatest supportive in everything that I propose to do. Thanks for come back in our life!!!Thanks for everything my love!!!!

To all colleagues and friends: Leonardo, Tassiana, João Paulo, Mariana Ribeiro, Marco Aguiar, Juliana Giusti, Ivan, Raquel, Rodrigo, Edson, Fernanda, Paulinha, Ana Carolina, Flavia Fernandes, Bruno, Luana, Carlos, warlen, to all others who contributed in any way for this work, friendship , exchange of experiences and socializing .

To Brazil, for adopting me as his stepson. Now I carry in my heart this great country!.

To FAPESP, process number (2011/16282-0 and 2013/02005), for the economic support in this research.

Abstract

The skeletal muscle atrophy is a common phenomenon in many chronic systemic diseases such a sepsis, chronic heart failure, chronic obstructive pulmonary disease, chronic kidney disease, diabetes, AIDS and cancer. These diseases may be accompanied by a complex metabolic syndrome characterized by muscle wasting, denominated cachexia. The molecular pathways responsible for cachexia are not completely understood, however, evidence suggest that pro-inflammatory cytokines like Tumor Necrosis Factor (TNF)-α and Interferon (INF)-γ have a key role in molecular pathways related to loss of function and muscle mass. The complexity of mechanisms controlling gene expression in this process suggests the involvement of additional regulatory molecules, such as microRNAs; these RNA molecules encoded by the genome regulate the function of skeletal muscle during development and various muscle diseases. MicroRNAs orchestrate common pathways or biological function, this unique feature gives rise as an effective tool for determining the pathways involved in specific diseases or biological processes. The hypothesis of this work is that the muscle atrophy induced by TNF-α and INF-γ has a microRNAs expression profile that allow the identification of regulatory networks and molecular pathways.

Contents

1. LITERATURE REVIEW

1.1. Skeletal Muscle

Skeletal muscles comprise approximately 40-50% of body mass and are responsible for basic functions such as locomotion, metabolism and respiration[1,2]. In order to allow movement, the organization of muscle cells is highly structured so as to generate and sustain mechanical tension. The cytosol of myofibers is packed with contractile proteins that are assembled into repetitive structures, the basal unit of which is constituted by the sarcomere. These are made up of actin and myosin filaments arranged in highly ordered, almost crystalline arrangements, as well as hundreds of regulatory proteins such as the troponin–tropomyosin complex, and scaffolding and cytoskeletal crosslinking proteins such as α-actinin, myomesin and the kinase titin. Several sarcomeres, arranged in register and surrounded by sarcoplasmic reticulum, form myofibrils. Various organelles such as mitochondria, for ATP generation, and sarcoplasmic reticulum, for calcium release are embedded among the myofibrils. This ordered assembly of contractile proteins and organelles differs from the cytosolic organization of the other cells of our body where mitochondria, endoplasmic reticulum and proteins move freely within the cytosol. Moreover, the myofiber is an enormous cell that can measure several centimeters in length and can contain hundreds of nuclei [3,4] (**Figure 1**).

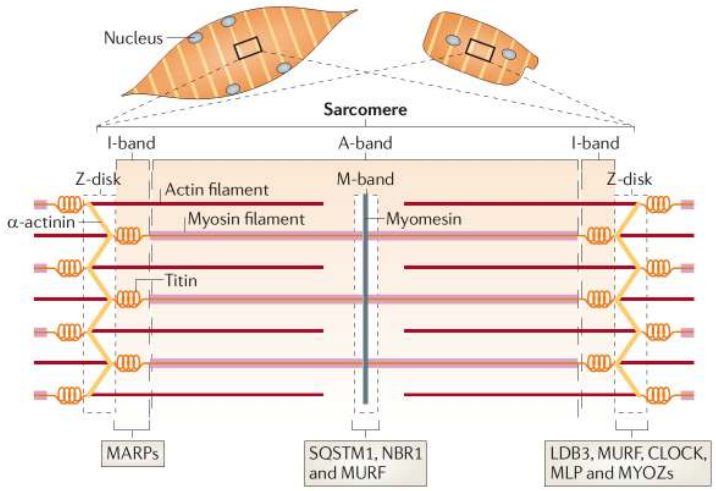

Figure 1 Striated muscle structure. The contractile machinery of skeletal muscle is formed from long arrays of sarcomere units, which are joined into myofibrils. The sarcomere (bottom) is constructed from interdigitating, antiparallel filaments of actin and myosin, the elastic titin filaments and the

crosslinker proteins for actin — α-actinin, myosin and myomesin. (adapted from Braun and Gautel, 2011 [4]).

1.2. Atrophy of Skeletal Muscle

The muscles have a high plasticity in response to changes in functional demands, resistance induce skeletal muscle hypertrophy, which is characterized by increased protein synthesis, fiber diameter and strength[5–9]. In contrast, conditions of disuse, immobilization, denervation, microgravity, aging and food restriction result in loss of muscle mass, known as muscle atrophy. Muscle atrophy is characterized by a decrease in the amount of protein, fiber diameter and the reduction of strength[4–6,8,9]. Several lines of evidence suggest that the atrophy of skeletal muscle is controlled by the coordinated action of key regulatory pathways involving IGF1-AKT-FoxO, myostatin, transcriptional factor NfκB and inflammatory cytokines [revised Braun & Gautel 2011[4]]. Subsequently, multiple proteolytic systems, such as those involving lysosomal proteases (cathepsins), the calcium-dependent calpains and ubiquitin-dependent proteolysis (UP) are activated to degrade most muscle proteins[10–12] (**Figure 2**).

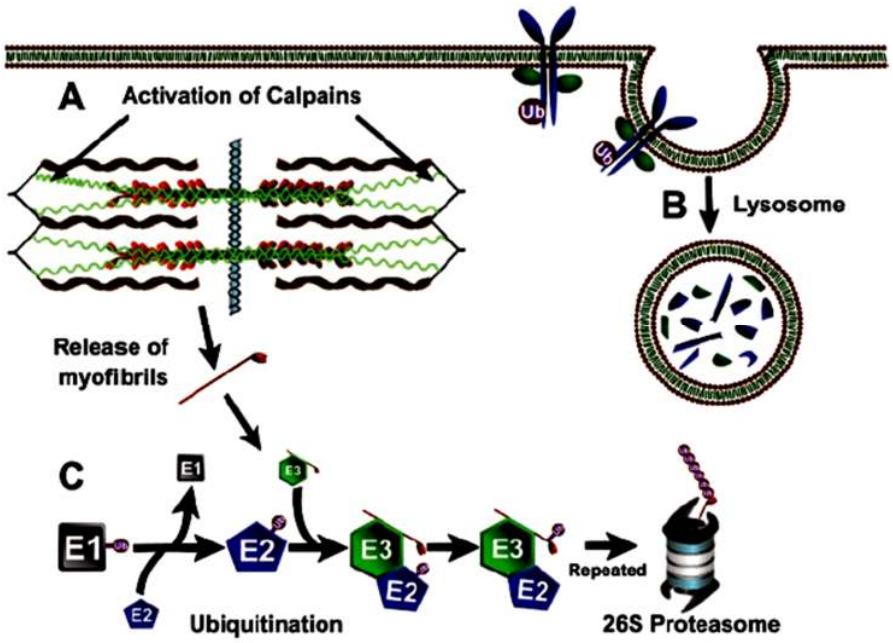

Figure 2. The proteolytic systems involved in muscle atrophy (A) activation of calcium-dependent calpains (B) lysosomal proteases (cathepsins) and (C) ubiquitin-dependent proteolysis. (adapted from Jackman & Kandarian, 2004[7]).

1.3. Cachexia

The skeletal muscle atrophy is also a common phenomenon in many chronic systemic diseases such as sepsis, chronic heart failure, chronic obstructive pulmonary disease, chronic kidney disease, diabetes, AIDS and cancer[13–15]. These diseases may be accompanied by a complex metabolic multifactorial syndrome characterized by decreased muscle mass, with or without loss of fat, called cachexia[13,15–18]. The most prominent clinical feature of cachexia is the weight loss in adults or growth disorders in children (excluding endocrine disorders)[16]. Cachexia arises from a metabolic disorder of these chronic diseases, creating an environment that can be characterized by inflammation, loss of appetite (anorexia) and low testosterone levels and other hormone anabolic and anemia. The decrease in food intake and anorexia resulting in loss of body mass and muscle, resulting in a condition of asthenia, immobility and cardiac or respiratory failure[14–16].

The cachectic state is particularly important in cancer, representing poor prognosis and decreased response to treatment radio and chemotherapy, more than 50% of cancer patients suffer from cachexia and, remarkably, approximately 30% of cancer-related deaths are estimated as a result of cachexia[13,14,19]. Depending on the tumor type, site and mass, weight loss occurs in 30 – 80% of cancer patients, for instance patients with pancreatic or gastric cancer have the highest frequency of weight loss, while patients with non-Hodgkin's lymphoma, breast cancer, acute nonlymphocytic leukemia, and sarcomas have the lowest frequency of weight loss[19]. Although certain tumor types are more commonly associated with cachexia, even with the existence of tumors with similar growth patterns and identical origins, one of which induces cachexia while the other does not[19–21]. Thus, in pancreatic cancer, 85% of patients become cachectic, but 15% do not. This implies variations in tumor phenotype that result in differences in a limited number of genetic events or gene expression[20], or host genotype[22,23], which contribute to the development of cachexia. In patients with pancreatic cancer, weight loss is a presenting symptom with a median weight loss of 14.2% of their illness stable weight[24] (**Figure 3**). This weight loss is progressive over the next 6 months, increasing to a median of 24.5% at the last assessment before death (**Figure 3**).

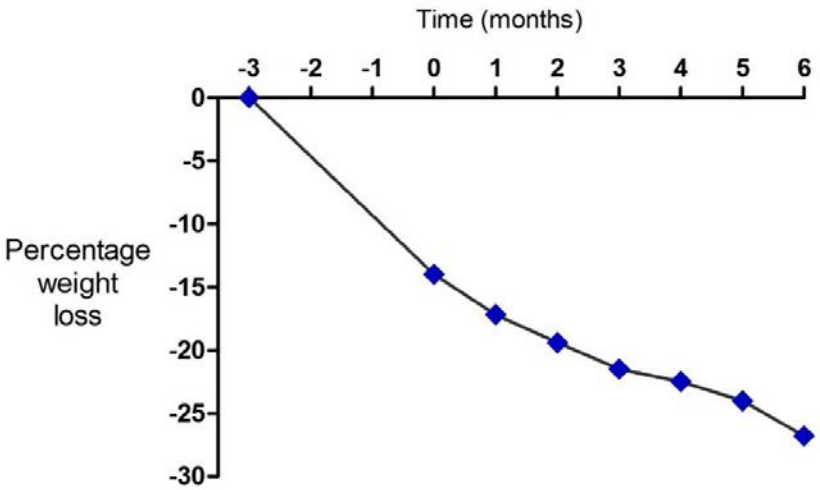

Figure 3. Time course of weight loss in patiens with advanced pancreatic cancer (n=20). At diagnosis, 85% of patients have lost weight. [Adapted from wigmore et al[24]].

Although the overall weight loss, the cachectic patients had lost their body fat and their skeletal muscle, and there was also a significant decrease in mineral content, suggesting erosion of bone (**Table 1**). This marked loss of skeletal muscle explains why patients with cachexia have a reduced mobility, and thus quality of life, together with a shorter life span, since loss of respiratory muscle function will lead to death from hypostatic pneumonia[25]. Death of patients occurs with 25–30% total body weight loss[24]. A similar situation is found in patients with acquired immunodeficiency syndrome (AIDS), where death is imminent when they have lost 34% of their ideal body weight[26]. Respiratory failure has been found to be responsible for the death of 48% of cancer patients[19].

Table.1.

Parameter	Normal, Kg	Cachectic, Kg
Total Body weight	65,6	44,9
Total fat	17,3	3,1
Muscle protein	2,8	0,7
Nonmuscle protein	8,3	8,1
Intracellular water	19,1	12,9
Extracellular water	15,1	17,5
Minerals	3,0	2,6

Comparison of body composition of cachectic cancer patients with normal controls. Adapted from Tisdale[19], 2009, Data from Fearon, 1992[27].

It is not known precisely how or why cancer so frequently develops in such a way as to induce cachexia. Cachexia has commonly been considered a paraneoplasic syndrome in

which tumor-derived factors induce widespread alterations in gene expression or metabolic flux that may function to release intermediate metabolites, which can then be used by the tumor for growth and expansion[21]. Cachexia can be considered a state of ‘‘auto cannibalism’’ in which the tumor survives at the expense of the host. In contrast, many of the metabolic changes in cachexia are the result of activated immune and neuroendocrine responses that are common to trauma or sepsis and are thus more likely related to a generic response to injury. In this model, cachexia may be regarded as the downside of a double-edged sword designed to respond to tumor-related noxious stimuli such as pain or tissue necrosis.

1.4. Molecular pathways in cachexia

The molecular pathways responsible for cachexia are not completely understood, however, evidence suggests that proinflammatory cytokines such as interleukin (IL)-1β, IL-6, tumor necrosis factor alpha (TNF-α) and interferon gamma (IFN-γ) have a key role, especially in the development of cellular and molecular alterations that result in loss of function and muscle mass[3,21,28]. Among these evidences point out that: 1) inflammatory cytokines inhibit differentiation of skeletal muscle *in vitro*[29–32] ; 2) pro-inflammatory cytokines induce specific muscle protein degradation in differentiated myotubes[33–37]; 3) high levels inflammatory cytokines cause alterations in the extracellular matrix and prevents the regeneration of skeletal muscle fibers inhibiting the differentiation of stem cells into muscle myofibers[38,39] and, most notably, 4) elevated levels of cytokines have been observed under conditions that induce muscle atrophy such as sepsis, AIDS, chronic heart failure and cancer[40,41].

Central Role of E3 Ligases in Atrophy Loss of skeletal muscle mass is generally due to reduced protein synthesis, increased degradation, or a relative imbalance of the two [42,43]. The signaling pathways that are thought to control these processes are shown in **Figure 4**. One prominent subset of the pro-cachectic molecular mechanisms can be traced as follows: proinflammatory cytokines such as TNFa, TWEAK, IL-1, IL-6 signal into 3 established pathways, the NF-kB pathway, STAT pathway, and p38 MAP kinase. These signaling mediators are required to up regulate the expression of the key E3 ligases such as , tripartite Motif Containing 63- E3 Ubiquitin Protein Ligase, TRIM63 (Alias: MuRF1 in the **Figure 4**) , and F-Box Protein 32, FBXO32 (Alias: Atrogine-1 in the **Figure 4**), which mediate sarcomeric breakdown and inhibition of protein synthesis[9,10,42]. TRIM63 is upregulated in

multiple settings of muscle atrophy[11]. This E3 ubiquitin ligase is responsible for mediating the ubiquitination of the thick filament of the sarcomere, Myosin (MYH)[44], and other thick filament components[45]. The cytokine TWEAK, in particular, induces TRIM63 up-regulation via NF-kB, resulting in MYH loss[46]. Inhibition of classical NF-kB is sufficient to significantly decrease tumor-induced muscle loss, at least in mice, in part, by inhibiting the up-regulation of TRIM63 [47,48].

FBXO32 also serves as a marker of acute muscle atrophy, being up regulated in multiple settings of cachexia[49], in addition to immobilization, denervation, and glucocorticoid excess[11]. FBXO32 up-regulation occurs via p38 activation[50] and by the induction of the C/EBPb transcription factor, which itself is activated through p38 phosphorylation[51]. FBXO32 induces the ubiquitination of an eIF3f, which is part of the protein translation machinery[52,53]. However, it is not clear if this is sufficient to decrease protein synthesis. The demonstration that both TRIM63 and FBXO32 contribute to skeletal muscle atrophy was provided by studies of knockout animals—in the absence of either TRIM63 or FBXO32, rates of atrophy are diminished[11]. Thus, inflammatory cytokines secreted by tumors directly induce signaling pathways that up-regulate enzymes that induce skeletal muscle protein turnover.

The mass of protein within a muscle is regulated by the net interplay between protein synthesis and degradation. In rodent models of cancer associated muscle wasting, both decreased synthesis and increased degradation have been described[54,55]. One of the best-characterized mechanisms for inducing protein synthesis is through IGF1 (insulin-like growth factor 1) signaling. IGF1 is up-regulated in skeletal muscle normally during resistance exercise[56]. The pathway that mediates hypertrophy downstream of IGF1 activation is IRS1/PI3K/Akt/mTOR (**Figure 4**)[57]. Akt induces activation of protein synthesis by blocking repression of mTOR, which in turn maintains muscle mass through two distinct complexes, known as TORC1 and TORC2[58,59]. The TORC1 complex requires an adaptor protein known as Raptor, which is required for normal muscle maintenance[58].

TORC1 signals to the p70S6 kinase and 4E-BP pathways, which induce ribosome formation and induce protein synthesis. TORC2 signaling controls autophagy, which also plays a role in muscle maintenance[60–62]. Under atrophy conditions, autophagy is induced in addition to ubiquitin-mediated proteolysis. In addition to activating TORC1 signaling, Akt also phosphorylates the Foxo (or Forkhead) family of transcription factors. FOXO1 and FOXO3 play a key role in inducing transcriptional up-regulation of TRIM63 and

FBXO32[63,64]. Apparently these transcription factors are required, since IGF1/Akt mediated Foxo phosphorylation and subsequent inhibition of Foxo transport to the nucleus is sufficient to block the up-regulation of the E3 ligases. In addition, transgenic overexpression of FOXO3 in skeletal muscle is sufficient to induce dramatic skeletal muscle wasting[65], while recent evidence supports that inhibition of Foxo spares muscle loss in a mouse model of cancer cachexia[66].

In addition to regulating the ubiquitin-proteasome pathway, Foxo transcription factors directly regulate genes coding for the autophagy pathway, which like the ubiquitin system also contributes to the degradation of muscle proteins to promote atrophy [60,62]. In autophagy, organelles are sequestered in autophagosome vacuoles that fuse with lysosomes and become digested by lysosomal enzymes[67]. Autophagy genes and the lysosomal proteolytic system are activated during denervation and cancer, and in both cases contribute to atrophy through the activity of Foxo[60,62,66]. A unique finding determined that analogous to Akt, FOXO3 is negatively regulated by PGC-1a[68]. PGC-1a is itself down-regulated in muscles from tumor-bearing mice and other wasting conditions, and transgenic expression of PGC-1a rescues muscle loss in part by inhibiting Foxo3 and through the production of metabolic products. PGC-1a is highly induced during exercise, and one of the primary roles of this factor is to regulate mitochondrial biogenesis and oxidative phosphorylation in myofibers, characteristic of type I, fatigue-resistant, muscles [69,70]. Interestingly, in cancer cachexia, muscle atrophy is selective to type II fast twitch myofibers, while type I oxidative fibers are relatively spared of similar catabolic effects[21]. Therefore, it is possible that this sparing effect results from PGC-1a inhibition of Foxo3 activity in type I myofibers. Attempts to screen for PGC-1a activators represents a promising therapeutic avenue to prevent muscle atrophy in cancer or other catabolic conditions[71].

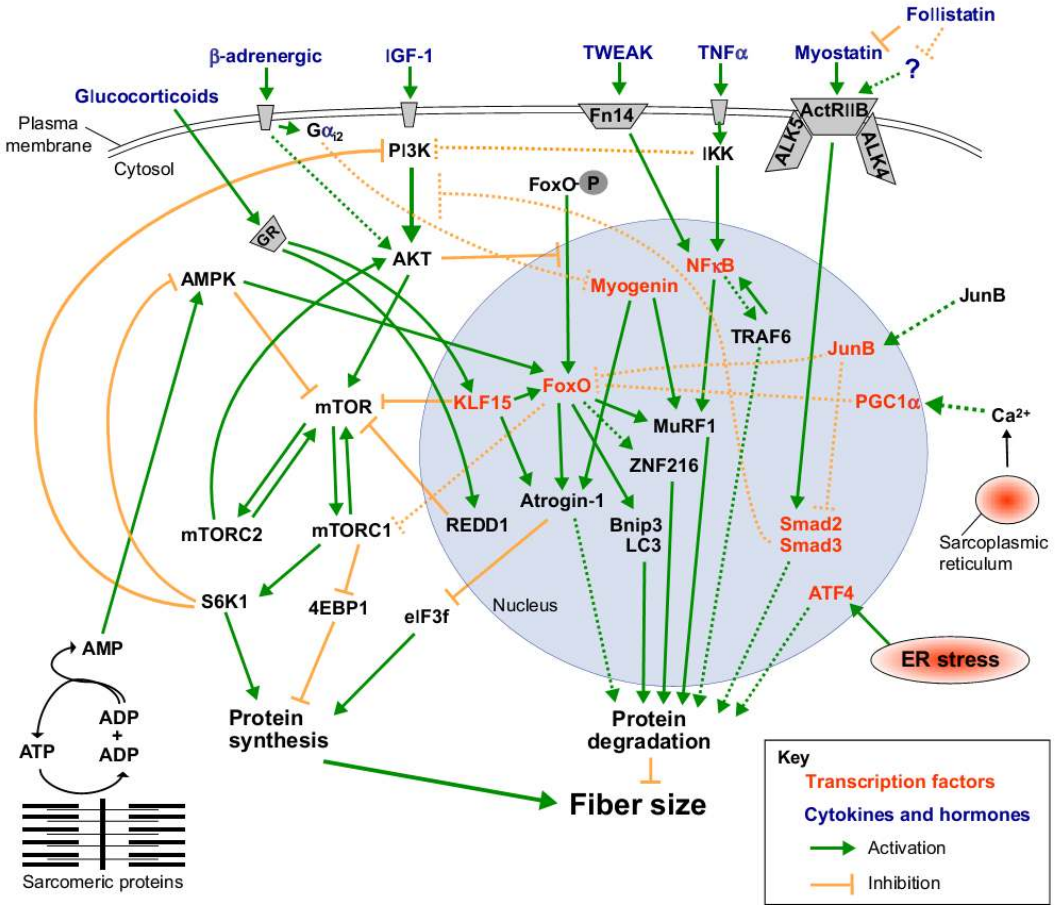

Figure. 4. Major pathways that control muscle fiber size. Protein synthesis and degradation are regulated by several different stimuli, which activate multiple signaling pathways, many of which converge at common intermediates and crosstalk with one another. Dotted lines depict pathways whose molecular mechanisms and role in adult skeletal muscle have yet to be completely defined. (adapted from Bonaldi and Sandri 2013[9]).

1.5. Small RNAs

Almost 90% of the human genome is actively transcribed, and most of these transcripts is composed by non-coding RNAs (ncRNA). ncRNAs are important regulatory molecules involved in diverse physiological and cellular processes, being composed of long RNAs and small RNAs[72]. Since then, new technologies in large-scale sequencing and bioinformatics analyzes have emerged and led to the discovery of new classes of small RNA in various organisms from yeast to humans[73,74].

These RNAs are classified by their biogenesis and function, but there is still no clear demarcation between the classes of non-coding RNA (ncRNA)[74,75]. The small RNAs are related to many biological processes, including development, differentiation, proliferation,

and pathological processes[73]. The main biological function, as it is known today is the regulation of gene expression, being involved in the regulation of the genome and transcriptome[74].

So far, there are known the following classes of small RNA: microRNAs (miRNAs), small nucleolar RNAs (snoRNAs), small nuclear RNAs (snRNAs), trans-acting siRNAs (tasiRNAs), cis-acting siRNAs (casiRNAs), natural antisense siRNAs (natsiRNAs), piwi-interactin RNAs (piRNAs), tRNA-derived fragments (TRFs), tRNA-derived stress-induced fragments (tiRNAs), endogenous small interfering RNAs (endosiRNA), exogenous small interfering RNAs (exosiRNA), piRNA-like small RNAs (piRNA-like), repeat associated small interfering RNA (rasiRNA), as shown in **Table 2**.

Table 2 Types of small, noncoding RNAs and their cellular functions.

Name	Biogenesis	Length (nt)	Source	Functions
miRNA	Drosha, Dicer	17-25	Plants, algae, protists, animals	mRNA stability, translational repression of endogenous transcripts
endosiRNA	Dicer	21-24	Plants, Fungi, animals	Posttranscriptional regulation of mRNA and transposons during development
exosiRNA	Dicer	~24	Plants, Fungi, animals	Transcriptional, posttranscriptional regulation of mRNA and transposons, defense against viral genes
natsiRNA	DCL1,2	21-24	Plants	Posttranscriptional gene silencing during development, salt tolerance, pathogen resistance
casiRNA	DCL3	24	Plants	Methylation of transposon loci in genome
tasiRNA	DCL4	21	Plants	Amplification of microRNA initiated posttranscriptional gene silencing
piRNA	Non-Dicer	26-31	Germ cells	Transposon regulation, germ line development
piRNA-like	Non-Dicer	24-30	Drosophila, *C. elegans*	Unknown
rasiRNA	Non- Dicer	26-31	Plants, Animals	Genomic stability by regulating transposons, germ cell development
tiRNA	Non-Dicer	30-40	Yeast, Drosophila, animals	Inhibition of translational initiation
tRFs	ELAC2	17-26	Animals	Cellular proliferation
PASR	Non-Dicer	22-200	Animals	Unknown
TinyRNA	Non-Dicer	17-18	Animals	Transcription star site
TSSa-RNA	Non-Dicer	20-90	Animals	Maintenance of transcription?
PROMPT	Non-Dicer	<200	Animals	Activation of transcription?

snoRNA	RNase III-like exonucleases	60-300	Eukarya	rRNA and snRNA modifications
snRNA	RNA Pol II	~150	Eukarya	Splicing

microRNA (miRNA), endogenous small interfering RNAs (endosiRNA), exogenous small interfering RNAs (exosiRNA), natural antisense siRNAs (natsiRNAs), cis-acting siRNAs (casiRNAs), trans-acting siRNAs (tasiRNAs), piwi-interacting RNAs (piRNAs), piRNA-like small RNAs (piRNA-like), repeat associated small interfering RNA (rasiRNA), tRNA-derived stress-induced fragments (tiRNAs), tRNA-derived fragments (tRFs), promoter-associated small RNAs (PASR), Tiny RNA(TinyRNA), TSS-associated RNAs (TSSa-RNA), promoter upstream transcripts (PROMPT), small nucleolar RNA (snoRNA), small nuclear RNA (snRNA).Adapted of Esteller 2011; Dey et al. 2012[74].

1.6. Micro-RNA

miRNAs are a class of small non-coding regulatory RNAs most studied, with size ranging from 17 to 25 nucleotides, and its first mention was made by Victor Ambros lab during the study of the role of lin-14 in the development of the nematode *Caenorhabditis elegans*. The authors observed that a fragment of 22 nt RNA, showed a partial complementarity to a region of non-coding portion of the gene under study, and led to inhibition of its translation[76]. In 2000, the group of Gary Ruvkun showed the presence of miRNAs in various organisms, indicating that this type of pos-transcriptional regulation could be present in different species[77]. The miRNAs are named as miR-more numbers (eg miR-133), however, there are some exceptions. The microRNAs of similar sequences are usually distinguished by an additional letter followed by the number of microRNA (eg mir-133a). A mature microRNA sequence with identical may appear in different genomic loci with different precursor sequences. In such cases, different miRNA genes are usually distinguished by additional number another end of the sequence (eg, mir-133a-1).According to their genomic location of the genes encoding miRNA are classified as intergenic, intronic or exonic (**Figure 5**).

Most genes of miRNAs have multiple isoforms (paralogous), which are probably the result of gene duplication. For instance, the human genome has 12 loci for miRNAs let-7 family. Paralogs generally have identical nucleotide sequences at positions 2-7 on the 5 'end of the miRNA. As these six nucleotides, called seed, are fundamental bases for pairing with the target mRNA, it is believed that the paralogs act redundantly. However, since the 3 'sequences of the miRNA also contribute to the target binding and how the pattern of expression of these miRNAs are generally different, members of the family may have different roles *in vivo*[75,78].

Approximately 50% of mammalian miRNA loci are found very close to other miRNAs. These agglomerates miRNAs are transcribed from a single polycistronic transcription unit (PTU)[79]. Some miRNAs are generated from the noncoding PTU while others are transcribed by PTU encoding proteins (for a review see Kim et al. Al 2009 [80]). Approximately 40% of miRNA loci are located in the intronic region of non-coding transcripts, while approximately 10% are located in the non-coding PTU. miRNAs in PTUs encoding proteins are generally found in intronic regions, which correspond to approximately 40% of all miRNA loci.

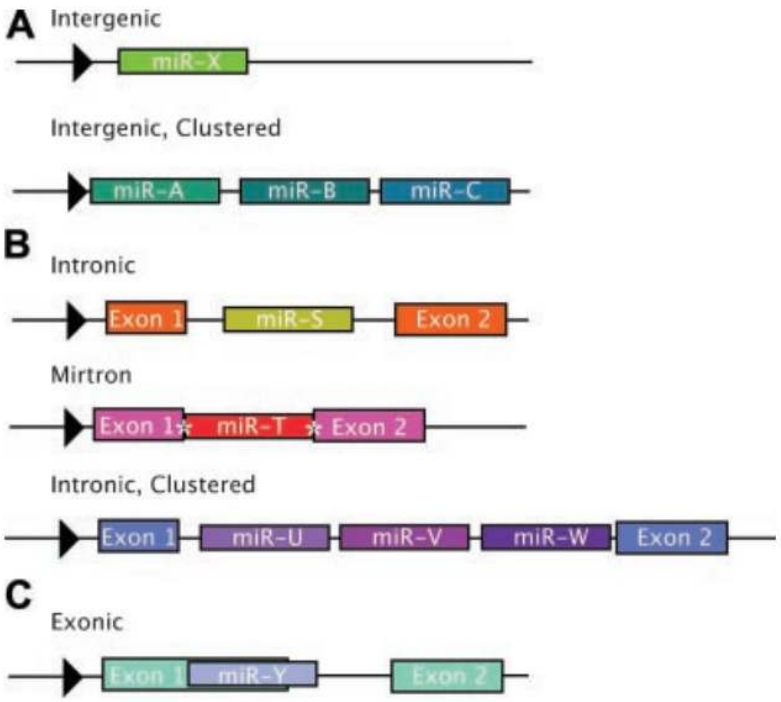

Figure 5. Genomic organization of miRNAs. Intergenic miRNAs are under the control of its own promoter, which may be organized as a single gene or like a cluster (A). The intronic miRNAs are located in intronic regions of a functional transcriptional unit and under the control of a promoter of a gene encoding protein as a single intronic miRNA and intronic cluster or as a mirtron (B) exonic miRNAs (C) are rare and often comprise an exon and intron of the gene are contained. Adapted of: Olena et al, 2010 [81]

Just as the organization of miRNAs in the genome has different arrangements, their biogenesis displays different pathways: 1) the canonical 2) the mirtrons and 3) the Argonaut-2 (Ago2)[82]. In general, the biogenesis of miRNAs occurs via several enzymatic cleavage to generate a mature miRNA. The canonical pathway (**Figure 6A**) starts by transcription of the gene encoding the miRNA by the polymerase type II, generating a named miRNA primary transcript (pri-miRNA) that undergoes polyadenylation and 5´cap. In the nucleus, the pri-

miRNA is processed to pre-miRNA by the enzyme RNase III (Drosha), which requires a cofactor, protein DGCR8 (DiGeorge syndrome critical region gene 8) in humans (Pasha in C. elegans and D. Melagonaster)[83–86]. The DGCR8 with Drosha form a large complex known as the Microprocessor complex, which in humans has ~ 650 kDa[84–86]. This complex recognizes and cleaves the pri-microRNA molecule resulting in a hairpin structure with approximately 70 bp, the pre-microRNA[87,88].

After the nuclear processing, each pre-microRNAs are exported to the cytoplasm by exportin-5 (exp5), being converted to mature and functional microRNAs by the enzyme Dicer (RNAase III)[89–91]. After cleavage by Dicer, a double-stranded molecule of approximately 22 nucleotide RNA associated with the protein Argonaut to form the complex of RNA-induced silencing (RISC)[80]. One of the strands of approximately 22 nucleotides remains into protein Argonaut like a mature microRNA (miRNA) while the other strand (miRNA *) could be degraded or remains like a functional miRNA. In the same way as there is the selection of a siRNA[92,93], the strand that has its 5 'end forming the more unstable duplex with its partner seems to preferentially survive as mature microRNA in RISC[82,88,92,93].

The biogenesis of mirtrons (**Figure 6B**) differs from the canonical, since it is not processed by Drosha, the pri-miRNAs undergoes splicing and are processed by the enzyme Ldbr, thus taking the structure of hairpin. Then the 5' tailed mirtrons have their tails trimmed by a nuclease not yet known and 3' tailed mirtrons have his tail processed by the exosome. At the end are generated the pre-miRNAs that are exported to the cytoplasm by XPO5, the next steps are the same to those of the canonical pathway[75,82,94,95].

The route of Ago2 was described in 2010 and is independent of Dicer initially the pri-miRNA is processed by Drosha/DGCHRB complex and later Ago2 cleaves the 3' tail, resulting the pre-miRNA. The following steps to generate the mature miRNA are still unknown, as **Figure 6C**[82].

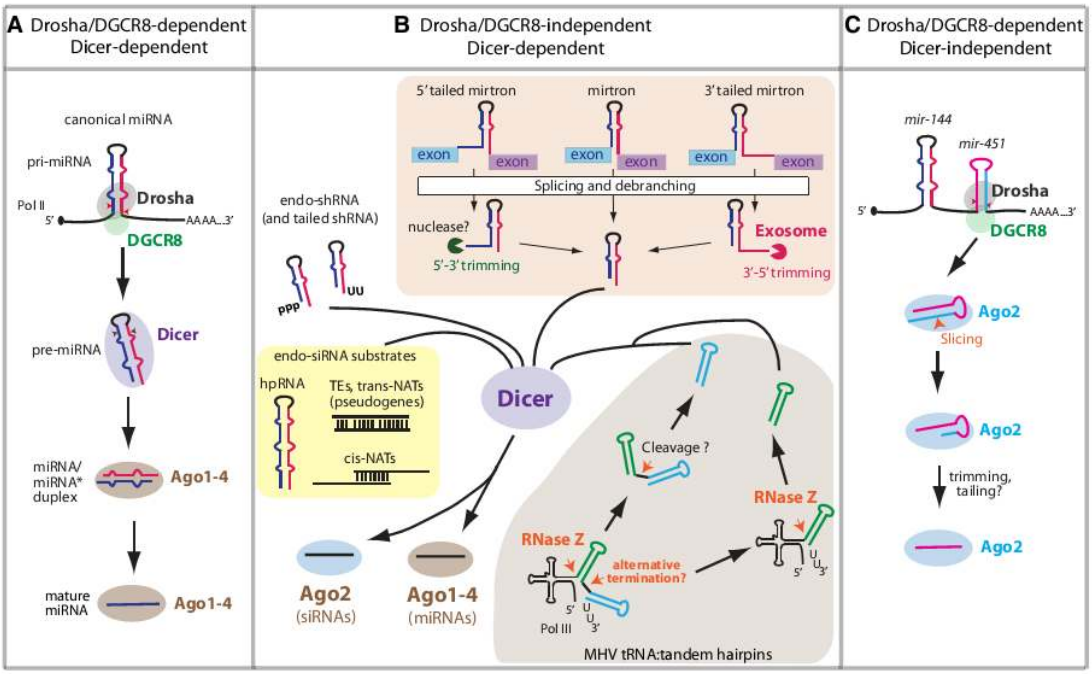

Figure 6. Canonical and Major Alternative miRNA Biogenesis Pathways in Animals.A-canonical biogenesis pathway: pre-miRNAs generated by cleavage of pri-miRNA by Drosha. The B-biogenesis pathway through mirtrons splicinge processing enzyme (Ldbr) generating mature miRNA. C- pri-microRNA is Drosha/DGCR8 processed, resulting in a clip of approximately 18nt which is incorporated into Ago2. All roads generate pre-miRNAs are exported to the cytoplasm by XPO5/EXP5, cleavage by Dicer and RISC complex. (adapted from Yang & lai, 2011[82]).

1.7. Mechanisms of post-transcriptional regulation by miRNAs

The miRNA active complex is incorporated into the RNA-induced silencing complex known as RISC. This complex is composed of the miRNA by the enzyme Dicer and the proteins Ago (1-4) of the subfamily Argonaut[96] (Kawamata and tomari 2010). miRNAs bind to their target mRNAs with the aid of the RISC complex, leading to a reduction in translation or inducing degradation of the mRNA[97]. The connection miRNA: mRNA occurs by a complementary 7 to 8 bases in the 5 'portion of the miRNA. This recognition sequence of miRNAs, which allows its binding to one or more sites of mRNA is known as seed sequence[98].

As a rule, the interaction miRNA: mRNA occurs in the 3 'untranslated region (UTR) when the imperfect matching between the miRNA and the target mRNA occurs, the translation is blocking and protein levels are decreased. However, when the écompleto pairing occurs also in mRNA degradation [99]. Recently it was reported that the activities of miRNAs in the degradation of mRNAs can be as or even more important than its activity in blocking

translation[100]. It is estimated that miRNAs regulate the translation of more than 60% of the genes encode proteins[75].

These post-transcriptional regulators play important roles in many biological processes, including growth, cell differentiation, development and disease (Alvarez-Garcia and MISKA 2005; INUI et al. 2010). Regardless of their action mode miRNAs directly affect the amount of protein produced leading to a marked change in cell physiology. A miRNA can interact with several hundred mRNAs, it is clear that miRNAs are among the most important regulators of the human genome[101] (BARTEL2009). To date more than 21,000 miRNAs have been discovered in several species and are currently 2578 known human microRNAs and 1908 mouse microRNAs (miRBase V.20, http://microrna.sanger.ac.uk/).

1.8. MicroRNAs in Skeletal Muscle

Several miRNAs are specifically or highly expressed in skeletal muscle. In addition, expression of muscle-specific miRNAs (miR-1, -133, -206 and -208) is regulated by transcription networks involving Serum response factor (SRF), Myogenic Differentiation 1(MYOD), and myocyte enhancer factor-2 (MEF2). The muscle-specific miRNAs (miR-1, -133, -206, -208,-208b and -499) are involved in a number of processes including myogenesis (proliferation, differentiation and specification of the type of fiber), regeneration and hypertrophy muscle fibers. miRNAs miR-208a, 208b, and -499 are each encoded by a distinct gene intron myosin heavy chain (MYH), respectively MYH6 , MYH7 and MYH7b. Van Rooij *et al* 2008 have recently proposed the existence of a network composed of these three miRNAs, called MyomiR, encoded by myosin genes, which is involved in the regulation of MYH expression and the muscle fibers type[102]. Interestingly, some non-muscle-specific miRNAs also regulate the differentiation and muscle regeneration after injury[103,104].

1.9. MicroRNAs in Skeletal Muscle Diseases

Currently, although the number of genes related to the development of muscle diseases increases every year and histological tissue pathology is well documented, the molecular pathways involved remain poorly understood[9,105]. However, several studies indicate that significant miRNA expression is altered in diseases of skeletal muscle and, in some cases, a single miRNA can cause disease[106,107]. miR-206 ,an important miRNA to skeletal muscle, is elevated in the diaphragm muscle of mdx mice, an animal model of muscular dystrophy[108].

Similarly, it was recently demonstrated that the level of expression of muscle specific miRNA miR-499 is also increased in a model of muscular atrophy in rats, suggesting activation of the network MyomiR[102,109]. Moreover, the expression levels of miR-1 and miR-133a are reduced in a model of hypertrophy of skeletal muscle in mice[107]. It was also demonstrated a mechanism involving genetic interactions between transcription factors NF-kB and YYI and miR-29; that regulates the differentiation of myoblasts and functions as a tumor suppressor in rhabdomyosarcomas, a tumor resulting from the deregulation of the proliferation of muscle cells[110].

Comprehensive studies of the expression patterns revealed miRNAs that a total of 185 miRNAs are altered in samples of ten different diseases of skeletal muscle - Five miRNAs (miR-146b, miR-221, miR-155, miR-214 and miR-222) were constantly regulated in almost all samples that were analyzed[106], suggesting a possible involvement of miRNA-mediated regulatory mechanisms in muscle diseases. In addition to these studies of miRNA expression in muscle disease, a genetic link directly connected miRNA with muscle hypertrophy[111]. A mutation that is responsible for the exceptional muscularization of Texel Sheep was mapped as a single mutation G / T in the region 3 'UTR of mRNA encoding Myostatin, a member of the family of transforming growth factor (TGFb); myostatin is negative regulator of muscle growth. This mutation creates a binding site for miRNAs miR-206 and miR-1, leading to repression of translation myostatin, which causes a phenotype similar to the "double-muscled" resulting from loss of myostatin in mice, rats and humans[112,113].

1.10. Genomic profile global microRNA and mRNA in skeletal muscle

Recent research involving global profile microRNA expression and mRNAs have identificated several new genes related to muscle wasting in different muscle diseases, as described in **Table 3**. Of the below table, we emphasize the study of Bhatnagar et al., 2010[114] which examined the global gene expression using mRNA microarray technology in cultured cells treated with TNF-α, this treatment induced a differential expression of several genes involved in distinct molecular pathways. However, this work does not assess the global gene expression of microRNAs and, in addition, the catabolic action of TNF-α may require the presence of other pro-inflammatory cytokines such as TWEAK (TNF-related weak inducer of apoptosis-), IL 6 and IFN-γ. In fact, the combination of TNF-α and INF-γ is necessary to decrease expression of muscle specific genes, including the

Myod in muscle cells culture[37,38]. To our knowledge, to date, no one study used the high-performance sequencing mRNA (RNA-Seq) integrated with the global expression profile of microRNAs to elucidate the molecular pathways involved in muscle atrophy induced by TNF-α and INF-γ.

Table 3.

Atrophy condition	Genomic profile	Approach	Pathways	Ref
Immobilization (Rat)	mRNA	DD	A	115
Starvation (Rat)	mRNA	Microarray (30000*)	A	49
hindlimb suspension (Rat)	mRNA	Microarray (8700*)	A,B,C,D,E,F	116
Sarcopenia (human)	mRNA	Microarray (18000*)	G,H,I,J,K,L	117
Starvation (C2C12 cells)	mRNA	Microarray (22000*)	A,C,F,I	118
Treatment TNF-α/INF-γ (C2C12 cells)	mRNA	Microaray (12000*)	A,F,M,N	119
hindlimb suspension (ratos)	miRNA	Microarray (350*)	O,P	109
TNF-α treatment (C2C12 cells)	mRNA	Microarray (25000*)	A,I,M,N,Q	114
TWEAK treatment (C2C12 cells)	mRNA miRNA	Microarray (25000*) and TLDA (650*)	A,C,F,G,I,L,M,O	120

Studies of the genomic profile global miRNA and /or mRNA in muscle atrophy. The main pathways or genes identified were: A) ubiquitin dependent proteasomal system, B) Chaperones, C) Oxidative Stress, D) calpain, E) lysosomal proteases, F) Myod, G) Myh, H) transporter glutamine, I) inflammatory cytokines, J) Apoptosis, K) Splicing System, G) Wnt signaling, M) NFkB signaling, N) System iNOS, O) Network MyomiR, P) miR-23, miR-221, miR-148b and miR-338 , Q) myogenesis. *: Number of probes used in the experiments; TLDA: TaqMan low density array (Life Technologies, USA), DD: Differential Display.

1.11. Molecular Networks

Reductionism, which has dominated biological research for over a century, has provided a wealth of knowledge about individual cellular components and their functions. Despite its enormous success, it is increasingly clear that a discrete biological function can only rarely be attributed to an individual molecule. Instead, most biological characteristics arise from complex interactions between the cell's numerous constituents, such as proteins, DNA, RNA and small molecules[121–126]. Therefore, a key challenge for biology in the twenty-first century is to understand the structure and the dynamics of the complex intercellular web of interactions that contribute to the structure and function of a living cell.

The development of high-throughput data-collection techniques, allows for the simultaneous interrogation of the status of a cell's components at any given time. In turn, new technology platforms, such as protein chips or semi-automated yeast two-hybrid screens, help to determine how and when these molecules interact with each other. Various types of interaction webs, or networks, (including protein–protein interaction, metabolic, signaling and transcription-regulatory networks) emerge from the sum of these interactions. None of these networks are independent, instead they form a 'network of networks' that is responsible for the behavior of the cell. Thus a perturbation in one gene can be propagated through the interactions, and affect other genes in the network. However, the fact that we observe similar disease phenotypes despite different genetic causes suggests that these different causes are not unrelated but rather deregulate the same component of the cellular system[127,128]. Therefore in studies of complex diseases researchers increasingly focus on groups of related/interconnected genes, referred to as modules or subnetworks. So a major challenge of contemporary biology is to embark on an integrated theoretical and experimental program to map out, understand and model in quantifiable terms the topological and dynamic properties of the various networks that control the behavior of the cell.

Many approaches are available for the analysis of individual types of data. However, integration and curation of multiple 'omic' data sources are more challenging[129] . Typically, there is little overlap among the proteins and genes identified by different methods[130], and the overlap between experimental findings and known pathways is very low. Previous publications have shown that a more coherent view of the underlying biological processes can be obtained by using a network approach in which the hits from 'omic' experiments are mapped onto a network of protein–protein interactions. Given the high rates of false positives and negatives in these data, the resulting networks are frequently too large and noisy to interpret directly, leading to a number of algorithmic approaches to the problem[131–144]. Flow optimization has been used to reconstruct pathways by inferring genetic hits and transcriptional data[144], and this method is available as a web server[137]. In another approach, transcriptional data obtained from gene knock-out experiments are integrated with interactome and causal paths are identified by linear programming[139]. Bayesian networks have been used to integrate siRNAdata in insulin signaling[141] and copy number and gene expression data for finding drivers in diseases[131]. A maximum-likelihood-based approach has been applied to reveal causal paths in transcriptional regulation by integrating gene knockout

experiments[143]. Other approaches include network inference from gene expression[134], electric circuits[136,138,140] and network propagation[142].

One successful approach to this problem is constrained optimization to identify a subset of the 'omic' hits that are connected directly or indirectly by high probability interactions[135]. This is achieved by searching for the solution to the prize collecting Steiner tree (PCST) problem[132,133,135]. In this approach, the detected proteins/genes in experiments are defined as 'terminal nodes' and seek to connect them to each other either directly or through other undetected proteins (Steiner nodes) using protein–protein and protein–gene interactions. A critical feature of the algorithm is that do not require it to connect all the terminal nodes. Rather, seek a network composed of high-confidence edges that ultimately link a subset of the termini. To identify this network, is made assigning costs to each interaction reflecting confidence that the interaction is real. In addition, is assigned penalties to the terminal nodes based on confidence in the proteomic or transcriptional data. The PCST algorithm identifies a relevant subnetwork by simultaneously minimizing the cost of edges included in the tree and the penalties of terminals that are excluded.

2. HYPOTHESIS

As 1) the plasma levels of TNF-α and IFN- γ are elevated in chronic diseases with skeletal muscle atrophy, 2) the combination of TNF-α and INF-γ deregulated the expression of various genes muscle-specific and 3) micro-RNAs control gene expression in different molecular pathways, the hypothesis of the present research is that skeletal muscle atrophy induced by TNF-α and IFN-γ has a characteristic expression profile of microRNAs and target mRNAs that allow identification of regulatory networks and molecular pathways involved in the muscle atrophy.

3. AIMS

This project aims to analyze in the skeletal muscle cells treated in vitro with TNF-α and IFN-γ:

- The effect of treatment time on the level of expression of MYH and MYOD.
- The overall profile of expression of microRNAs and mRNAs in treatment time with less gene expression of MYH and MYOD.
- Data integration of microRNAs and mRNAs to determine the pattern of correlation between changes in gene expression and reconstruction of a molecular network.

4. MATERIAL AND METHODS

4.1. Experimental Design

This study will use a mouse cell line C2C12 differentiated myotubes. This cell line is an important tool for the study of muscle atrophy, it expresses important cellular and molecular pathways in skeletal muscle and in addition, has a large amount of data available, including data from microarray[114,118–120]. The skeletal muscle atrophy was induced by TNF-α (10 ng / mL) and IFN-γ (100 U / ml) in different treatment times (0h, 6h, 12h, 18h, 24h and 48h). The gene expression of MYH and MYOD was monitored using RT-qPCR to determine the effect of treatment time on the level of expression of MYH and MYOD. This information was used to establish the time with lower gene and protein expression of MYH and MYOD to accomplish the global analysis of the expression of micro-RNAs and mRNAs using RT-qPCR TaqMan Low Density Arrays System and High Performance Sequencing (RNA-Seq), respectively. After that, the bioinformatics analysis were doing to construct the miRNA-regulatory network that was made combining: target genes of microRNAs, and the differential expression of microRNAs and mRNA.

4.2. Cell Culture

C2C12 cell line obtained from the Cell Bank of Rio de Janeiro was trypsinized and divided into two groups: an expansion group and a study group. In the expansion group, the cells were cultured in bottles with DMEM culture medium (Dulbecco's Modified Eagle's Medium - Life Technologies, USA) + 20% fetal calf serum (FCS - Life Technologies, USA) + 1% antibiotics (Penicillin-streptomycin stabilized solution - Life Technologies, USA) until reaching a confluence of 80%. Upon reaching this confluence (within 4 to 5 days), the cells were trypsinized: half of the cells were transferred to another flask to be expanded and the other half will be transferred to 6-well plates forming the study group. The cells of this group were culture with medium DMEM + 10% FBS + 1% antibiotic for 6 days to differentiate into myotubes, which were used for the control group and treatment with TNF-α (10 ng / ml), IFN-γ (100 U / ml) and TNF-α + IFN-γ (10ng/ml + 100 U / ml). The cells were treated with cytokines for different times (0h, 6h, 12h, 18h, 24h and 48h) during the experiment and were kept in Forma Scientific incubator (37°C, 5% CO2), whose medium is changed daily. Each experimental group will be performed in triplicate and have three biological replicates.

4.3. Determination of atrophy of C2C12 myotubes

Atrophy was analyzed using immunofluorescence directly into culture plates containing a glass slide for cell adhesion. The analysis was performed with differentiated cells with the cytokine treatment. The cells were washed with 0.1 M PBS, pH 7.4, fixed with 4% paraformaldehyde in PBS for 30 minutes at room temperature.

The cells were permeabilized with 0.2% Triton X-100 in PBS for 10 minutes at room temperature, washed with PBS and then prepared for immunoblotting myosin Myh IIa. Cells were treated with horse serum at 5% (Sigma) and bovine serum albumin at 2% (BSA, Sigma) and PBS for 30 minutes at room temperature and then incubated with a mouse anti-Myh IIa (Sigma; 1:100 in PBS) for 8 h at 4 ° C. After washing in PBS, samples were incubated with a secondary antibody conjugated to FITC (Vector DBA; 1:50 in PBS) for 1 hour at room temperature and subsequently assembled with Vecta Shield (DAPI). All samples were observed and photographed with a confocal fluorescence microscope (Leica HCS, Germany).

4.4 Gene Expression Profiles

4.4.1 Extraction of Total RNA

RNA extraction was performed using TRIZOL kit (Ambion, USA) according to the manufacturer's instructions. The RNA was quantitated by spectrophotometry using equipment NanoVue (GE Healthcare Life Sciences, USA). RNA samples were treated with DNA FreeTM Kit (Ambion, USA) to remove genomic DNA contamination.

4.4.2 Analysis of RNA quality

The quality of RNA was obtained by the RNA integrity number (RNA Integrity number, RIN) from the analysis of ribosomal RNAs based on microfluidics, using the 2100 Bioanalyzer system (Agilent, USA)[145,146].

4.4.3 Evaluation of Gene Expression by RT-qPCR

The RT-qPCR experiments are being carried out following the guidelines of MIQE: Minimum information for Publication of Quantitative Real-Time PCR Experiment[147].

c) Reaction of reverse transcription (mRNA)

Reverse transcription of mRNA was performed using the High Capacity kit RNA-to-cDNA Master Mix (Life Technologies, USA) following the manufacturer's guidelines. Were used for the reaction 4μL of Master Mix, 1 mg of total RNA and the volume made up to 20μL with nuclease-free water. The mixture was incubated under the following conditions: 25 ° C for 5 min., 42 ° C for 30 min. Followed by inactivation of reverse transcriptase at 85 ° C for 5 min.

d) Polymerase Chain Reaction in Real Time

For each reaction were applied 1μL GoTaq ® qPCR Mix master based on SYBR Green chemistry (Promega, USA), 5μL of RT reaction, and 1μL of primers (**Table 4**) to 10 mM and the volume was completed to 20μL with nuclease-free water. Thermocycling was performed on equipment 7300 Real-Time PCR System (Applied Biosystems, USA) according to the following conditions: GoTag Hot Start Polymerase activation 2 min at 95 °C followed by 40 cycles of 15 sec. at 95 °C and 1 min. 60 °C, finally, dissociation curve in the range of 60-95 °C. Relative gene expression was evaluated using the comparative quantification method [148]. All relative quantifications was assessed using REST software 2009 v 2.0.13, using the pair-wise fixed randomization test with 10,000 permutations [149], with PCR efficiencies calculated by linear regression from fluorescence increase in the exponential phase in the program LinRegPCR v 11.1 [150]. The gene expression change was considered: with fold change (FC) cutoffs ≥1.5 and significance p-values of ≤ 0.05.

Table 4.

Gene	NCBI REF Seq	Primers sequence	Amplicon (bp)
TRIM63	NM_080903.1	5′TGCCCTGCCAGCACAAC 5′GGATTGGCAGCCTGGAAGAT	61
FBXO32	NM_133521.1	5′GACCTGCATGTGCTCAGTGAAG 5′GGATCTGCCGCTCTGAGAAGT	76
MYOD1	NM_001107794.2	5′AAGCAGAGAGAGGAGCAAGCAGAA 5′ACTTTCACTCGAGGGTGAAGCAGT	92
MYH2	NM_012675.3	5′GCCACCACGCTCTTCTGTCT 5′GTCTGGGCCATGGAACTGAT	101
RPL13A	NM_022536.1	5′ CAAGACCTCCTGGCTAGACG 5′ CCGTACCACATCCATGCCTT	70

ACTB	NM_017101.1	5′ TCAACCCCACCGTGTTCTTC 5′ ACTTTGTCTGCAAACAGCTCG	82
TBP	NM_012512.2	5′ CGAGACCGATGTATATGCTTGC 5′GTCCAGATGATTCAGAGCTCCA	114

NCBI REF Seq: sequencia de referência NCBI; pb: pares de bases; TRIM63 (*tripartite motif containing 63*); FBXO32 (*F-box protein 32*); MYOD1 (*myogenic differentiation 1*); MAFbx (*F-box protein 32*); MYH2 (*myosin, heavy chain 2*); RPL13A (*60S ribosomal protein L13a*); ACTB (beta actin) and TBP (TATA-binding protein).

4.4.4 miRNA Expression Profile

The miRNA expression profile was analyzed using the platform TaqMan Low Density Array (TLDA). RNA samples were the same as those used for RNA-seq studies. Briefly, reverse transcription of microRNAs was performed using the kit TaqMan ® MicroRNA Reverse Transcription Kit (Life Technologies, USA) combined with Stem-loop Megaplex ™ RT Primers (Life Technologies, USA), following the manufacturer's guidelines. This system allows reverse transcription only mature microRNAs and is not affected by contamination with genomic DNA[151]. Were used for reaction 3μL (500 ng) of total RNA to which was added the following components of the kit: Megaplex ™ RT primers (10X), dNTPs with dTTP (100 mM) ™ MultiScribe Reverse Transcriptase (50 U/uL), 10X RT Buffer, RNase Inhibitor (20 U/uL) and the volume up to 4.5uL with nuclease-free water. The mixture was incubated under the following conditions: 40 cycles of 16 ° C for 2 min., 42 ° C for 1 min. and 50 ° C for 1 sec. followed inactivation of reverse transcriptase at 85 ° C for 5 min. Each cDNA sample was analyzed with the TLDA MicroRNA A + B Cards Set v3.0 (Life Technologies, USA) the most current version of the system, consisting of a PCR plates of 384 wells with primers and hydrolysis probes Specific which allows the identification of 379 mature microRNAs 5 and reference genes. Each assay (primers and probe) is capable of discriminating mature microRNAs that differ by only one base using a small amount of RNA[151,152]. As shown by Mestdagh et al. 2008[152], variations of instrument and handling of liquids is minimal in this system and therefore it is not necessary to perform PCR replicates. For each plate, 450μL of TaqMan ® Universal PCR Master Mix, No AmpErase ® UNG (2X), 6μL of the reaction product of reverse transcription and the final volume adjusted to 900μL with nuclease-free water. We used the following cycling conditions: 95 ° C for 10 min. Followed by 40 cycles of 95 ° C for 15s and 60 ° C for 1 min. The reactions were performed in System Real-Time PCR VIIa 7 (Life Technologies, USA). Cq values were calculated using the SDS 2.1 software using

the automatic setting of baseline and threshold of 0.2. The Cq (quantification cycle) refers to the meeting point between the amplification curve corrected for baseline and threshold (according to RDML, HTTP://rdml.org)[153].Relative quantification of gene expression was performed by the method of Cq comparative[154]. The high-throughput analysis and visualization of quantitative real-time PCR data was made in R using the library HTqPCR[155]. The gene expression change was considered: with fold change (FC) cutoffs ≥1.5 and significance p-values of ≤ 0.05.

4.4.5. mRNA Expression Profile

The RNA-seq was achieved on HiScanSQ platform (Illumina) using the services of the Laboratory of Animal Biotechnology, School of Agriculture Luiz de Queiroz (ESALQ), coordinated by Dr. Luiz Lehmann Coutinho. RNA libraries were created from each of two controls and two biological replicate cells for each treatment. RNA samples were the same as those used for the microarray analysis studies. The protocol will follow the manufacturer's instructions (available: http://goo.gl/hyslD). In summary, sequencing protocol includes preparation of the transcriptome analysis of RNA (5 mg total RNA), followed by fragmentation and purification of the messenger RNA. The next step is the amplification for the construction of cDNA libraries: hybridization and binding of adapters, reverse transcription, cDNA purification, followed by amplification and quantification of the amplified cDNA. This cDNA is diluted and used in generating clusters (amplification of specific fragments), and subsequently sequenced. Constructed libraries were 100 bp paired-end sequenced by an Illumina HiScanSQ instrument (Illumina, San Diego, CA, USA), Sequencing was performed on eight RNA samples in one lane of the flow cell, following manufacturer's instructions. Each lane produced 84–108 million raw paired reads. Data output in fastq file format contained information about sequences and quality (Phred quality score). Average Phred scores of ≥20 per position were used for alignment.

4.5. Bioinformatics Analysis

4.5.1 Alignment and Analysis of Differential Gene Expression

RNA samples were sequenced by the standard Illumina protocol to create raw sequence files (.fastq files) which underwent quality control analysis using FastQC (goo.gl/vFqiZ). The raw paired-end reads of the cDNA fragments were aligned to the mouse

(RefSeq, mm9) transcriptome, using a spliced junction discovery tool, TopHat version 1.3.2 allowing for unique alignments to the genome[156], and short-read alignment tool, Bowtie[156]. Given a file with aligned sequencing reads was made a count of how many reads map to each gene using the Python package HTSeq. Differential expression across each condition were identified using DEseq version 1.8.2[157](**Figure 7**). These methods represent a widely accepted analysis approaches of RNA-Seq data. The raw read counts were used as input to DESeq for calculation of normalized signal for each transcript in the Control and Treatment samples, and differential expression was reported as Fold Change along with associated p-values. Genes were called differentially expressed if the Pvalue was less than 0.05 and the absolute log fold change was greater than 1. DESeq calculates p-values using a negative binomial distribution which accounts for technical as well as biological variability. The DESeq approach is well suited for count data (read counts) as is the case for RNA-Seq experiments, and the method estimates variance in a local fashion for varying signal strength[157].

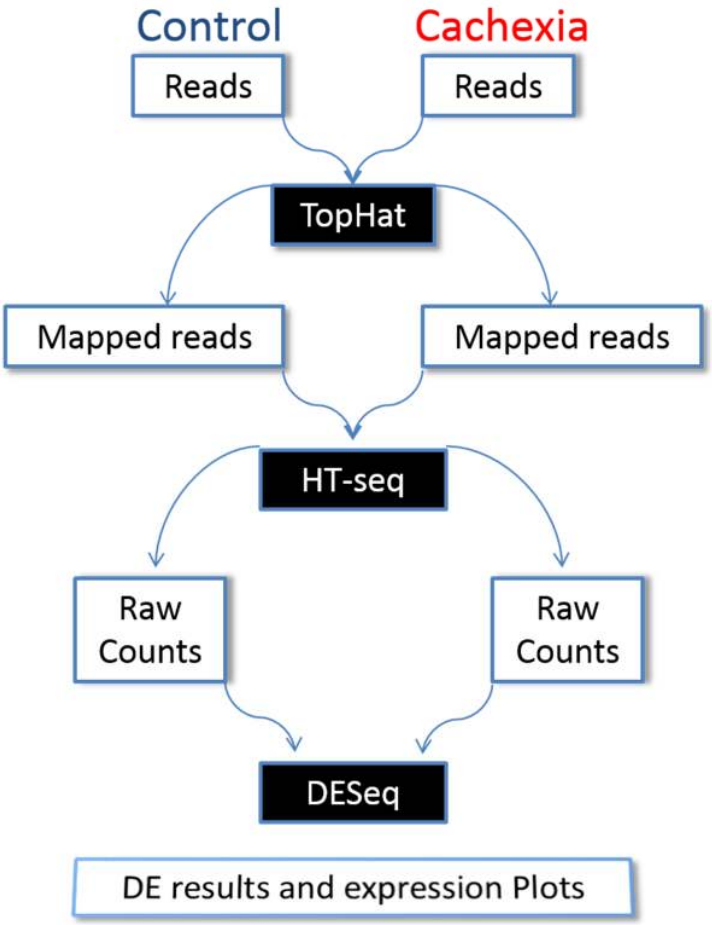

Figure 7. Schematic diagram of the pipeline in RNAseq data analysis. Black boxes represent the software used in each step, and the white boxes represent the output in each step in the pipeline.

4.5.2 Network Reconstruction

4.5.2.1 Interaction Network

The interaction network was built using an approach similar to those recently published for the construction of yeast interaction networks[139,140,144] and reviewed in Cloots and Marchal[158]. For every molecular interaction layer the different interactions were retrieved (protein–protein, pathway and transcriptional layer) and subsequently merged into an integrated network.

a) Protein-Protein layer

The protein-protein interaction data was obtained from HPRD, Release 9 [159], with 9,673 nodes and 39,204 protein-protein interactions (PPIs). Among the exclusively, experimentally derived protein-protein interaction databases, HPRD is the most complete and overlaps well with other PPI databases[160] suggesting that it is most likely to represent the full panorama of human Protein interactions.

b) Pathway layer

The pathway layer interaction data was obtained from curated pathway databases: Reactome[161], Panther (http://www.pantherdb.org/pathway), CellMap (http://cancer.cellmap.org), NCI Pathway Intercation Database (http://pid.nci.nih.gov), and KEGG (http://www.genome.jp/kegg/pathway.html), with 6316 nodes and 98590 interactions.

c) Transcriptional layer

The transcriptional layer 119 Transcription factors-DNA interactions map in promoter-proximal regulatory regions were obtained from curated ChIP-seq and ChIP-chip experiments deposited in the ENCODE[162].

4.5.2.2 Sub Network applying the prize-collecting Steiner tree method

We used the Goemans-Williamson formulation of the Prize- collecting Steiner Tree (PCST) problem[133,135]. Given an undirected graph $G=(V,E)$ where nodes $v \in V$ are associated with penalties $\pi_v \geq 0$ and edges $e \in E$ are associated with costs $c_e > 0$, the algorithm find a sub tree $F=(V_F,E_F)$ of G that minimizes the objective function

$$\sum_{e \in E_F} c_e + \sum_{v \notin V_F} \pi_v.$$

Nodes that have positive penalty values are called "termini". The nodes and edges were obtained from interaction network datasets (see above). Protein nodes to which experimental data could be mapped received positive penalty values (and therefore they were termini) and other nodes received zero penalties. The cost on edges was inversely related to the confidence on each interaction based on available evidence so that high confidence edges had lower costs and therefore would be preferentially selected to be in the solution. Further the algorith introduced a scaling parameter β to balance the penalties paid to exclude nodes with experimental observations and the costs of including edges to connect these nodes:

$$\sum_{e \in E_F} c_e + \sum_{v \notin V_F} \beta\pi_v.$$

The algorithm solved this optimization problem using the branch-and-cut approach[163]. For the costs in the interaction Network we defined two kinds: Interaction from the protein-protein layer and pathway layer were assigned a probability of 0.8, whereas interactions from pathway layer were assigned a probability of 0.6. We defined the penalties for proteins in the interaction graph using the fold changes derived from RNA-Seq expression data.

4.5.2.3 miRNA target prediction

Candidate miRNA–target relationships were predicted by at least one or more of the following target prediction algorithms (union set) extracted from: mirDB[164], TargetScan 5.1 (conservation and Non conservation sites)[165], DIANA-microT[166], PicTar (4-way, and 5-way)[167]. Additionally we used validated targets deposited in miRTarBase[168].

4.5.2.4 miRNA target–dysregulated network

We constructed the miRNA target–dysregulated network (MTDN) using candidate miRNA-target relationships and filtered to mapping only differentially expressed genes derived from RNA-Seq. To prioritize prostate cancer miRNAs, we defined 3 topological features for miRNAs in the MTDN. 1) D_{out} is the number of links from node *i* (number of dysregulated targets for miRNA *i*). 2)N_{miRNA} is the number of its coregulators, which are

miRNAs that share at least 1 target with miRNA *i* in the MTDN including itself and 3)$R_{pc\text{-}miRNA}$ is the proportion of miRNAs in its coregulator set.

To assess the significance of differences in these measures we used a permutation test to determine whether prostate cancer miRNAs features significantly differ from those of general background miRNAs, defined as all miRNAs in the MTDN except for disregulated miRNAs. We randomly selected the same number of miRNAs as disregulated miRNAs from general background miRNAs and computed average values for the 3 topological features. We repeated this procedure 10,000 times. The p-value for each feature is the fraction of feature values for random miRNA sets that are larger than the corresponding values for disregulated miRNAs.

4.5.2.5 Pathway and GO Enrichment Analysis

GO enrichment was performed using the BiNGO Cytoscape plugin[169], using a hypergeometric test with a Benjamini and Hochberg False Discovery Rate correction. A p-value cut-off of 0.05 was used to identify enriched processes. Additionally ClueGO was used to group and analyse the GO and KEGG enrichments[170]. Networks were visualized and analysed using Cytoscape[171].The **Figure 8** show a schematic representation of the overall pipeline used in the reconstruction of biological networks from the high-throughput data.

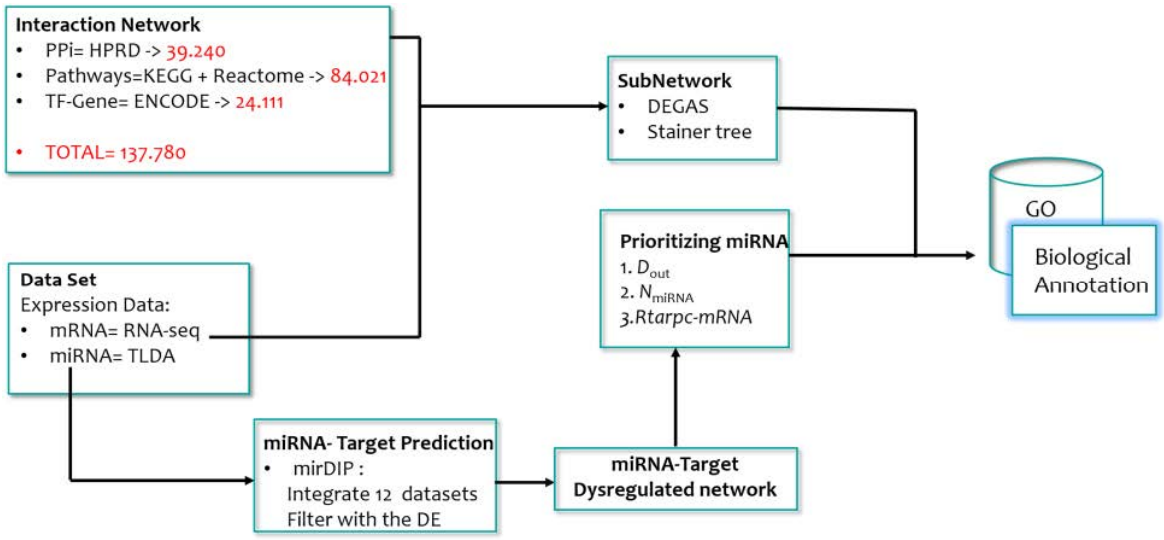

Figure 8. Schematic diagram of the pipeline in the molecular Network analysis. The pipeline shows the steps for the miRNA and mRNA data and the integration in a molecular network.

5. RESULTS

5.1. Differentiation C2C12 cells and analysis of atrophy.

The cells were differentiated into myotubes and subsequently treated with cytokines to form four experimental groups: 1) control, 2) TNF-α: treatment with TNF-α (10ng/mL), 3) IFN-γ: IFN-treatment γ (100U/ml) and 4) IFN-γ + TNF-α: combined treatment of TNF-α (10ng/mL) and INF-γ (100U/ml).

The atrophy of myotubes was observed by light microscopy, in groups treated with cytokines, as already shown in previous publications that same model[119]. However, in addition, to use the confocal immunofluorescent labeling of myosin Myh2. Thus, evidenced also decrease the diameter of myotubes and intensity of fluorescent labeling Myh2 and substantial loss of differentiated myotubes 18-h post treatments with cytokines (**Figure 9**).

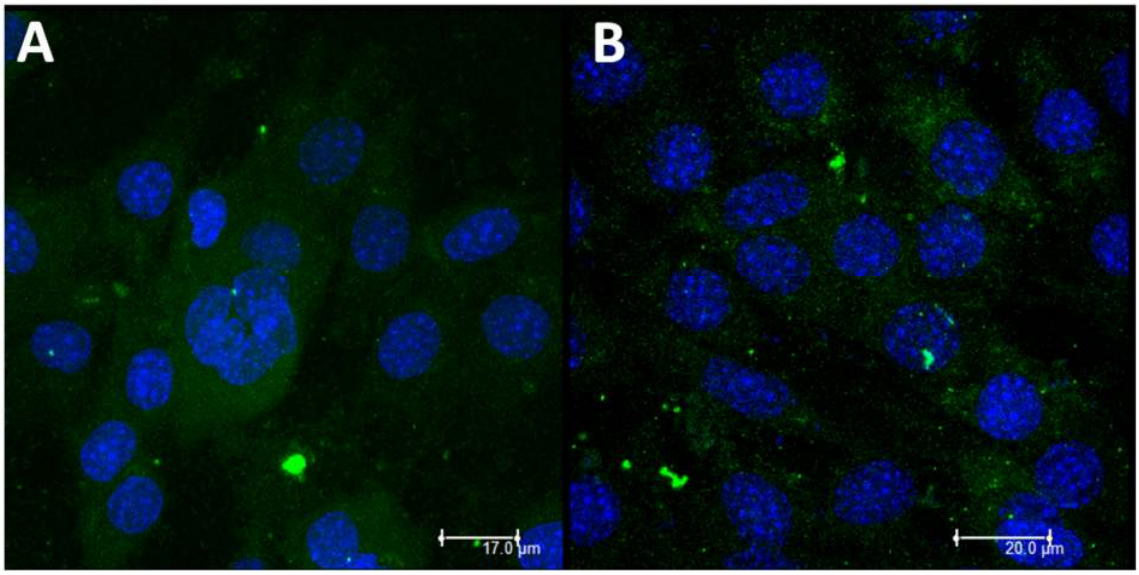

Figure 9. Immunostaining of myosin Myh2 (green) DAPI (blue) in C2C12 myotubes. A) control myotubes. B) myotubes after treatment with TNF-α + IFN-γ (10ng/ml + 100 U / ml) after 18 hours.

To define genes affected in myotubes during cytokine-dependent muscle fiber loss, total RNA from these cells at different times (0h, 6h, 12h, 18h, 24h and 48h) were collected. Spectrophotometric analysis of the samples showed RNA ratio 260/280 nm> 1.8; and the RNA quality determined by the number of the integrity of RNA (RNA Integrity number, RIN) was 8.9 ± 0.37 (**Table 5**).

Table 5– RNA quality and Integrity.

Group	Sample	[ng/µL]	260/280 nm	RIN
CT	Ct1	550	1,869	8,9
	Ct2	684	1,867	8,7
	Ct3	660	1,972	9,2
TNF-α	T1	710	1,842	8,4
	T2	519	1,85	9,0
	T3	354	1,851	8,9
IFN-γ	I1	458	1,982	8,7
	I2	578	1,989	9,4
	I3	580	2.010	8,6
TNF-α	TI1	612	1,923	8,8
INF-γ	TI2	429	1,832	8,7
	TI3	478	1,912	9,1

Ct: Control group; TNF-α (10 ng/ml), IFN-γ (100 U/ml) e TNF-α + IFN-γ (10ng/ml + 100 U/ml). RIN: RNA Integrity Number.

We analyze the effect of cytokine treatment time on expression levels of some genetic markers of atrophy in C2C12 myotubes. RNA-free genomic DNA from each sample was subjected to reverse transcription reaction and expression of MYOD1, MYH2, TRIM63 , FBXO32 were quantified using qPCR. The three experimental groups showed the same pattern of expression throughout the study. However, the data show that the combined effect of TNF-α and IFN-γ leads to greater changes in gene expression with reduced MYOD1 and MYH2 (98% and 78%, respectively) after 24 hours of treatment. Furthermore, the negative regulation of mRNA expression of MYOD1 is faster (90%) compared to Myh2 (50%) after 6 h of treatment. Additionally, treatment with TNF-α and IFN-γ, the atrogenes TRIM63 and FBXO32 show a 2-fold up-regulation after 18 h of treatment (**Figure 10**).

We and previous reports shown that treatment of C2C12 myotubes with cytokines augments the expression of muscle-specific E3 ubiquitin ligases atrogin and TRIM63 and augments the ubiquitination of select muscle proteins such as MYH and MYOD within 12–

24h of treatment[37,172]. In this study, we have performed mRNA and miRNA profiling at 18h of cytokines treatment to detect the expression of both early and late responsive genes.

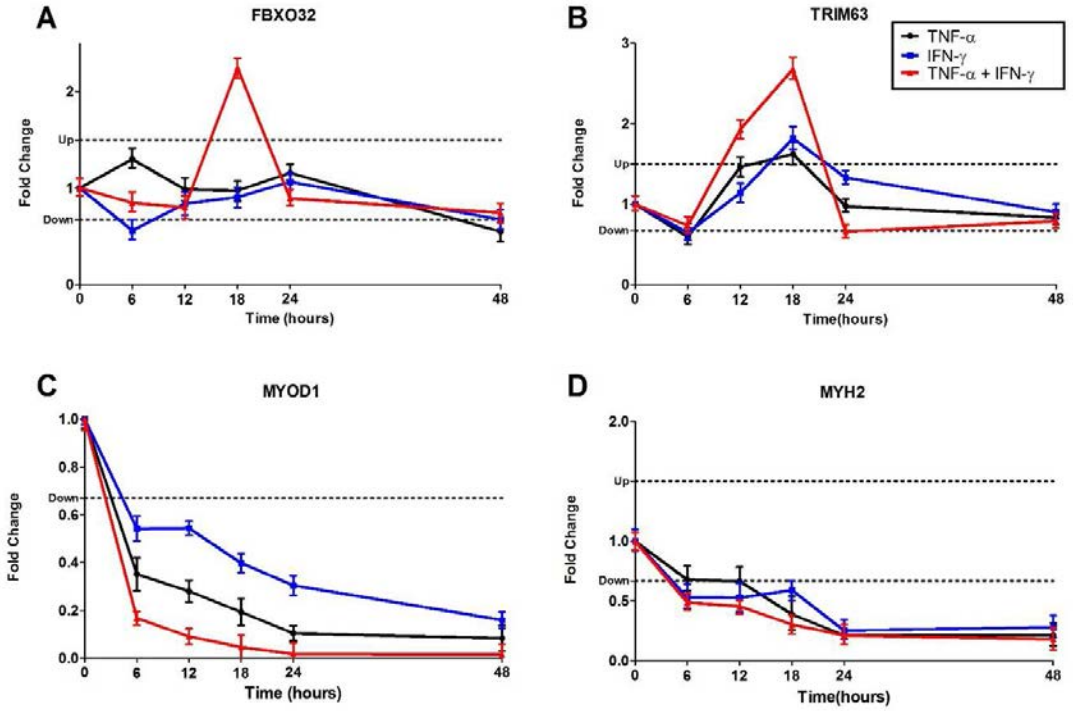

Figure 10. Gene expression A) FBXO32, B) TRIM63, C) MYOD1 and D) MYH2 estimated by RT-qPCR in cells treated with TNF-α (10ng/mL), INF-γ (100U/ml) and INF-γ + TNF-α (100U/ml and 10ng/mL, respectively). Expression normalized to the reference genes: beta actin (ACTB), TATA-binding protein (TBP) and ribosomal protein L13 (RPL13a). Data are expressed as "Fold change" (mean, n = 3).

5.2 RNA-seq Analysis of Global Gene Expression in Cytokines-Treated C2C12 Myotubes

We have used RNA-seq approach to identify the set of genes which cytokines regulates in cultured C2C12 myotubes. To detect the expression of both early and late responsive genes, we have performed mRNA profiling after 18h of cytokines treatment. Eight sequencing libraries were constructed using cDNA from independent experiments (two for each treatment and two control) and sequenced on an Illumina HiScanSQ. We obtained 17.4±3.3, 11.8±1.6, 14.9±0.6 and 20.5±3.5 million 100-nt reads from the TNF-α, IFN-γ, TNF-α plus IFN-γ and control libraries, respectively. The base calling accuracy, measures by the Phred quality score (Q score) was over 20 (supplementary figure S1).

5.2.1 Transcriptome Profiles

Out of approximately 25,794 annotated protein-coding genes, we filtered the genes with the fold change ≥ 2 and p- value < 0.05. Which yielded that TNF-α significantly affected the expression of a total of 437 genes, out of which 183 genes were down regulated and 254 genes were up regulated. While IFN-γ affected 807 genes, out of which 191 were up regulated and 616 up regulates, and finally the treatment with both cytokines affected the expression of more genes of a total of 2933 genes, out of which 1309 were down regulated and 1309 were up regulated (**Figure 12**). The volcano plot of differentially expressed genes with these cut-off p-values and fold changes is presented in the **Figure 11**.

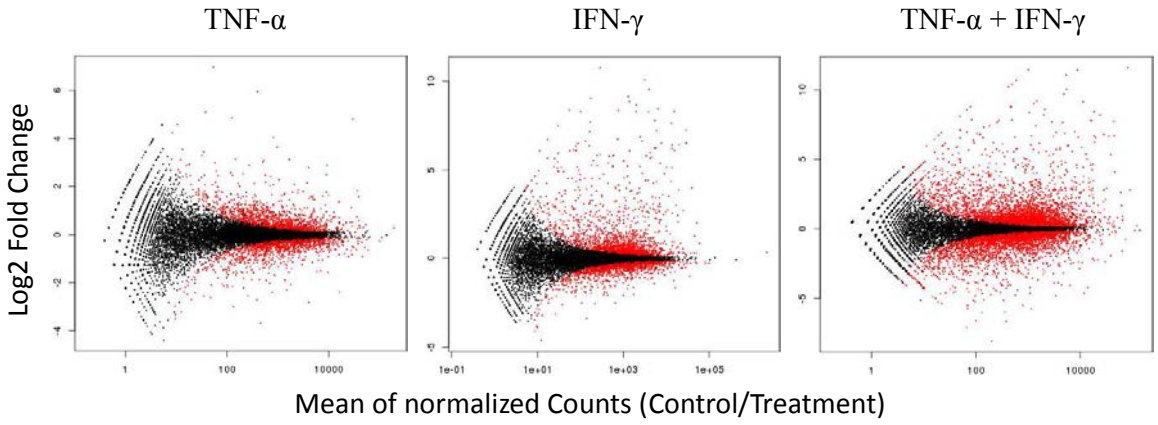

Figure 11 Volcano plots of differentially expressed genes in Cytokines-treated C2C12 myotubes. The dots in red, represent p adjusted-values (FDR) < 0,01.

We analyzed the intersection of differential expressed genes between the three treatments. The number of genes significantly regulated showed substantial overlap (**Figure 12**). Suggesting that TNF-α and IFN-γ activate a common muscle atrophy program, but with diferences to be consider, Whereas around 30% of the differential expressed genes in the TNF-α treatment were shared with the IFN-γ treatment (**Figure 12**)

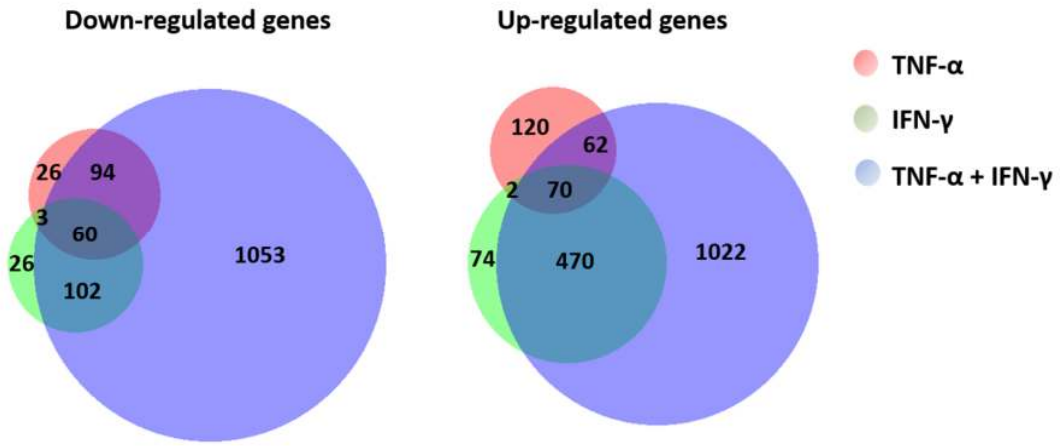

Figure 12. Venn diagram illustrating the overlap between the mRNAs identified as up-regulated and down-regulated in the treatment with TNF-α (10 ng / ml), IFN-γ (100 U / ml) and TNF-α + IFN-γ (10ng/ml + 100 U / ml).

Our data set shown genes were induced up to 100>-fold and were suppressed as much as 25-fold in Cytokine treated C2C12 myotubes (compared to controls). The magnitude and breadth of changes documented appear generally more extensive than alterations detectable in comparable microarray studies citokines induced atrophy on myotubes[114,119,120]. The principle of quantification by mRNA-seq is digital counting, which is free of background hybridization problems (or similar artifacts limiting sensitivity) and does not suffer from saturation of probes (known to diminish precision when quantifying high-expressing genes in microarrays)[173].

5.2.2 Functional clustering of genes

Based on the results from RNA-seq, the specific gene sequences were grouped into different categories according to their functions using Gene Set Enrichment Analysis. It appears that a function can be assigned to a large proportion of genes and it was surprising that some of these genes are interrelated and belonged either to a functional group or a biochemical pathway. As displayed in the **Tables 6 to 20**, a total of 15 groups were clustered in five major biological modules. There is actually overlapping of genes between the three cytokine treatments as shown in the venn diagram (**Figure 12**).

The following sections describe the genes displayed in the cytokines treatments in terms of the functional group they belong (column 1), the Symbol (column 2), the Description

of gene names (column 3), and the gene expression as measured using fold change (columns 4 to 6).

5.2.2.1 Structural Genes

5.2.2.1.1 Muscle Structural genes and Myogenic Factors

As expected, large decreases transcription of myofibrillar were obtained in atrophying myotubes. Among the down-regulated genes comprise several but not all components of the sarcomere, including components of the Thick and thin myofilaments (Actin, Myosins light and heavy chain isoforms, Troponins and Tropomyosins) and scaffold proteins like: Desmina that links the myofibrils laterally by connecting the Z-disks, Myomesin that anchoring the thick filaments to other filaments and the giant obscurin that play important roles in the assembly and stabilization of sarcomeres (**Table 6**). The gene IGFN1, a myosin-binding protein C, was down regulated in all the treatments and is of particular interest because has a regulatory role during the modulation of protein synthesis characteristic of muscular atrophy. Down regulation of these genes contributes to the deregulation of Skeletal Muscle Contraction seen in cancer cachexia. The Myogenic regulatory factors (MYOD1, MEF2C, MEF2A, and myogenin), was highly down regulated, which have been demonstrated previously, denoting a role for this transcriptions factors in the atrophy process.

Functional Group	Symbol	Description	TNF-α	IFN-γ	TNF-α + IFN-γ
Muscle Structural genes and Myogenic Factors	MYH7	myosin, heavy chain 7, cardiac muscle, beta	-4,248	-3,412	-6,693
	MYH1	myosin, heavy chain 1, skeletal muscle, adult	-1,613	-1,733	-5,907
	MYH2	myosin, heavy chain 2, skeletal muscle, adult	-1,500	-1,806	-5,227
	MYH7B	myosin, heavy chain 7B, cardiac muscle, beta	-1,000	-4,789	-4,044
	MYLK	myosin light chain kinase	-1,000	-5,774	-21,413
	MYL9	myosin, light chain 9, regulatory	-2,279	-2,762	-7,911
	MYLK4	myosin light chain kinase family, member 4	-1,728	-2,285	-4,301
	MYBPC1	myosin binding protein C, slow type	-1,000	-9,208	-7,027
	MYO18B	myosin XVIIIB	-1,874	-1,295	-2,071
	MYO1B	myosin IB	1,429	1,000	2,295
	TNNT1	troponin T type 1 (skeletal, slow)	-2,186	-2,434	-5,291
	TNNC2	troponin C type 2 (fast)	-1,578	-1,751	-4,112
	TNNT2	troponin T type 2 (cardiac)	-1,506	-1,431	-2,535
	TNNI1	troponin I type 1 (skeletal, slow)	-1,327	-1,373	-2,323
	TNNT3	troponin T type 3 (skeletal, fast)	-1,296	-1,415	-2,145

	TPM1	tropomyosin 1 (alpha)	-1,527	-1,913	-3,285
	TPM2	tropomyosin 2 (beta)	-1,560	-1,527	-2,855
	DES	desmin	-1,284	-1,369	-2,271
	IGFN1	immunoglobulin-like and fibronectin type III domain containing 1	-2,554	-8,772	-24,510
	OBSCN	obscurin, cytoskeletal calmodulin and titin-interacting RhoGEF	-1,435	-1,203	-2,407
	MYOM1	myomesin 1	-1,355	-1,000	-2,309
	ACTA1	actin, alpha 1, skeletal muscle	-1,352	-1,000	-2,115
	MYOD1	myogenic differentiation 1	-2,223	-1,664	-11,919
	MEF2C	myocyte enhancer factor 2c	-1,000	-1,000	-4,413
	MYOG	myogenin	-1,608	-1,397	-3,134
	MBNL1	muscleblind-like splicing regulator 1	-1,373	-1,138	-2,408
	MEF2A	myocyte enhancer factor 2A	-1,645	-1,411	-2,239

Table 6. Differential mRNA Expression of Muscle Structural genes and Myogenic Factors. Differential expression of mRNAs in Citokines-treated C2C12 myotubes measured by RNA-seq, expressed as Fold change ratios.

5.2.2.1.2 Extracellular matrix components

There was also a decrease in mRNAs for ECM proteins, such as collagens (I,III,IV,V, VI,XII, and XIV) m cadherin, laminin, Tenacin C, V-cam and nidogen 2 (**Table 7**), which may be related to the loss of protein and the potencial of muscle regeneration that occurs in the muscle atrophy in cachexia. However, for the treatments did not result in the same changes in RNA expression of some of the extracellular matrix genes. For instance, upon TNF-α plus INF-γ treatment, increased expression of mRNAs for collagens was noted (**Table 7**), but not the regulation of these in the treatment with a single cytokine. Change in mRNA levels for a range of matrix metalloproteases (MMPs) and Metalloproteases inhibitor (TIMP) was found (**Table 7**), and this genes have been proposed to function in remodeling and turnover of the extracellular matrix components during atrophy. The integrins (ITGA) are integral membrane proteins and are known to participate in cell adhesion as well as cell-surface mediated signaling, and upon citokines treatment was down-regulated (**Table 7**), mRNA levels for other matrix components, nicotinamide riboside kinase 2 (ITGB1BP3), were reduced (**Table 7**) and this gene has recently been shown to may play a role in the regulation of terminal myogenesis.

Functional Group	Symbol	Description	TNF-α	IFN-γ	TNF-α + IFN-γ
Extracellular matrix components	ITGBL1	integrin, beta-like 1	-2,503	-1,797	-7,457
	ITGA1	integrin, alpha 1	-2,939	-1,000	-4,177
	ITGA11	integrin, alpha 11	-2,170	-1,000	-3,578
	ITGA10	integrin, alpha 10	-1,000	-2,601	-3,200
	ITGA3	Integrin, Alpha 3	-1,652	-1,000	-2,607
	CDH11	Cadherin 11	1,321	2,999	2,764
	CDH15	M cadherin	-2,077	-1,868	-8,673
	COL6A2	collagen, type VI, alpha 2	0,558	0,588	0,139
	COL6A3	collagen, type VI, alpha 3	0,541	0,479	0,160
	COL6A1	collagen, type VI, alpha 1	1,000	1,000	0,215
	COL14A1	collagen, type XIV, alpha 1	1,000	1,000	0,245
	COL12A1	collagen, type XII, alpha 1	1,000	1,000	0,265
	COL4A2	collagen, type IV, alpha 2	0,732	0,588	0,310
	COL3A1	collagen, type III, alpha 1	0,923	0,812	0,327
	COL4A1	collagen, type IV, alpha 1	0,726	0,717	0,366
	COL1A1	collagen, type I, alpha 1	0,703	1,000	0,380
	COL5A1	collagen, type V, alpha 1	0,870	1,000	0,444
	COL1A2	collagen, type I, alpha 2	0,766	1,000	0,483
	LAMA2	laminin, alpha 2	-1,798	-1,461	-4,124
	LAMA1	laminin, alpha 1	-2,035	-1,000	-9,833
	MMP7	matrix metallopeptidase 7	-2,250	-3,054	-9,044
	MMP16	matrix metallopeptidase 16	-0,645	-1,558	-3,631
	MMP8	matrix metallopeptidase 8	1,956	-1,320	-3,464
	MMP14	matrix metallopeptidase 14	-1,119	-1,261	-2,270
	MMP23	matrix metallopeptidase 23	-1,000	-1,000	-2,258
	MMP15	matrix metallopeptidase 15	-1,614	-1,601	-2,228
	TIMP2	TIMP metallopeptidase inhibitor 2	-1,218	-1,138	-2,162
	MMP3	matrix metallopeptidase 3	3,384	0,715	1,188
	TIMP1	TIMP metallopeptidase inhibitor 1	2,727	1,759	4,800
	PRELP	proline/arginine-rich end leucine-rich repeat protein	-2,108	-1,679	-14,859
	ITGB1BP3	nicotinamide riboside kinase 2	-2,300	-2,279	-10,684
	NID2	Nidogen 2	-1,422	-1,367	-5,200
	TNC	tenascin C	-1,247	-1,749	-3,116
	VCAM	Vascular Cell Adhesion Molecule 1	-6,539	1,715	1,832

Table 7. Differential mRNA Expression of Extracellular matrix components. Differential expression of mRNAs in Citokines-treated C2C12 myotubes measured by RNA-seq, expressed as Fold change ratios.

5.2.2.2 Cell Proteolytic systems and cell death

5.2.2.2.1 Ubiquitin Proteasome System

Many of the atrogenes encode proteins involved in protein breakdown, mainly by the Ub-proteasome system. Among the up regulated genes comprise several but not all components of the 26S proteasome, including subunits of the alternative regulator 11S complex (PSME1 and PSME2) and of the 20S core particle (PSMB8, PSMB9, and PSMB10), proteins that encode Ubiquitin-activating enzymes (UBA7), ubiquitin-like modifier family (UBD) and Proteasome assembly chaperone (PSMG4) responsible for the assembly of proteasome (**Table 8**). Induction of these genes probably contributes to the increased protein degradation seen in these atrophying muscles. Finally, just in the atrophy induced by IFN-γ treatments, there was an up regulation of Ubiquitin Specific Peptidase (USP) (**Table 8**), genes that associates reversibly with the 19S complex, and may be important in recycling poly Ubiquitin chains back to Ubiquitin monomers.

Functional Group	Symbol	Description	TNF-α	IFN-γ	TNF-α + IFN-γ
Ubiquitin Proteasome System	UBD	ubiquitin D	1,000	308,892	1394,456
	PSMB9	proteasome activator subunit 9	2,251	67,424	73,439
	PSMB8	proteasome activator subunit 8	2,654	28,355	25,858
	UBA7	ubiquitin-like modifier activating enzyme 7	1,962	12,703	14,442
	PSMB10	proteasome activator subunit 10	2,472	14,186	11,661
	USP18	ubiquitin specific peptidase 18	1,000	7,617	10,490
	PSME1	proteasome activator subunit 1	1,856	6,422	6,850
	PSME2	proteasome activator subunit 2	1,701	5,035	4,715
	USP53	ubiquitin specific peptidase 53	1,000	1,000	4,208
	USP45	ubiquitin specific peptidase 45	1,000	1,563	3,770
	USP25	ubiquitin specific peptidase 25	1,319	2,414	2,504
	USP12	ubiquitin specific peptidase 12	1,319	2,050	2,245
	USP42	ubiquitin specific peptidase 42	1,000	2,105	2,116
	PSMG4	proteasome assembly chaperone 4	1,000	2,033	1,916
	USP2	ubiquitin specific peptidase 2	-1,684	-1,595	-3,011

Table 8. Differential mRNA Expression of Ubiquitin Proteasome System. Differential expression of mRNAs in Citokines-treated C2C12 myotubes measured by RNA-seq, expressed as Fold change ratios.

5.2.2.2.2 Oxidative stress

The Increased oxidative stress appear as a mechanic that triggers muscle atrophy, in addition to being close related to mechanisms of autophagy and apoptosis. Among the genes related to oxidative stress was found an up regulation of Nitric oxide synthase (NOS) (**Table 9**). A downstream target of TNF-α and IFN-γ pathways is the NOS2 gene. NOS2 will induce NO, that react with free radical superoxide to form peroxynitrite ($OONO^-$), the release of which leads to down regulation of MyoD mRNA. The transcription factor (ATF4), which promotes the expression of oxidative stress responsive genes as glutathione peroxidase 3 (GPX3), are induced just, upon TNF-α plus INF-γ treatment (**Table 9**). Together, these changes suggest a role for activation of an oxidative stress response in atrophying muscles, as has been suggested by others.

Functional Group	Symbol	Description	TNF-α	IFN-γ	TNF-α + IFN-γ
Oxidative stress	NOS2	nitric oxide synthase 2	6,905	11,044	105,031
	ATF4	activating transcription factor 4	1,000	1,276	2,620
	GPX3	Glutathione Peroxidase 3	0,777	1,227	2,011
	NOS1	nitric oxide synthase 1	-4,168	-3,659	-12,870

Table 9. Differential mRNA Expression of Oxidative stress genes. Differential expression of mRNAs in Citokines-treated C2C12 myotubes measured by RNA-seq, expressed as Fold change ratios.

5.2.2.2.3 Apoptotic Pathways- autophagy-lysosome system

The group included the proapoptotic genes of the BCL-2 family (BCL2L1, BBC3, BAX and BID), the mitochondrial voltage-dependent anion channel (VDAC1), the activator of caspases PMAIP1 and Capsases (CASP1, 4,7and 12), were strongly and moderately up-regulated under TNF-α plus INF-γ and INF-γ treatments respectively (**Table 10**). BCL-2 family cooperates or are activator proteins which leads to the loss in membrane potential increasing the opening of VDAC1 gene, the release of cytochrome c and caspases activation. It's noteworthy that caspases are implicated in not canocial functions. For instance, CASP1 can form part of the inflammasome, a key part of IL-1 processing during inflammation, whilst CASP12 can reduces activation of NFκB in response to TNF-α. Change in mRNA levels for nuclear lamina genes (LMNB1 and LMNB2) and was found (**Table 10**), and this genes have been related as targets of many caspases in the deregulation of nuclear architecture during apoptosis.

On the other hand, in the TNF-α plus INF-γ treatments, there was also an up regulation in mRNAs for autophagy-lysosome system proteins, such as the tumor protein p53 inducible nuclear protein 1 (TRP53INP1) required for autophagosome formation and processing and as a scaffold protein that recruits MAP1LC3A, However, the associated genes MAP1LC3A and TRP53INP2 were down regulated. In contrast, key regulator of the process were up regulated as ubiquitin specific peptidase 13 (USP13) that mediates deubiquitination of BECN1 (protein of the regulatory complex that induces LC3 recruitment to the nascent autophagosome).In addition this genes apparently bind LC3 and can therefore recruit the grow autophagosome to mitochondria. Interestingly, BNIP3 and BNIP3L promotes crosstalk between apoptosis and autophagy and may be triggered by common pathways, and sometimes this results in combined autophagy and apoptosis responses.

Functional Group	Symbol	Description	TNF-α	IFN-γ	TNF-α + IFN-γ
Apoptotic Pathway	PMAIP1	phorbol-12-myristate-13-acetate-induced protein 1	1,000	1,000	11,145
	CASP4	caspase 4, apoptosis-related cysteine peptidase	1,963	3,646	8,350
	BCL2L1	BCL2-like 1	1,000	1,898	4,415
	CASP1	caspase 1, apoptosis-related cysteine peptidase	1,500	6,207	4,282
	BBC3	BCL2 binding component 3	1,000	1,000	4,043
	CASP7	caspase 7, apoptosis-related cysteine peptidase	1,000	4,124	3,611
	BAX	BCL2-associated X protein	1,175	1,409	2,701
	CASP12	caspase 12, apoptosis-related cysteine peptidase	1,000	2,285	2,458
	BID	BH3 interacting domain death agonist	1,267	2,293	2,371
	VDAC1	voltage-dependent anion channel 1	1,000	0,893	2,052
	LMNB2	lamin B2	-1,000	-1,596	-3,671
	LMNB1	lamin B1	-0,757	-1,000	-3,992
Autophagy-lysosome system	TRP53INP1	tumor protein p53 inducible nuclear protein 1	1,000	2,256	7,357
	BNIP3	BCL2/adenovirus E1B 19kDa interacting protein 3	1,431	1,000	3,617
	BNIP3L	BCL2/adenovirus E1B 19kDa interacting protein 3-like	1,442	0,899	2,522
	USP13	ubiquitin specific peptidase 13	1,000	0,695	2,104
	MAP1LC3A	microtubule-associated protein 1 light chain 3 alpha	-1,471	-1,425	-2,243
	TRP53INP2	tumor protein p53 inducible nuclear protein 2	-1,000	-1,506	-2,277

Table 10. Differential mRNA Expression of Apoptotic Pathways- autophagy-lysosome system genes. Differential expression of mRNAs in Citokines-treated C2C12 myotubes measured by RNA-seq, expressed as Fold change ratios.

5.2.2.3 Inflammatory Cytokines and signaling pathway

5.2.2.3.1 TNF-α Pathway

As expected our data revealed increased expression of the TNF-α/NFκB pathway even with the IFN-γ treatment (**Table 11**). Both canonical (NFKB1: p105/p50) and alternative (NFKB2: p100/p52) NF-kB signaling pathways in my tubes were up regulated. The NFκB inhibitor family (NFKBIA, NFKBIB, NFKBIZ, NFKBIE) that inhibits and regulated the DNA binding of NFκB were up-regulated, suggesting feed-back regulation of this transcription factor. Adapter molecule that regulates the activation of NF-kappa-B and JNK such as the TNF receptor associated factor (TRAF) protein family and their associated proteins (TRAF1, TRAF6, TRAF3IP2 and TRAFD1) were up regulated, highlighting the up regulation of TRAF6 a protein required for the activation of FoxO3 and AMPK in muscle atrophy, and for the induction of ubiquitin-proteasome and autophagy-lysosome systems. We also found up regulation in the mRNA levels downstream the pathway in the component of a protein kinase signal transduction cascade (MAP3K1 and MAP3K8). Finally there were a regulation of some genes downstream the path such as the TNF-α induced proteins (TNFAIP2 and TNFAIP3) and molecular components that trigger the activation of the path, such as the cytokine TNF-α and their receptor (TNFRSF1A).

Functional Group	Symbol	Description	TNF-α	IFN-γ	TNF-α + IFN-γ
TNF-α Pathway	TNF	tumor necrosis factor	1,000	1,000	22,442
	TNFAIP2	tumor necrosis factor, alpha-induced protein 2	1,435	6,708	10,939
	TNFAIP3	tumor necrosis factor, alpha-induced protein 3	1,517	1,000	5,977
	NFKBIZ	Nuclear Factor Of Kappa Light Polypeptide Gene Enhancer In B-Cells, zeta	1,324	2,609	5,216
	NFKBIA	Nuclear Factor Of Kappa Light Polypeptide Gene Enhancer In B-Cells, alpha	1,761	0,803	3,486
	NFKBIB	Nuclear Factor Of Kappa Light Polypeptide Gene Enhancer In B-Cells, beta	1,000	1,000	3,248
	NFKBIE	Nuclear Factor Of Kappa Light Polypeptide Gene Enhancer In B-Cells, epsilon	2,254	1,000	3,127
	TRAF1	TNF receptor-associated factor 1	1,000	1,000	4,592
	TRAFD1	TRAF-type zinc finger domain containing 1	1,000	4,229	3,347
	MAP3K1	mitogen-activated protein kinase kinase kinase 1, E3 ubiquitin protein ligase	1,397	0,673	4,060
	MAP3K8	mitogen-activated protein kinase kinase kinase 8	1,497	1,547	3,372
	TRAF3IP2	TRAF3 interacting protein 2	1,000	1,000	2,496
	TRAF6	TNF receptor-associated factor 6	1,000	1,000	2,239

	TNFRSF1A	tumor necrosis factor receptor superfamily, member 1A	1,213	1,611	2,157
	NFKB1	Nuclear Factor Of Kappa Light Polypeptide Gene Enhancer In B-Cells 1	1,418	1,000	2,135
	NFKB2	Nuclear Factor Of Kappa Light Polypeptide Gene Enhancer In B-Cells 2	1,284	0,811	1,843
	TRAF3IP3	TRAF3 interacting protein 3	-1,000	-3,741	-2,647

Table 11. Differential mRNA Expression of TNF-α Pathway. Differential expression of mRNAs in Citokines-treated C2C12 myotubes measured by RNA-seq, expressed such as Fold change ratios.

5.2.2.3.2 INF-γ Pathway

As expected our data revealed increased expression of the INF-γ/Jak/stat pathway just in the IFN-γ treatments (**Table 12**). The upstream regulator of the pathway the enzymes Janus kinases (JAK1 and JAK2) were up regulated, this kinases phosphorylates the STATs proteins that were also up regulated (STAT1 and STAT2) that translocate to the cell nucleus where they act as transcription activators. Other interesting up regulated genes related to the pathway are the Tripartite motif proteins (TRIM21, TRIM25 and TRIM34), that are ubiquitin E3 ligase that mediating ubiquitination of proteins that leads to the production or regulation of interferons. Finally there were a regulation of the INF-γ receptor (IFNAR2) and highlighting the induction around 400 folds of the major histocompatibility complex (MHC) class II transactivator, CIITA, which binds to myogenin and inhibits its activity.

Functional Group	Symbol	Description	TNF-α	IFN-γ	TNF-α + IFN-γ
INF-γ Pathway	CIITA	Class II, Major Histocompatibility Complex, Transactivato	1,000	1745,682	446,826
	TRIM21	tripartite motif containing 21	1,485	9,698	11,385
	STAT1	signal transducer and activator of transcription 1	1,000	14,739	9,952
	TRIM34	tripartite motif containing 34	1,000	7,711	7,718
	STAT2	signal transducer and activator of transcription 2	1,446	4,681	4,522
	IFNAR2	interferon (alpha, beta and omega) receptor 2	1,760	2,071	3,716
	TRIM56	tripartite motif containing 56	1,236	2,685	3,649
	JAK2	Janus kinase 2	3,057	2,604	3,324
	JAK1	Janus kinase 1	1,123	1,337	2,336
	TRIM25	tripartite motif containing 25	1,000	2,405	2,320

Table 12. Differential mRNA Expression of INF-γ Pathway. Differential expression of mRNAs in Citokines-treated C2C12 myotubes measured by RNA-seq, expressed such as Fold change ratios.

5.2.2.3.3 IL-6 Pathway

The treatments with both cytokines trigger an up-regulation up to 33 fold of IL-6 citokine (**Table 13**). Also, were up regulated the interleukin 6 receptor (IL6RA), the enzymes Janus kinase (JAK3) and the response transcription activator STAT3 (**Table 13**). The gene EBPB were up regulated, an important transcriptional activator that specifically binds to an IL-1 response element in the IL-6 gene.

Functional Group	Symbol	Description	TNF-α	IFN-γ	TNF-α + IFN-γ
IL-6 Pathway	IL6	interleukin 6	4,377	2,630	33,066
	JAK3	Janus kinase 3	1,926	1,000	5,010
	STAT3	signal transducer and activator of transcription 3	1,454	1,967	2,624
	CEBPB	CCAAT/enhancer binding protein (C/EBP), beta	1,374	1,000	2,363
	IL6RA	interleukin 6 receptor	1,418	1,000	2,215

Table 13. Differential mRNA Expression of IL-6 Pathway. Differential expression of mRNAs in Citokines-treated C2C12 myotubes measured by RNA-seq, expressed such as Fold change ratios.

5.2.2.3.4 Cytokines

The treatments with both cytokines trigger an up-regulation of proinflammatory chemokines (IL1A, TNSFSF9, TNFSF10, CSF, CCL2, CCL5, CCL7,CCL8,CCL9 and CXCL5), that are related to induced cell death and produced in response to stimulation with other cytokines such as TNF-α. Simultaneusly were up regulation of some receptor (TNFRSF9, TNFRSF11B, TNFRSF10B, TNFRSF22, TNFRSF23, IL4RA, IL12RB1 and IL15RA) (**Table 14**).

Functional Group	Symbol	Description	TNF-α	IFN-γ	TNF-α + IFN-γ
Cytokines	IL1A	interleukin 1, alpha	1,000	1,000	139,770
	CCL5	chemokine (C-C motif) ligand 5	12,374	2,405	129,790
	TNFSF10	tumor necrosis factor superfamily, member 10	1	106,6537	44,1413
	CCL2	chemokine (C-C motif) ligand 2	5,670	4,693	12,330
	CCL7	chemokine (C-C motif) ligand 7	2,891	4,808	7,118
	CCL8	chemokine (C-C motif) ligand 8	2,385	5,198	6,574
	TNFSF9	tumor necrosis factor superfamily, member 9	1,4923	1	5,352
	CCL9	chemokine (C-C motif) ligand 9	2,987	1,000	4,632
	CSF1	Colony Stimulating Factor 1	1,280	1,461	2,658
	CXCL5	chemokine (C-X-C motif) ligand 8	3,550	1,000	2,318
	TNFRSF11B	tumor necrosis factor receptor superfamily, member 11b	1,000	1,964	2,088
	IL18BP	interleukin 18 binding protein	1,000	54,455	25,995
	TNFRSF9	tumor necrosis factor receptor superfamily, member 9	5,523	1,000	17,326

	IL15RA	interleukin 15 receptor, alpha	1,000	6,849	11,923
	TNFRSF23	tumor necrosis factor receptor superfamily, member 23	1,387	1,351	7,001
	TNFRSF22	tumor necrosis factor receptor superfamily, member 22	1,453	1,660	6,435
	TNFRSF10B	tumor necrosis factor receptor superfamily, member 10b	1,000	1,523	5,141
	IL4RA	interleukin 4 receptor	2,111	1,000	2,436
	IL12RB1	interleukin 12 receptor, beta 1	1,000	1,000	2,140
	CXCR4	Chemokine (C-X-C Motif) Receptor 4	-3,225	-0,864	-2,188
	IL1R1	interleukin 1 receptor, type I	-0,699	-1,721	-4,411

Table 14. Differential mRNA Expression of Cytokines. Differential expression of mRNAs in Citokines-treated C2C12 myotubes measured by RNA-seq, expressed such as Fold change ratios.

5.2.2.4 Muscle growth and differentiation

5.2.2.4.1 IGF1-AKT-FOXO Signaling Pathway

Insulin-like growth factor-1 is a major determinant of muscle growth and plays a key role in compensatory hypertrophy. IGF-1 and downstream signaling molecules (PIK3C2B and PIK3R3) were down regulated, and the IGF-1 binding proteins (IGFBP2, IGFBP3, IFGBP4, IFGBP5, IFGBP6) which binds IGF-1 either inhibit or stimulate the growth promoting effects, were deregulated (**Table 15**). Also the pathway are related to FOXO3, a transcription factor that promote protein degradation that was up regulated when the myotubes were treated with both cytokines. Also FOXO3 could be inhibited by PPARGC1B that were down regulated. Simultaneously to the down regulation of PPARGC1B the gene PPARD, a potent inhibitor of PPARGC1B, were up regulated. The genes NEB and WASF1 that can control actin nucleation, muscle hypertrophy by IGF1-Akt pathway were down regulated.

Functional Group	Symbol	Description	TNF-α	IFN-γ	TNF-α + IFN-γ
IGF1-AKT-FOXO Signaling Pathway	IGF1	insulin-like growth factor 1	-1,715	-2,189	-28,409
	IGFBP5	insulin-like growth factor binding protein 5	-1,895	-3,215	-18,762
	DEPDC6	DEP domain containing MTOR-interacting protein	-1,514	-2,103	-6,873
	IGFBP4	insulin-like growth factor binding protein 4	-1,000	-1,000	-5,299
	PIK3C2B	phosphatidylinositol-4-phosphate 3-kinase, catalytic subunit type 2 beta	-1,502	-1,598	-4,531
	PPARGC1B	peroxisome proliferator-activated receptor gamma, coactivator 1 beta	-1,000	-1,000	-3,333
	NEB	Nebulin	-1,449	-1,423	-3,332
	PIK3R3	phosphoinositide-3-kinase, regulatory subunit 3 (gamma)	-1,418	-1,000	-2,322

	WASF1	WAS protein family, member 1	-1,000	-1,000	-2,226
	IGFBP6	insulin-like growth factor binding protein 6	-1,640	-1,000	-2,018
	PIK3C2A	phosphatidylinositol-4-phosphate 3-kinase, catalytic subunit type 2 alpha	1,000	1,197	2,137
	FOXO3	forkhead box O3	1,000	1,000	2,189
	IGF2BP2	insulin-like growth factor 2 mRNA binding protein 2	1,250	1,274	2,471
	PPARD	peroxisome proliferator-activated receptor delta	1,000	1,000	3,311
	PIK3R5	phosphoinositide-3-kinase, regulatory subunit 5	2,857	1,000	7,158
	IGFBP3	insulin-like growth factor binding protein 3	0,652	2,800	7,180

Table 15. Differential mRNA Expression of IGF1-AKT-FOXO Signaling Pathway. Differential expression of mRNAs in Citokines-treated C2C12 myotubes measured by RNA-seq, expressed such as Fold change ratios.

5.2.2.4.2 TGFβ Signaling Pathway

There were a decrease in mRNAs for protein of the transforming growth factor (TGF) pathway, including ligands (TGFB2 and TGFB3), receptor (TGFRB2) and the transcription factors (SAMD2 and SMAD3) (**Table 16**). Furthermore, in the treatment with both cytokines the genes SMAD7 and SMURF1, related to the negative feedback of the pathway, were up regulated. SMAD7 binds the E3 ubiquitin ligase SMURF1, this complex interacts with TGF-beta receptor leading to the degradation.

Functional Group	Symbol	Description	TNF-α	IFN-γ	TNF-α + IFN-γ
TGFβ Signaling Pathway	TGFB3	transforming growth factor, beta 3	-1,890	-1,467	-18,657
	TGFB2	transforming growth factor, beta 2	-2,961	-3,286	-5,631
	SMAD3	SMAD family member 3	-1,298	-1,418	-2,402
	TGFBR2	transforming growth factor, beta receptor I	-1,000	-1,172	-2,366
	SMURF1	SMAD specific E3 ubiquitin protein ligase 1	1,000	1,390	2,304
	SMAD7	SMAD family member 7	1,000	1,477	2,499

Table 16. Differential mRNA Expression of TGFβ Signaling Pathway. Differential expression of mRNAs in Citokines-treated C2C12 myotubes measured by RNA-seq, expressed such as Fold change ratios.

5.2.2.4.3 WNT-Notch Signaling Pathway

Wnt and Notch signaling pathways are essential to myogenic cell fate decisions during development and tissue repair. This two pathways were down regulated when has been treated with bot cytokines. There were a decrease in mRNA for the ligands (JAG1 and WNT10A),

the membrane receptor (NOTCH1), transcriptional activators and repressor (RBPJ and HEY1) and the inducible proteins downstream the pathway (WISP1 and WISP2) (**Table 17**).

Functional Group	Symbol	Description	TNF-α	IFN-γ	TNF-α + IFN-γ
Notch Signaling Pathway	Notch1	Notch1	0,443	1,000	3,361
	Rbpj	Recombination Signal Binding Protein For Immunoglobulin Kappa J Region	1,463	1,000	3,234
	Jag1	Jagged 1	-1,736	-1,000	-2,401
	Hey1	Hairy/Enhancer-Of-Split Related With YRPW Motif 1	-5,921	-3,385	-2,535
WNT Signaling Pathway	Wisp1	WNT1 inducible signaling pathway protein 1	-1,383	-2,100	-6,031
	wisp2	WNT1 inducible signaling pathway protein 2	-1,169	-1,144	-5,376
	Lef1	Lymphoid Enhancer-Binding Factor 1	-1,000	-2,830	-4,097
	WNT10a	Wingless-Type MMTV Integration Site Family, Member 10A	-1,000	-2,394	-3,165
	Ccnd1	cyclin D1	-1,196	-1,245	-2,979

Table 17. Differential mRNA Expression of WNT-Notch Signaling Pathway. Differential expression of mRNAs in Citokines-treated C2C12 myotubes measured by RNA-seq, expressed such as Fold change ratios.

5.2.2.5 Transcriptional and Translational control

5.2.2.5.1Transcriptional control

During the phase of muscle atrophy in the combined treatment with both cytokines, there were deregulation in transcription activators and factor, such as the up regulation of JUN, JUNB, CREB5,CREBL4 and FOS as well as the down regulation of TCF4 and FOXO6 (**Table 18**).This evidence that atrophy involves a complex regulatory network of transcription factors.

Functional Group	Symbol	Description	TNF-α	IFN-γ	TNF-α + IFN-γ
Transcriptional control	JUNB	jun B proto-oncogene	1,543	1,258	3,489
	CREB5	cAMP responsive element binding protein 5	1,000	1,000	3,717
	FOS	FBJ murine osteosarcoma viral oncogene homolog	1,000	1,000	3,617
	CREB3L4	cAMP responsive element binding protein 3-like 4	1,000	1,000	3,221
	JUN	jun proto-oncogene	0,724	1,342	2,578
	TCF4	transcription factor 4	-1,211	-1,401	-2,102
	FOXO6	forkhead box O6	-2,058	-2,459	-5,045

Table 18. Differential mRNA Expression of Transcriptional control genes. Differential expression of mRNAs in Citokines-treated C2C12 myotubes measured by RNA-seq, expressed such as Fold change ratios.

5.2.2.5.2 Translation Control

Several up-regulated atrogenes such as EIF4EBP1, and EIF2AK2 inhibit translation initiation factors and could indicate a reduction in translation in muscle (**Table 19**). These adaptations could help reduce 5cap-dependent translation that occurs when growth factors and nutrients are decreased while allowing cap-independent translation which tend to be important in stressed cells.

Functional Group	Symbol	Description	TNF-α	IFN-γ	TNF-α + IFN-γ
Translation	EIF4E3	eukaryotic translation initiation factor 4E family member 3	1,348	5,243	5,539
	EIF2AK2	eukaryotic translation initiation factor 2-alpha kinase 2	1,000	3,082	3,279
	EIF4EBP1	eukaryotic translation initiation factor 4E binding protein	1,198	1,000	2,911

Table 19. Differential mRNA Expression of Translation Control genes. Differential expression of mRNAs in Citokines-treated C2C12 myotubes measured by RNA-seq, expressed such as Fold change ratios.

5.2.2.5.3 Chromatin Regulation

The Chromatin modifications appear a mechanism in the regulation of the gene expression in the combined treatment with both cytokines. Among the genes related to chromatin regulation were found the up regulation of histone variants (HIST1H1C, HIST1H1D, HIST1H1E, HIST1H2BC and HIST1H4I) (**Table 20**). The Histone deacetylase 11 (HDAC11), enzyme that gives a tag for epigenetic repression and plays an important role in transcriptional regulation was down regulated.

Functional Group	Symbol	Description	TNF-α	IFN-γ	TNF-α + IFN-γ
Chromatin Regulation	HDAC11	histone deacetylase 11	-1,858	-1,000	-2,130
	HIST1H1C	histone cluster 1, H1c	1,000	1,347	3,407
	HIST1H1E	histone cluster 1, H1e	1,000	1,000	2,297
	HIST1H2BC	histone cluster 1, H2bc	1,000	1,000	2,561
	HIST1H1D	histone cluster 1, H1d	1,000	1,000	3,330
	HIST1H4I	histone cluster 1, H4i	1,000	1,000	9,094

Table 20. Differential mRNA Expression of Chromatin Regulation genes. Differential expression of mRNAs in Citokines-treated C2C12 myotubes measured by RNA-seq, expressed such as Fold change ratios.

5.3 Identification of Differentially Expressed MicroRNAs in Cytokines-Treated Myotubes

It is estimated that among several thousand human genes, up to one-third of the mRNA, are potential targets for regulation by miRNAs encoded in the genome. To understand the regulatory mechanisms induced by cytokines that occur at the post-transcriptional and involves interaction with microRNA binding sites in mRNA, we investigated the effect of atrophy induced by cytokines INF-γ and TNF-α on the expression of microRNAs using low density arrays.

We used the following exclusion criteria for trials for gene expression analysis: 1) Crossing Threshold (Ct) ≤ 33, 2) failure determination algorithm of the exponential phase of amplification, 3) standard deviation between replicas <0.5, 4) ΔCt <1 between the replica group, 5) Outlier identified by the analysis software. The proper normalization of the data minimizes the effects of variations and systematic techniques is a prerequisite for achieving significant biological change. However, there is still a lot of inconsistency on the performance of recommendations and commonalities in experiments for the global analysis of the expression of microRNAs.

Five dierent normalisation methods are currently implemented in HTqPCR. Three of these (Rank invariant scaling, DeltaCt and Geometric Mean) will scale each individual sample by a given value, whereas the remaining two (Quantile and Rank invariant normalization) will change the distribution of Ct values. For the deltaCt normalization we used the highest stability of the five genes which show little variability in Ct values between different experimental groups (**Figure 13**).Comparing the raw and normalised values gives an idea of how much correction has been performed (**Figure 14**).To examine the general distribution of data both before and after normalisation we plotting the densities of the different normalisation methods to lends insight into how they differ (**Figure 15**).We select Geometric mean normalization to perform the differential expressio as there are some indications that this normalization is optimal for miRNA studies, because calculates the average Ct value for each sample, and scales all Ct values according to the ratio of these mean Ct values across samples[174].

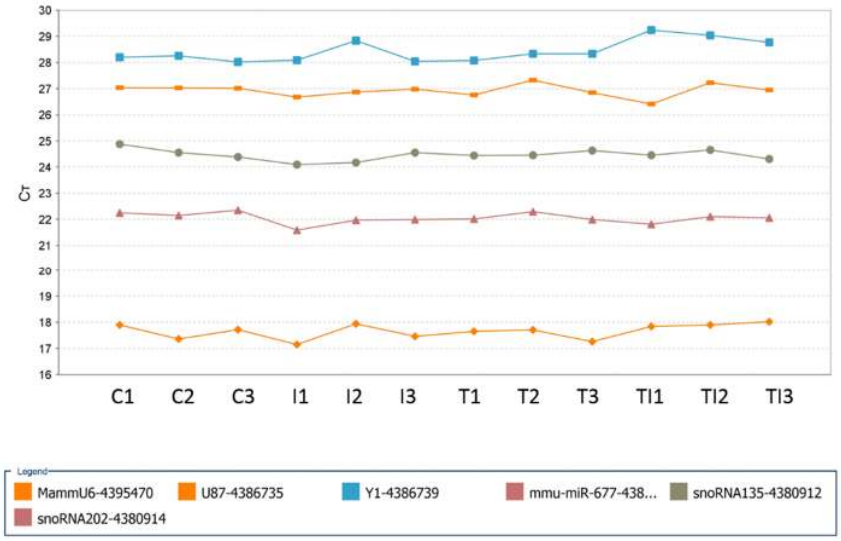

Figure 13. Analysis Ct values of endogenous genes used in this study, C1, C2, C3: control group, T1, T2, T3: TNF-α (10 ng / ml), I1, I2, I3: IFN-γ (100 U / mL) and TI1, TI2, TI3: TNF-α + IFN-γ (10ng/ml + 100 U / ml).

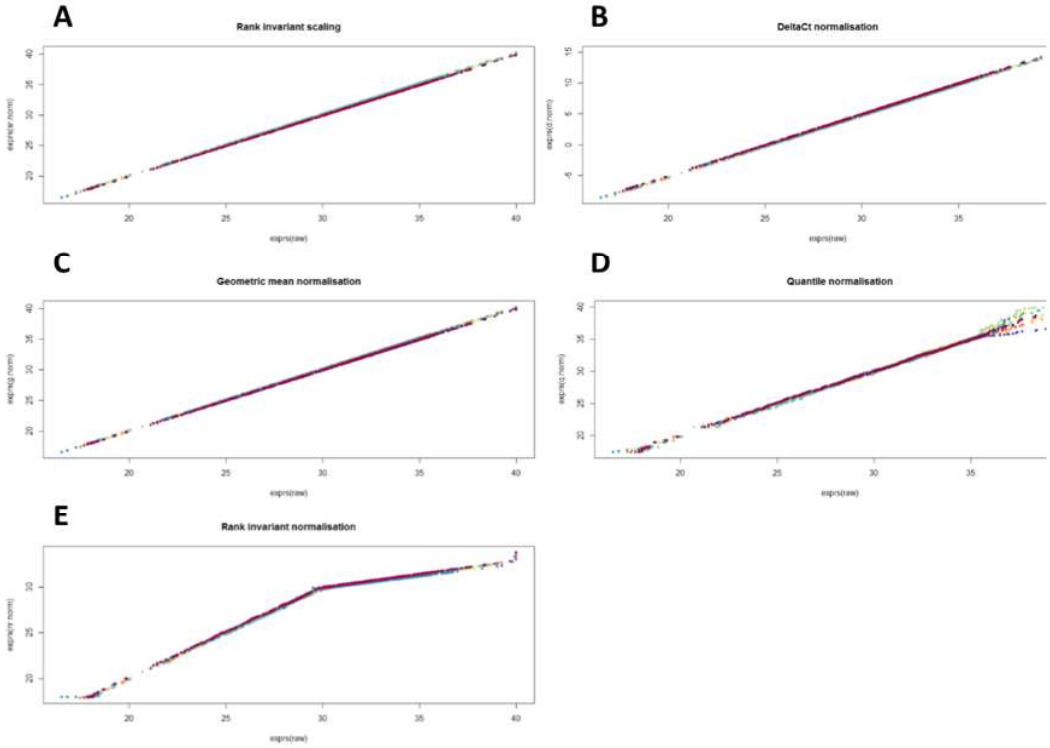

Figure 14. Normalized versus raw data, using a separate colour for each sample. The raw data is plotted along the x-axis and the normalised along y.A) Rank invariant scaling, B) Delta CT, C)Geometric Mean, D) Quantile, E) Rank Invariant Normalization.

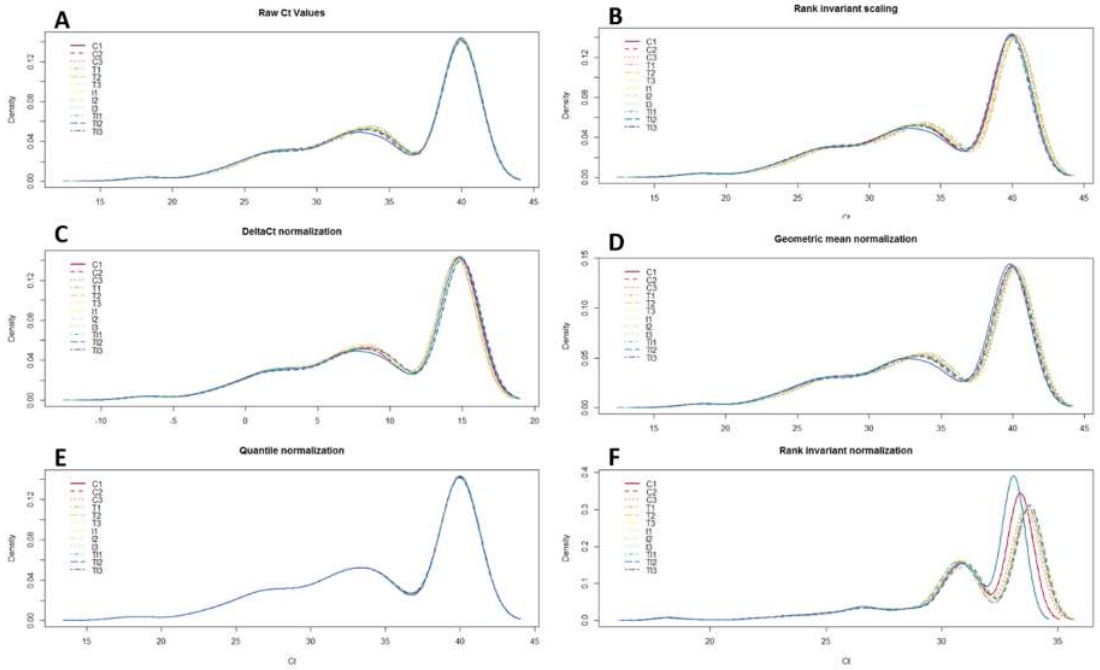

Figure 15. Densities of Ct values for all samples before and after each of the normalisation methods. The peak at the high end originates from features with "Undetermined"Ct values,which are assigned the Ct value 40 by default. A) Raw Data, B) Rank invariant scaling, C) Delta CT, D)Geometric Mean, E) Quantile, F) Rank Invariant Normalization.

For testing the significance of differences in Ct values between samples we use Linear Models for Microarray Data (LIMMA) with the control group defined like reference for the analysis. Subsequently, we generated a heat map (**Figure 16**) with the microRNAs that constitute a molecular signature atrophy by cytokines IFN-γ and TNF-α. Each column of Heat map is a group of samples, and each row is probes of miRNA. The color and intensity of each square represents the relative expression of a miRNA for each sample. The relative expression of a set of microRNA is determined by transforming the expression values ΔΔCt. Negative values (green) indicates that the expression is lower than average and positive values (red) indicate expression values are larger than average ($p \leq 0.05$).

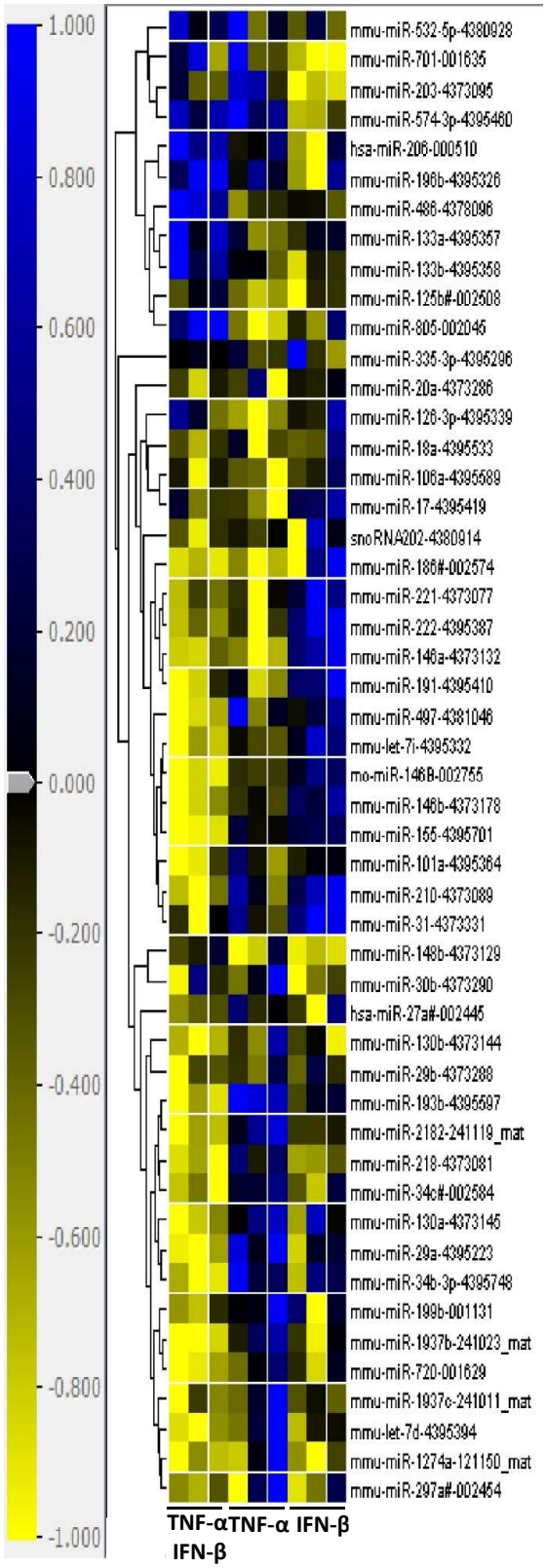
1.000
0.800
0.600
0.400
0.200
0.000
-0.200
-0.400
-0.600
-0.800
-1.000
mmu-miR-532-5p-4380928
mmu-miR-701-001635
mmu-miR-203-4373095
mmu-miR-574-3p-4395460
hsa-miR-206-000510
mmu-miR-196b-4395326
mmu-miR-486-4378096
mmu-miR-133a-4395357
mmu-miR-133b-4395358
mmu-miR-125b#-002508
mmu-miR-805-002045
mmu-miR-335-3p-4395296
mmu-miR-20a-4373286
mmu-miR-126-3p-4395339
mmu-miR-18a-4395533
mmu-miR-106a-4395589
mmu-miR-17-4395419
snoRNA202-4380914
mmu-miR-186#-002574
mmu-miR-221-4373077
mmu-miR-222-4395387
mmu-miR-146a-4373132
mmu-miR-191-4395410
mmu-miR-497-4381046
mmu-let-7i-4395332
mo-miR-146B-002755
mmu-miR-146b-4373178
mmu-miR-155-4395701
mmu-miR-101a-4395364
mmu-miR-210-4373089
mmu-miR-31-4373331
mmu-miR-148b-4373129
mmu-miR-30b-4373290
hsa-miR-27a#-002445
mmu-miR-130b-4373144
mmu-miR-29b-4373288
mmu-miR-193b-4395597
mmu-miR-2182-241119_mat
mmu-miR-218-4373081
mmu-miR-34c#-002584
mmu-miR-130a-4373145
mmu-miR-29a-4395223
mmu-miR-34b-3p-4395748
mmu-miR-199b-001131
mmu-miR-1937b-241023_mat
mmu-miR-720-001629
mmu-miR-1937c-241011_mat
mmu-let-7d-4395394
mmu-miR-1274a-121150_mat
mmu-miR-297a#-002454
TNF-α
TNF-α IFN-β
IFN-β

Figure. 16. Heatmap of gene expression of Top fifthy microRNAs that are on the molecular signature of atrophy induced by cytokines TNF-α (10 ng / ml), IFN-γ (100 U / ml) and TNF-α + IFN-γ (10ng/ml + 100 U / ml).

Statistical analysis of microRNAs that were differentially expressed in samples treated with cytokines was performed by applying a filter p-value ≤ 0.05 and at least 1.5 of Fold change(increase or decrease in expression). The analysis of 760 microRNAs that were surveyed resulted in three lists of: A) 67 (40 Up regulated and 27 Down regulated), B) 68 (48 Up regulated and 20 Down regulated) and C) 92 (49 Up regulated and 43 Down regulated), miRNA regulated for treatments TNFα, IFN-γ and TNF-α+IFN-γ respectively (**Table 21**). The analysis of the Venn diagram shows the involvement of common microRNAs in different treatments with cytokines, these data suggest the involvement of the same molecular pathways in the process of cell atrophy. Additionally, have also been identified microRNAs with specific differences for each treatment (**Figure 17**).

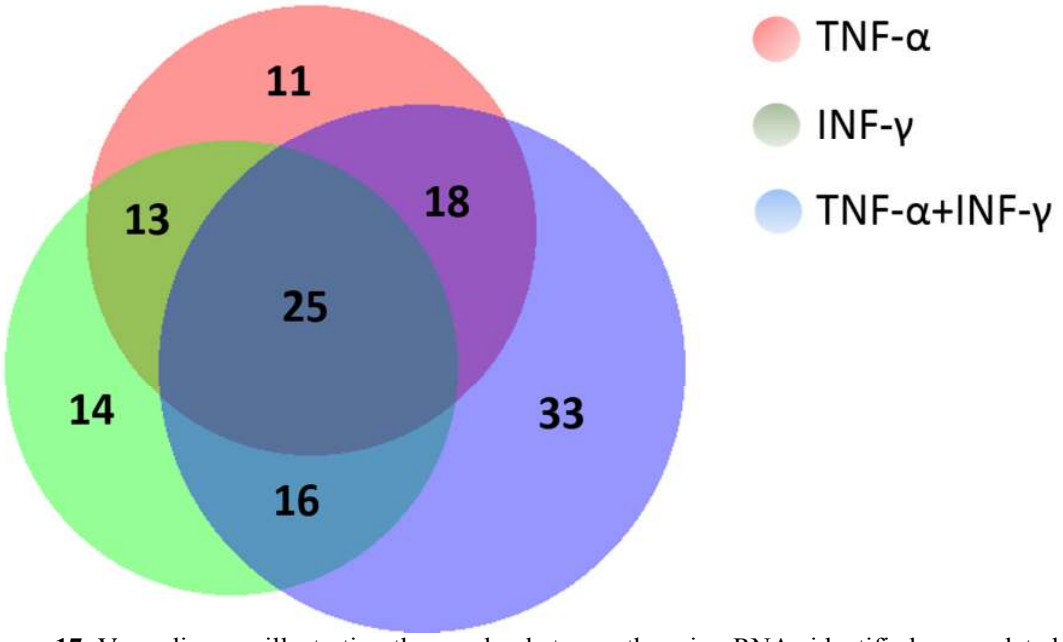

Figure 17. Venn diagram illustrating the overlap between the microRNAs identified as regulated in the treatment with TNF-α (10 ng / ml), IFN-γ (100 U / ml) and TNF-α + IFN-γ (10ng/ml + 100 U / ml).

miRNA	TNF-α	IFN-γ	TNF-α+IFN-γ
let-7a-1-3p	1,088	1,110	0,667*
let-7c-1-3p	1,680*	0,836	1,186
let-7g-3p	0,856	0,626*	0,744
let-7i-3p	6,557*	0,951	3,021*
mir-101a-3p	1,423	1,413	2,038*
mir-107-3p	1,832*	1,986*	0,969
mir-1191	2,608*	1,365	1,692*
mir-1198-5p	2,270*	1,999*	1,954*
mir-125a-3p	0,617*	1,060	0,367*
mir-125b-2-3p	3,699*	3,228*	2,141*
mir-126a-3p	1,546*	1,107	1,115
mir-126a-5p	1,386	1,636*	0,808
mir-128-3p	0,838	0,912	0,508*
mir-129-2-3p	1,075	0,369*	1,000
mir-1306-5p	0,216*	2,369*	0,619*
mir-133a-3p	0,833	0,748	0,547*
mir-133b-3p	0,749	0,855	0,454*
mir-135b-5p	1,819*	1,305	2,175*
mir-142-3p	0,289*	1,358	0,484*
mir-146a-5p	2,336*	1,055	2,249*
mir-146b-5p	1,614*	1,599*	2,340*
mir-148b-3p	1,764*	2,091*	1,537*
mir-148b-5p	0,597*	0,352*	0,937
mir-150-5p	0,609*	1,127	0,921
mir-153-3p	0,907	3,169*	1,071
mir-155-5p	1,985*	1,620*	5,563*
mir-15a-3p	0,636*	0,818	0,717
mir-16-1-3p	0,959	0,423*	0,679
mir-182-5p	1,860*	2,176*	1,395
mir-183-3p	1,661*	2,683*	1,894*
mir-1839-5p	1,037	1,338	1,669*
mir-186-3p	2,137*	0,124*	2,381*
mir-1896	1,104	1,349	0,647*
mir-1897-5p	0,620*	1,415	0,611*
mir-18a-3p	8,112*	3,565*	3,197*
mir-18a-5p	1,723*	1,457	1,762*
mir-190b-5p	0,503*	1,364	0,749
mir-191-3p	0,970	2,576*	1,511*
mir-1928	0,728	0,221*	0,137*
mir-193b-3p	0,856	1,168	1,762*
mir-1941-3p	0,652*	0,853	0,247*
mir-1943-5p	0,388*	0,067*	0,087*

mir-1948-3p	1,000	1,000	0,103*
mir-1949	1,058	1,515*	1,343
mir-1954	1,001	1,183	1,677*
mir-1981-5p	2,269*	1,988*	1,350
mir-199b-3p	1,096	1,353	1,588*
mir-1a-3p	2,012*	1,502*	1,037
mir-200b-3p	1,000	0,175*	1,000
mir-200c-3p	0,485*	0,396*	0,588*
mir-203-3p	0,987	3,594*	2,345*
mir-204-5p	2,617*	1,745*	1,533*
mir-206-3p	0,756	0,917	0,575*
mir-20a-3p	1,133	1,611*	1,610*
mir-20b-5p	1,665*	1,793*	2,160*
mir-211-5p	1,000	27,954*	1,000
mir-21-3p	1,968*	2,637*	2,622*
mir-218-1-3p	1,743*	1,298	1,716*
mir-218-5p	1,162	1,465	1,582*
mir-223-3p	0,567	1,557*	0,331
mir-23a-5p	0,421*	0,143*	1,000
mir-26b-3p	0,747	0,859	0,598*
mir-27a-5p	1,271	1,492	1,621*
mir-27b-5p	1,663*	0,850	0,604*
mir-296-3p	1,000	1,584*	0,939
mir-297a-5p	0,733	1,789*	2,422*
mir-29a-5p	1,763*	1,364	1,150
mir-29b-1-5p	1,345	1,349	1,589*
mir-29b-3p	1,345	1,154	2,018*
mir-322-5p	1,138	0,571*	0,575*
mir-32-5p	1,585*	1,455	0,729
mir-326-3p	1,201	1,543*	1,607*
mir-327	0,315	1,000	1,000
mir-335-3p	0,322	0,135	0,211
mir-339-5p	1,579*	1,235	0,336
mir-345-3p	0,799	1,536*	1,650*
mir-345-5p	0,986	1,765*	1,748*
mir-34b-5p	1,264	0,885	2,051*
mir-34c-3p	1,179	1,430	1,674*
mir-350-3p	0,528	0,640	0,401
mir-351-5p	0,721	0,707	0,578
mir-361-5p	1,074	1,605*	0,744
mir-362-5p	0,818	0,832	0,484*
mir-381-3p	0,086*	1,000	1,579*
mir-409-3p	0,442*	0,625*	0,887
mir-411-5p	3,421*	9,945*	1,618*

mir-425-5p	1,572*	1,809*	1,406
mir-449a-5p	0,688	0,592	0,474
mir-449b	1,637*	0,391	1,022
mir-450a-5p	1,100	1,280	2,054*
mir-450b-3p	2,240*	2,086*	1,025
mir-465b-5p	0,660*	0,577*	0,936
mir-466a-3p	1,000	2,333*	0,681*
mir-466b-3p	0,503*	1,702*	1,085
mir-466g	1,375	0,647*	0,566*
mir-466k	0,759	0,925	0,556*
mir-467b-5p	1,564*	1,735*	1,616*
mir-467c-5p	1,966*	1,842*	2,887*
mir-467d-5p	0,385*	2,786*	1,353
mir-486-5p	0,776	0,737	0,385*
mir-501-3p	0,954	0,722	0,559*
mir-503-5p	1,520*	1,072	1,432
mir-542-3p	4,180*	2,685*	2,487*
mir-542-5p	0,678	0,710	0,618*
mir-547-3p	0,780	2,167*	1,899
mir-574-3p	0,538*	0,913	0,555*
mir-582-5p	0,991	0,860	0,588*
mir-590-5p	1,313	1,714*	0,792
mir-598-3p	1,000	1,000	0,404*
mir-615-5p	0,561*	1,077	0,057*
mir-669a-5p	0,713	0,323*	0,842
mir-669l-5p	1,167	1,000	0,089*
mir-669m-5p	1,312	1,626*	2,086*
mir-669o-5p	0,326*	1,000	1,000
mir-671-5p	0,627*	0,750	0,515*
mir-696	1,193	1,276	0,611*
mir-700-3p	0,528*	0,361*	0,635*
mir-701-5p	0,783	5,072*	0,698*
mir-712-5p	0,996	1,054	0,584*
mir-741-3p	0,681	1,230	0,540*
mir-744-3p	1,727*	0,873	0,801
mir-7a-5p	1,259	0,344*	1,495*
mir-873-5p	9,653*	1,000	4,148*
mir-875-5p	1,519*	1,715*	1,609*
mir-878-3p	1,000	3,256*	0,339
mir-881-3p	0,266	2,904*	1,893*
mir-9-3p	0,616	1,632*	0,786
mir-96-5p	1,000	1,000	0,401
mir-98-5p	1,556*	1,949*	2,075*
mir-99a-3p	1,876*	1,380	0,601*

mir-99b-3p	1,971*	1,883*	1,639*

Table 21. List of differentially expressed microRNAs atrophy induced by cytokines TNF-α (10 ng / ml), IFN-γ (100 U / ml) and TNF-α + IFN-γ (10ng/ml + 100 U / mL) after 18h treatment. *represent p adjusted-values (FDR) < 0,05.

Some of the important miRNA with known/putative targets and differentially regulated by Citokines are presented in **Figure 18**. miRNAs, such as mir-18a-5p, mir-146a-5p and mir-29a-5p appear to be TNF-α specific (**Figure 18 A**). On the other hand miRNAs suas as Let7a-5p, mir-211-5p, mir-20a-3p and mir-200b-3p appear to be IFN-γ specific (**Figure 18 B**). Additionally there are common deregulated miRNAs between the TNF- α and IFN- γ treatment such as mir-18a-3p, mir-125-2-3p, mir-21-3p, mir-148b-3p, mir-20b-5p, mir-155-5p, mir146b-5p, mir-1a-3p and mir 200c-3p (**Figure 18 C**). Finally our results showed that only the combined treatment of cytokines (TNF-α plus IFN-γ) deregulated the expression of muscle-specific mir-133a-3p, mir-133b-3p and mir-206-3p, and several other miRNAs including mir-29b-3p, mir-29-1-5p and mir-206-3p (**Figure 18 D**).

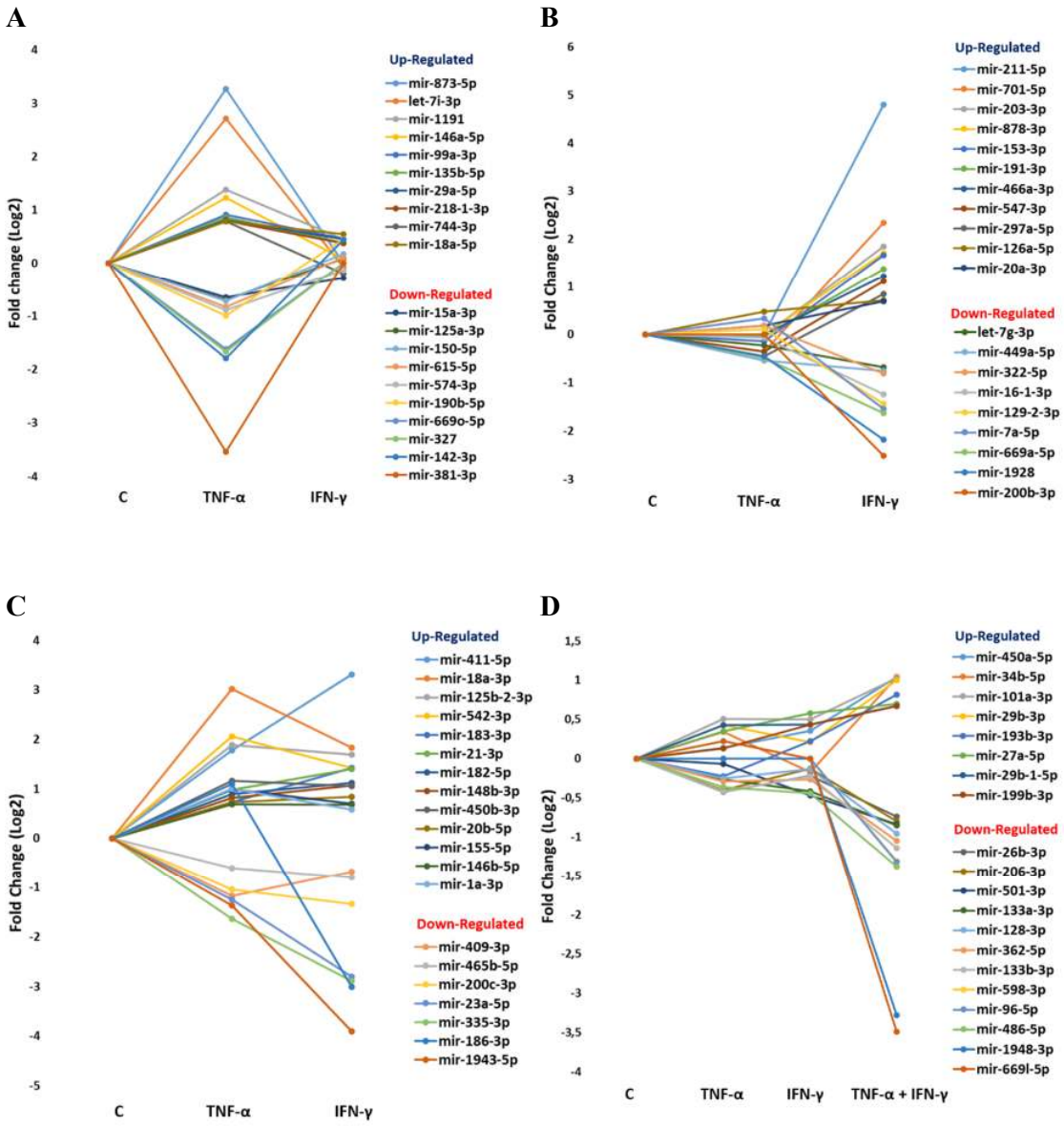

Figure 18. Differential expression of miRNAs in Citokines-treated C2C12 myotubes measured by low-density miRNA array. C2C12 myotubes were treated with TNF-α (10 ng / ml), IFN-γ (100 U / ml) and TNF-α + IFN-γ (10ng/ml + 100 U / mL) for 18h. Untreated C2C12 myotubes under exactly similar conditions served as control (C). A) Deregulation of mirRNAs TNF- α specific. B) Deregulation of mirRNAs IFN-γ specific. C) Deregulation of common mirRNAs in tretments and D) Synergistic deregulation of miRNA. The normalized expression ratios were plotted for each miRNA are mean. Deregulation was considered when the log2 Fold change was |0.58| and p-values <0.05.

5.4 miRNA-Target deregulated network

We first identified miRNA–target pairs with significant deregulation in Control versus Cytokine treatments data sets based on the negative correlation in the fold change (eg: miRNA up-regulated and mRNA down-regulated). Using an FDR threshold of 0.05 and also an absolute Fold change ≥1,5 and ≥2 for miRNA and mRNA respectively. We detected the next topology for each treatment: 1) TNF-α treatment, 151 deregulations between 36 miRNAs and 99 target genes; 2) IFN-γ treatment, 92 deregulations between 52 miRNAs and 180 target genes and for 3) TNF-α+IFN-γ treatment, 1757 deregulations between 87 miRNAs and 1051 target genes. We found that the miRNAs deregulate at least 2 targets, and approximately, one third of mRNAs are co-deregulated by 2 or more miRNAs. As shown in **Figures 19 to 21**, most deregulations in the network are connected and form a large connecting subnetwork. These results indicate a complicated combination in terms of both target multiplicity and miRNA cooperatively. After that, we identified miRNA–target pairs experimentally validated. We detected 31, 34 and 41 validated targets for TNF-α, INF- γ and TNF-α+IFN-γ treatment respectively

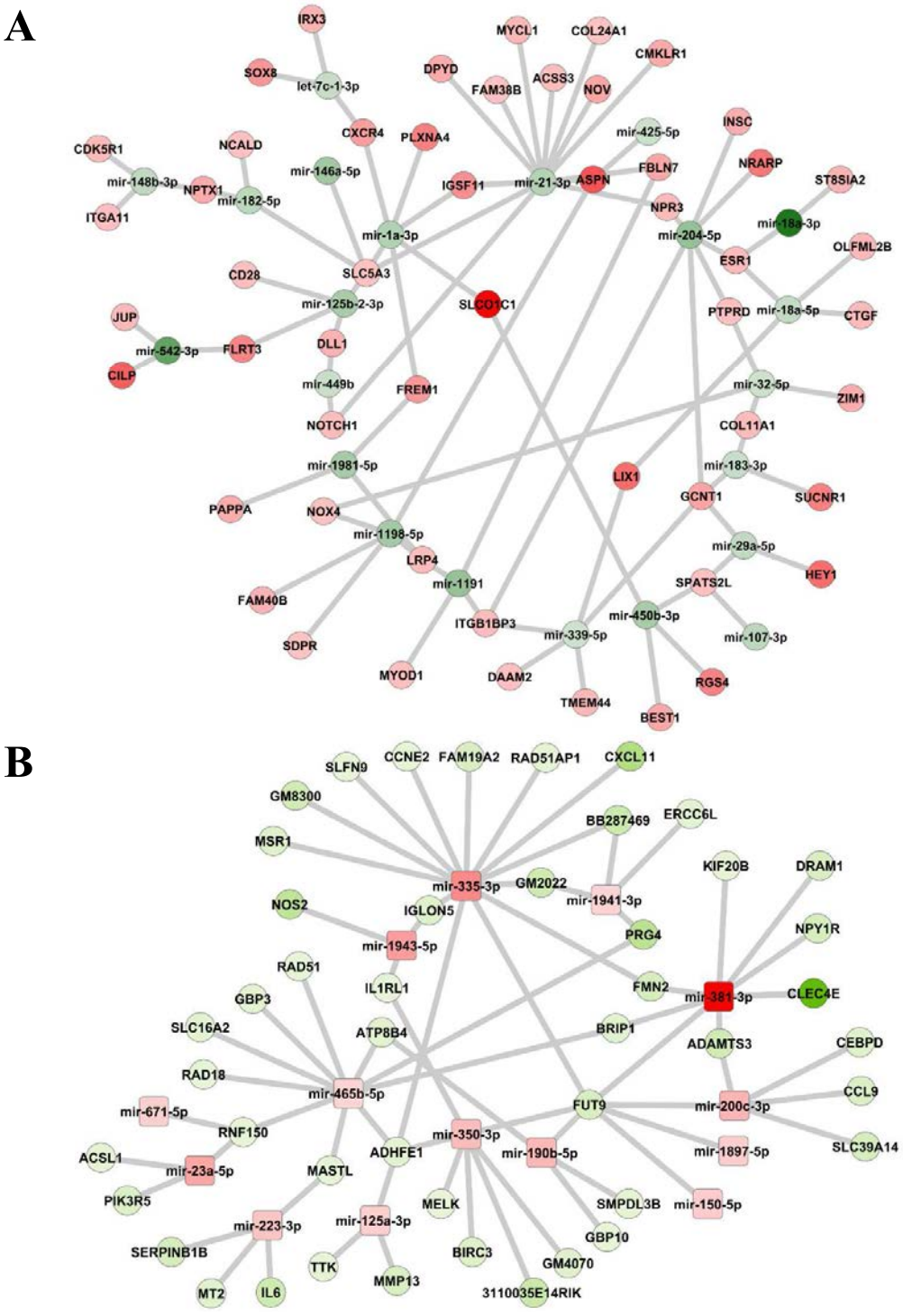

Figure 19. miRNA-mRNA deregulated subnetworks in TNF-α treated myotubes. A) Subnetworks of miRNA-mRNA interactions involved in mRNA negative regulation, **B**) Subnetworks of miRNA-mRNA interactions involved in mRNA positive gene regulation. The solid lines connecting molecules here represent a predicted interaction miRNA-mRNA. Circle node shape represent mRNA, and rectangle node shape represents miRNA. Nodes are colored based on the log2 fold change of the differential expression of the underlying gene. Red indicates down–regulation, green up-regulation.

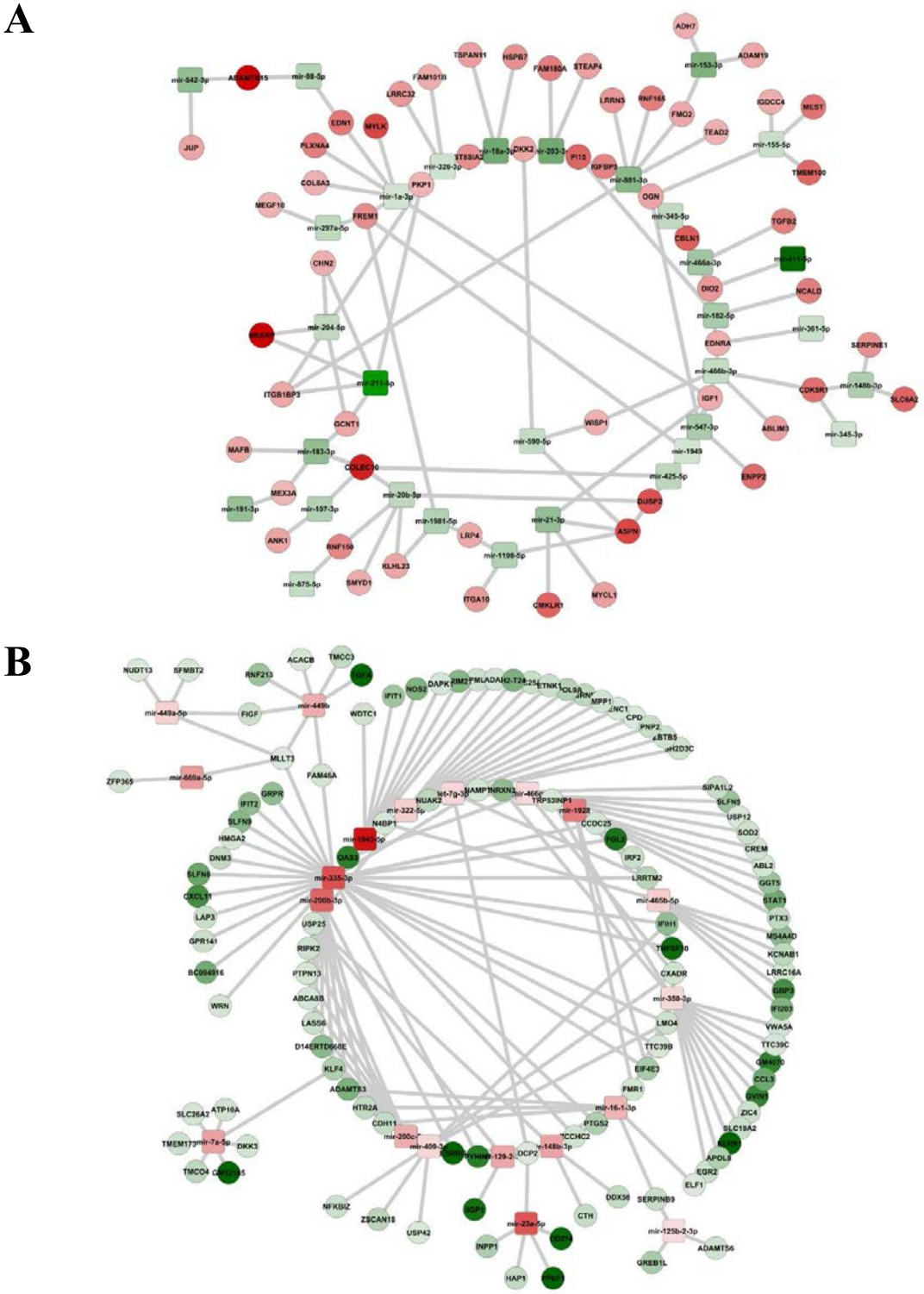

Figure 20. miRNA-mRNA deregulated subnetworks in IFN-γ treated myotubes. A) Subnetworks of miRNA-mRNA interactions involved in mRNA negative regulation, **B**) Subnetworks of miRNA-mRNA interactions involved in mRNA positive gene regulation. The solid lines connecting molecules here represent a predicted interaction miRNA-mRNA. Circle node shape represent mRNA, and rectangle node shape represents miRNA. Nodes are colored based on the log2 fold change of the differential expression of the underlying gene. Red indicates down–regulation, green up-regulation.

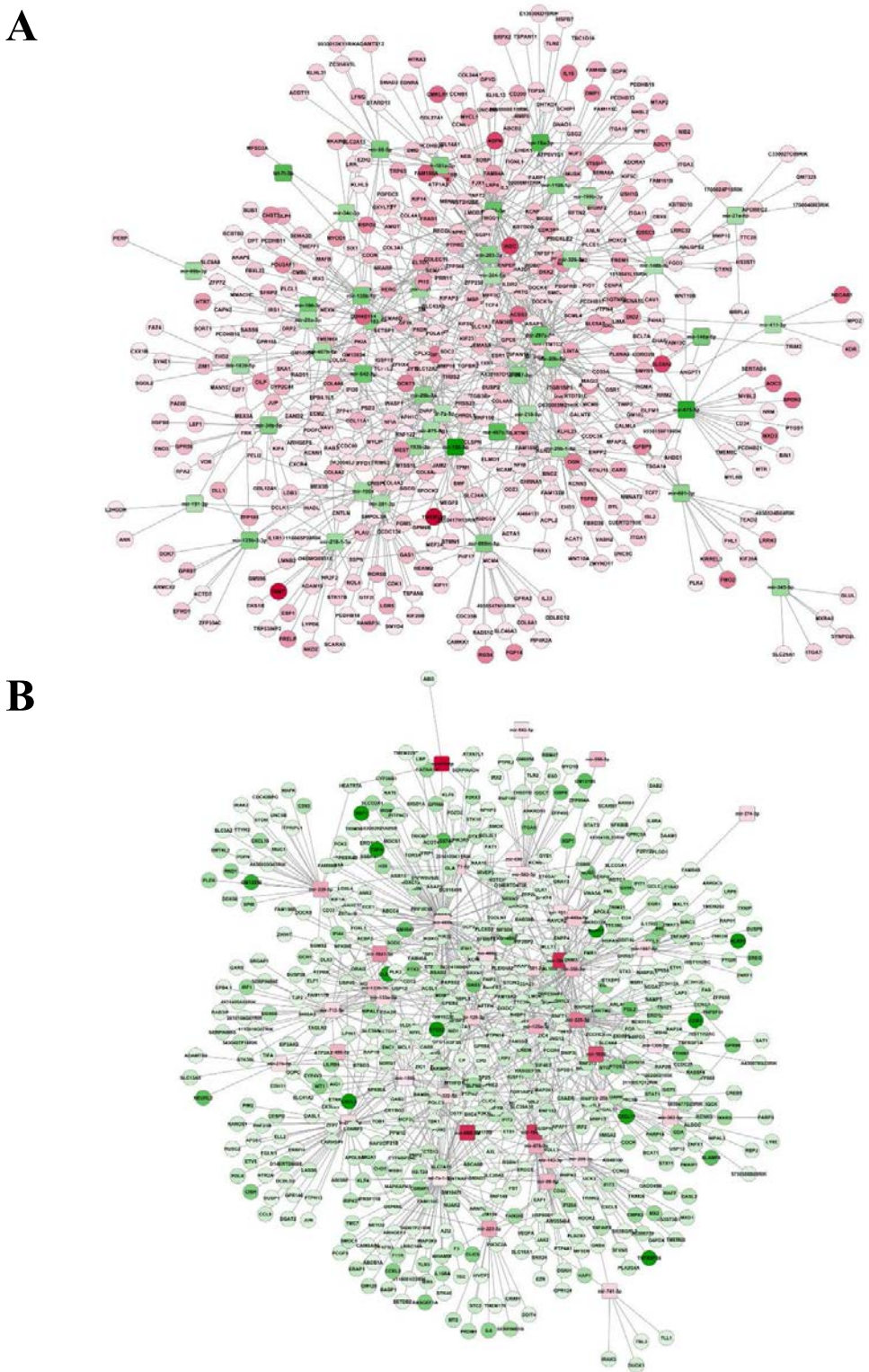

Figure 21. miRNA-mRNA deregulated subnetworks in TNF-α + IFN-γ treated myotubes. A) Subnetworks of miRNA-mRNA interactions involved in mRNA negative regulation, **B**) Subnetworks of miRNA-mRNA interactions involved in mRNA positive regulation. The solid lines connecting molecules here represent a predicted interaction miRNA-mRNA. Circle node shape represent mRNA, and rectangle node shape represents miRNA. Nodes are colored based on the log2 fold change of the differential expression of the underlying gene. Red indicates down–regulation, green up-regulation.

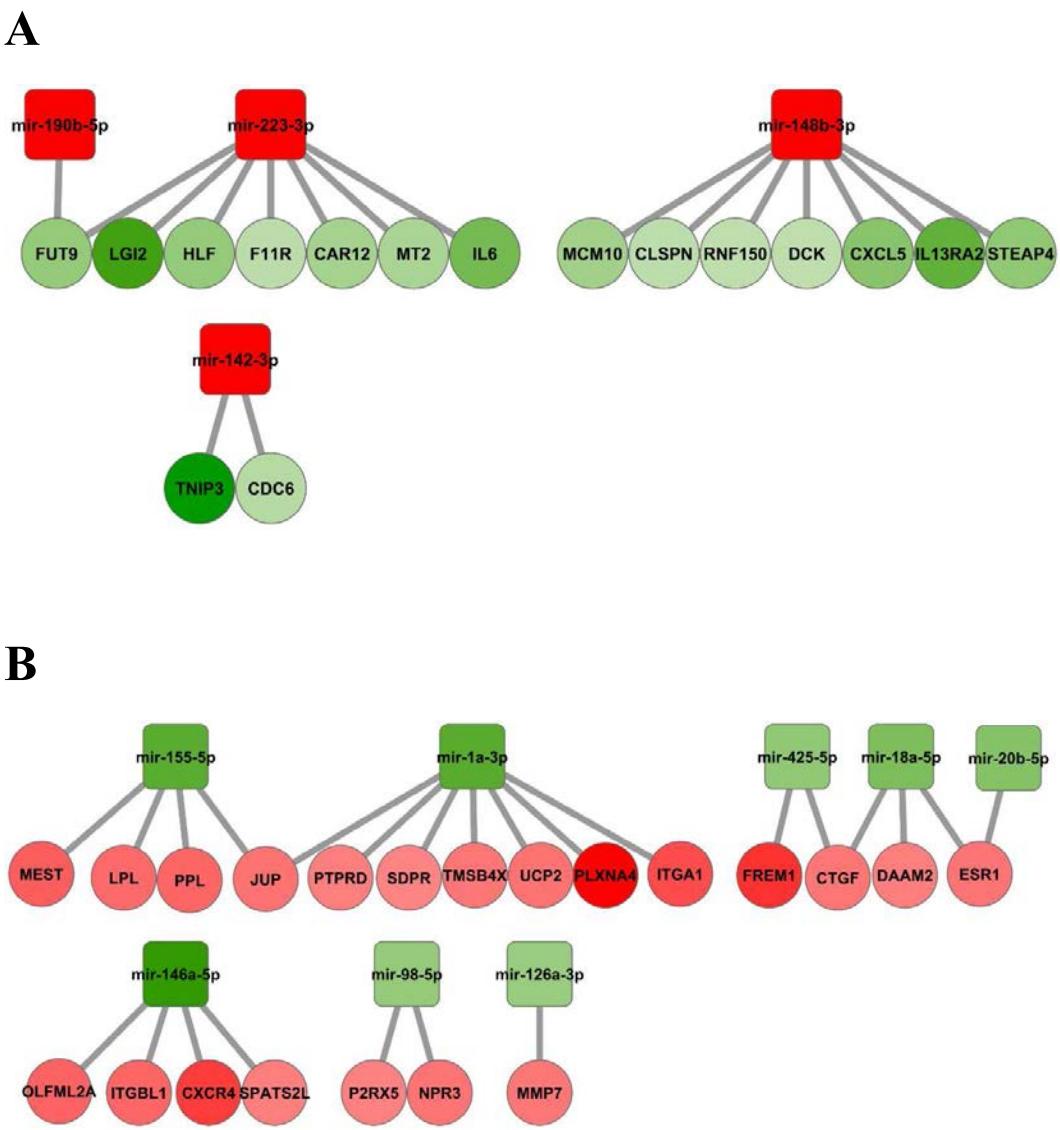

Figure 22. miRNA-mRNA validated deregulated subnetworks in TNF-α treated myotubes. A) Subnetworks of miRNA-mRNA validated interactions involved in mRNA positive regulation, **B**) Subnetworks of miRNA-mRNA validated interactions involved in mRNA negative gene regulation. The solid lines connecting molecules here represent a predicted interaction miRNA-mRNA. Circle node shape represent mRNA, and rectangle node shape represents miRNA. Nodes are colored based on the log2 fold change of the differential expression of the underlying gene. Red indicates down–regulation, green up-regulation.

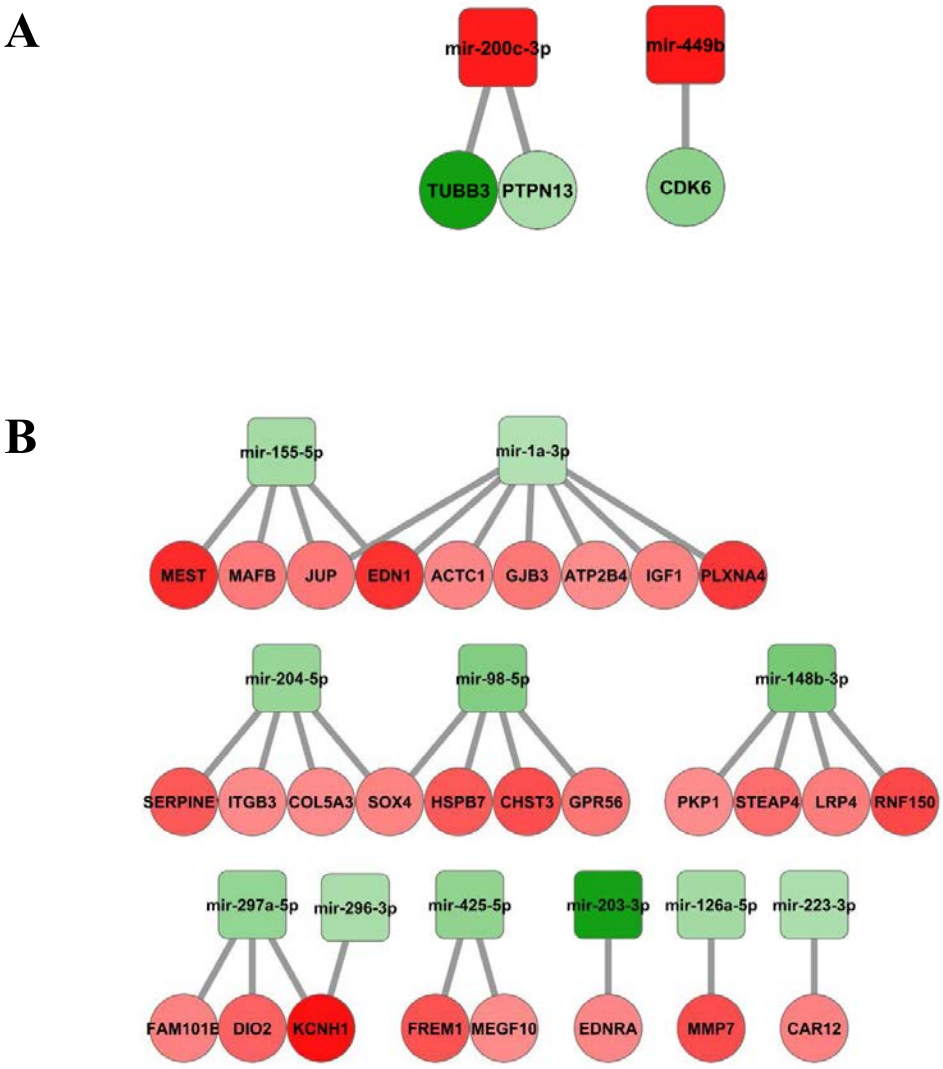

Figure 23. miRNA-mRNA validated deregulated subnetworks in INF-γ treated myotubes. A) Subnetworks of miRNA-mRNA validated interactions involved in mRNA positive regulation, **B)** Subnetworks of miRNA-mRNA validated interactions involved in mRNA negative gene regulation. The solid lines connecting molecules here represent a predicted interaction miRNA-mRNA. Circle node shape represent mRNA, and rectangle node shape represents miRNA. Nodes are colored based on the log2 fold change of the differential expression of the underlying gene. Red indicates down–regulation, green up-regulation.

A

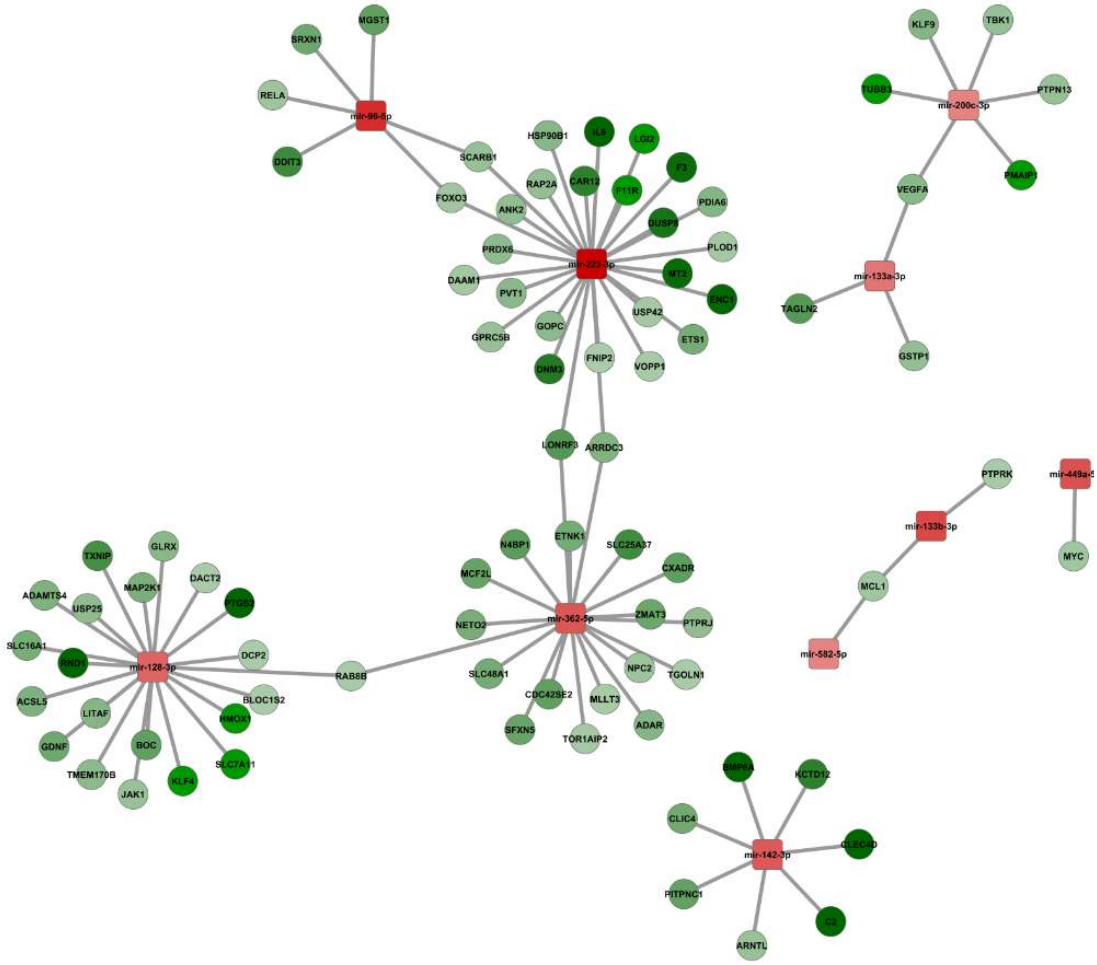

Figure 24. miRNA-mRNA validated deregulated subnetworks in TNF-α+INF-γ treated myotubes. A) Subnetworks of miRNA-mRNA validated interactions involved in mRNA positive regulation. The solid lines connecting molecules here represent a predicted interaction miRNA-mRNA. Circle node shape represent mRNA, and rectangle node shape represents miRNA. Nodes are colored based on the log2 fold change of the differential expression of the underlying gene. Red indicates down–regulation, green up-regulation.

B

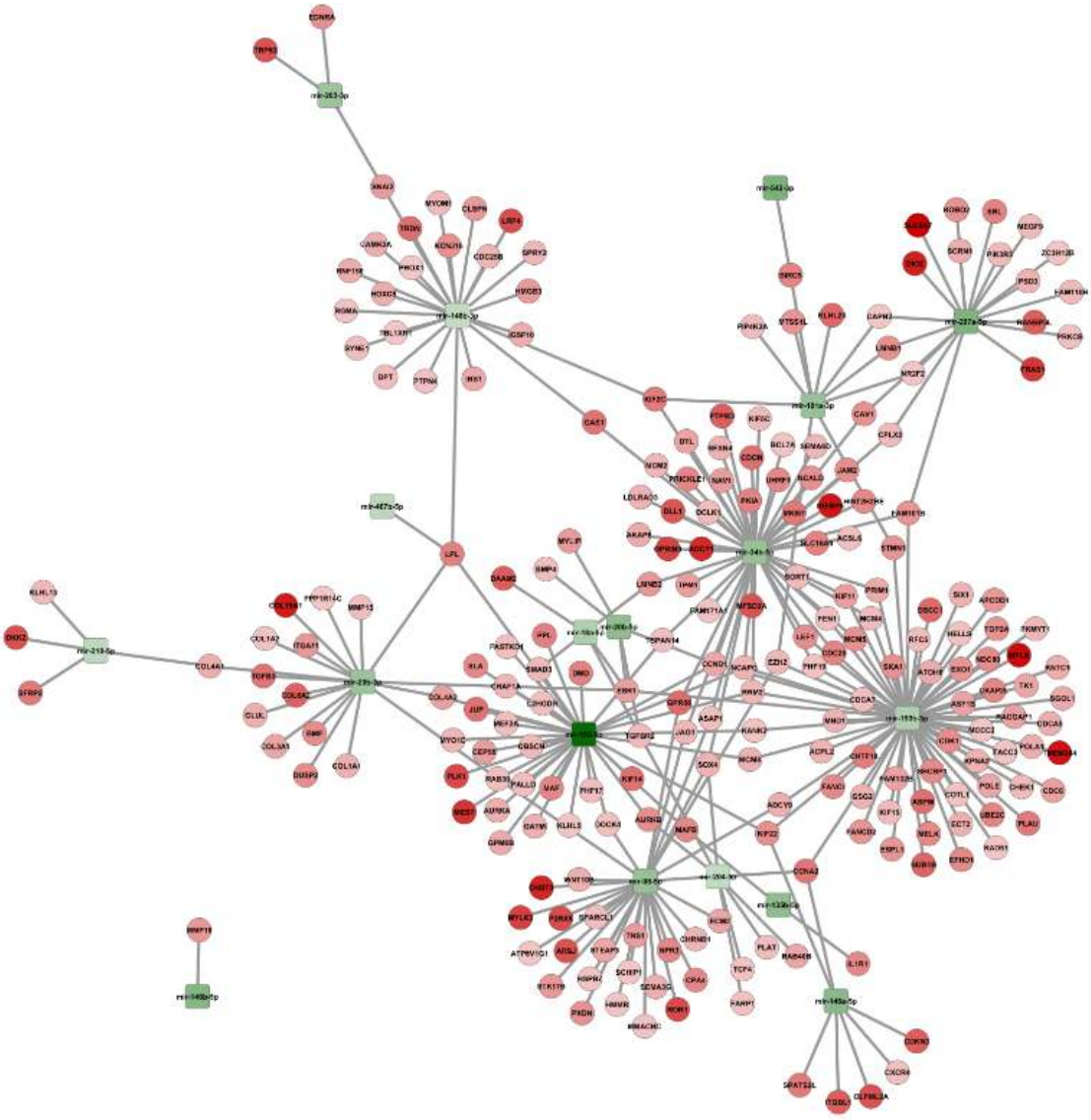

Figure 24. miRNA-mRNA validated deregulated subnetworks in TNF-α+INF-γ treated myotubes. B) Subnetworks of miRNA-mRNA validated interactions involved in mRNA negative gene regulation. The solid lines connecting molecules here represent a predicted interaction miRNA-mRNA. Circle node shape represent mRNA, and rectangle node shape represents miRNA. Nodes are colored based on the log2 fold change of the differential expression of the underlying gene. Red indicates down–regulation, green up-regulation.

5.5 The subnetwork solution recapitulates known biology of Myoyubes

Initally prize-collecting Steiner tree was run using the 500 most differentially expressed genes of the myotubes treated with TNF-α, a pathlength of 5 in the network, a lower bound on probability for a path at 1e-4, and 40-best paths in the cause-effect networks with different costs. Network of size 338 nodes were generated (**Figure 25**). When we interpret the network, it is clear that these networks are mostly enriched for genes in the response to stress (GO:6950, e-22, 93 genes), defense response(GO:6952, e-21, 54 genes) and immune system response (GO:2376, e-19, 67). The regulatory gene sets were omitted from these results as they are always enriched when we look for regulatory paths.

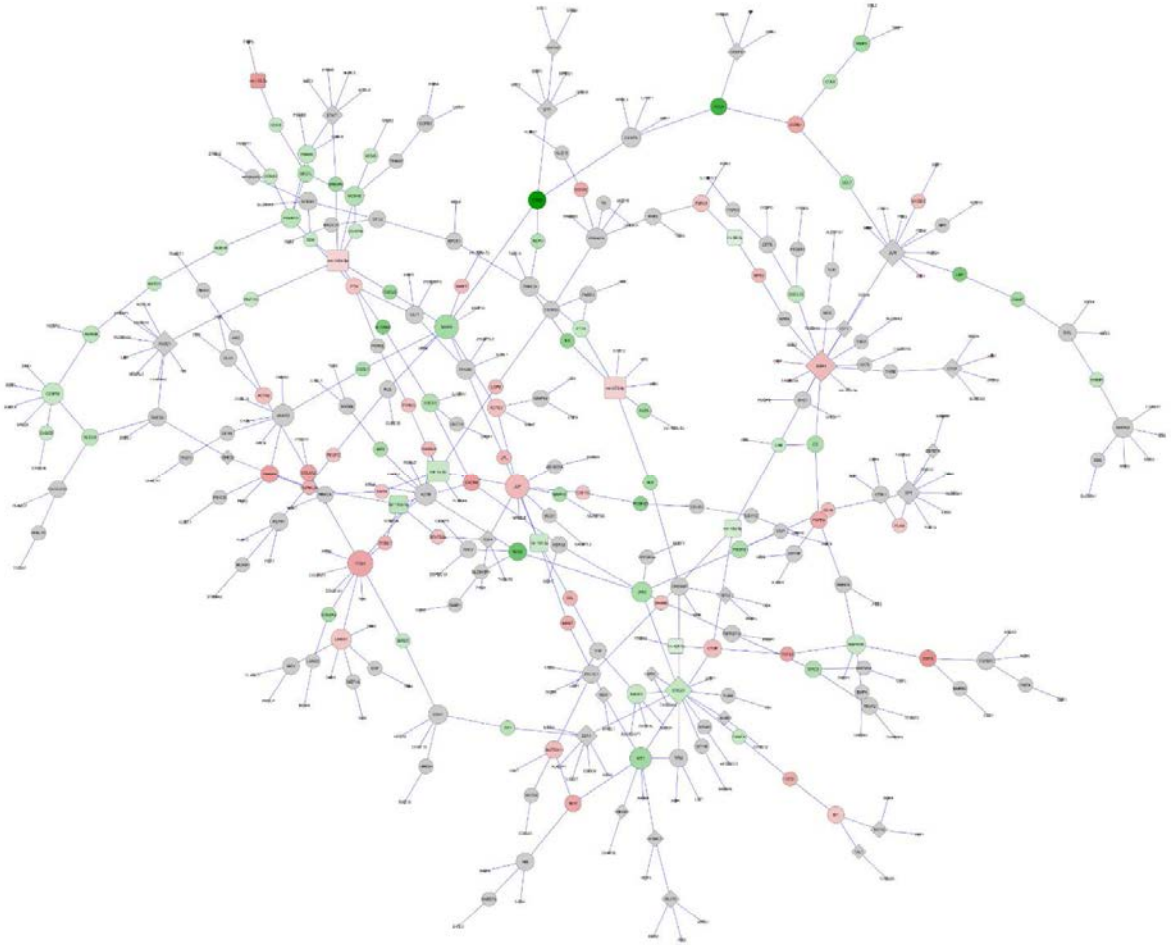

Figure 25. Subnetworks in TNF-α treated myotubes Result of Steiner tree network of 338 genes selected for 500-most differentially expressed genes, lower bound on probability of 1e-4, 40 best paths. Nodes are colored based on the log2 fold change of the differential expression of the underlying gene. Red indicates underexpression, blue overexpression and grey means no differential expression data is provided. The network nodes, Cicle: mRNA, Diamond: Transcription Factors, and Rectangules: miRNAs.

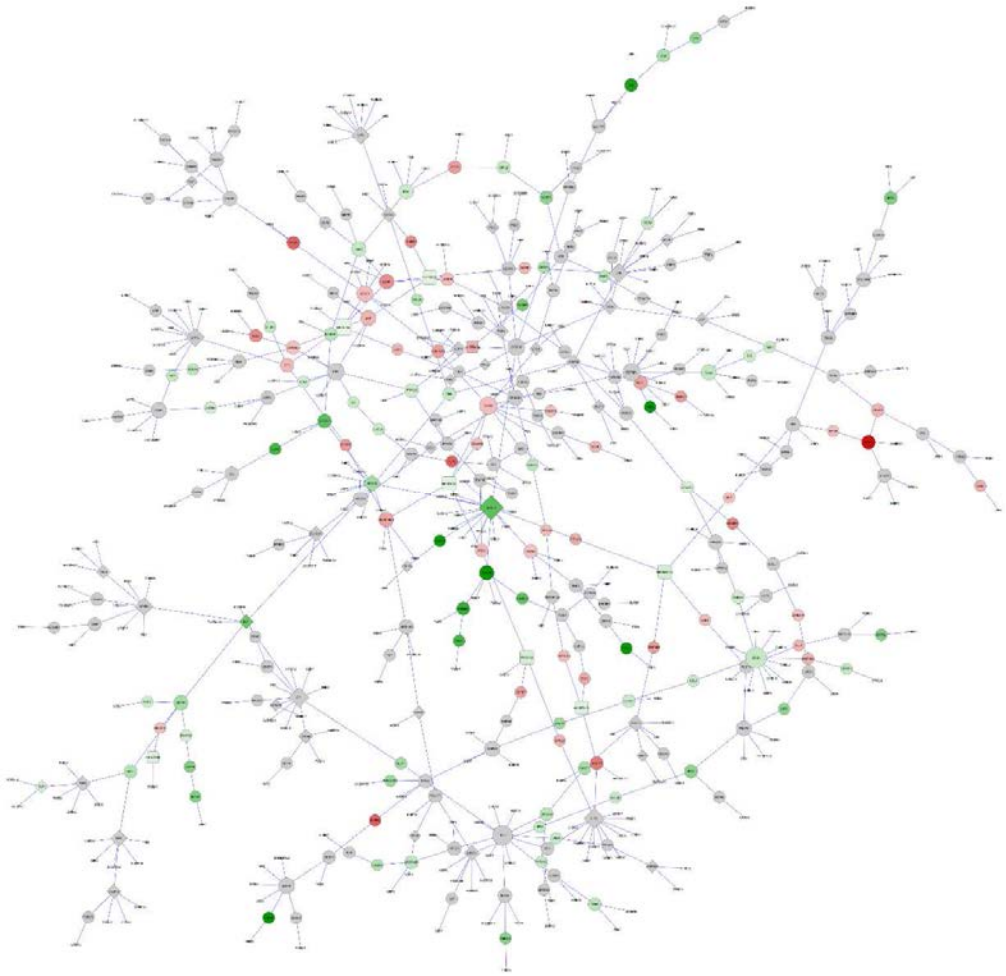

Figure 26. Subnetworks in TNF-α treated myotubes Result of Steiner tree network of 338 genes selected for 500-most differentially expressed genes, lower bound on probability of 1e-4, 40 best paths. Nodes are colored based on the log2 fold change of the differential expression of the underlying gene. Red indicates underexpression, blue overexpression and grey means no differential expression data is provided. The network nodes, Cicle: mRNA, Diamond: Transcription Factors, and Rectangules: miRNAs.

6. ANALYSIS

Cytokine trigger pleiotropic molecular pathways in skeletal muscle cells

Although there is significant amount of literature suggesting the role of citikines in skeletal muscle wasting[34,35,37,38,114], the molecular mechanisms by which citokines induces muscle loss remain poorly understood. This study is the first to define the pattern of miRNA and mRNA changes in myotubes in several Cytokines stimuli that cause muscle wasting and the first uncover the pathways by wich INF-γ might be regulating skeletal muscle mass . These transcriptional profiles define a set of genes in common pathways that are consistently up- or down-regulated in cytokines treatment; together, these adaptations represent a program of changes in molecular networks associated with development of atrophy. Most of these alterations in mRNA and miRNA content are likely to reflect transcriptional changes, though differences in mRNA degradation rates or mRNA stability may also be contributing to the changes described here. Perhaps the strongest confirmation that this analysis provides valid information about the atrophy process is that many of the pathways identified here are known to have important functions in muscle wasting[7,120,175].

The pathways affected by Cytokines were grouped in three categories: Triggers pathways, effectors pathways and molecular targets. Interestingly, it has now become increasingly clear that skeletal muscle wasting in cytokines treatments leads to the regulation of these pathways in skeletal muscle suggesting the redundancy stimuli effect for muscle wasting phenotype.

Triggers pathways

Accumulating evidence strongly suggests that NF-kB is one the most important signaling pathways, the activation of which leads to skeletal muscle wastage[176]. NF-kB activation can occur through two parallel pathways. The canonical NF-kB signaling pathway involves the upstream activation of IkB kinase-b (IKKb) and subsequent phosphorylation and degradation of IkB proteins[177]. In contrast, the activation of the alternative NF-kB pathway requires the upstream activation of NF-kB-inducing kinase (NIK or MAP3K14) and IKKa and the proteolytic processing of NFkB2 (p100 subunit) into p52 protein[177]. The RNA-seq analysis in the present study showed that TNF-α increases the expression levels of both

NFkB1 and NFkB2 in skeletal muscle cells (Table 11). It was demonstrated recently in c2c12 myotubes that TNF-α induces NF-kB activity via canonical pathway initially, however a time-dependent increase in the components of alternative pathway was observed at later time points. These observations suggest that TNF-α alone might provide sufficient signal to activate alternative NF-kB pathway in skeletal muscle. It is also noteworthy that the activation of alternative NF-kB pathway in myotubes may be specific to TNF-α and the synergistic treatment exacerbates it.

IFN-γ, induces STAT1 and IRF-1 nuclear binding. The JAK/STAT pathway is a well-characterized pathway of IFN-γ signaling. It involves IFN- γ dimer binding to IFN- γ R1, IFN- γ R1 and IFN- γ R2 association, JAK1 and JAK2 activation, phosphorylation of Tyr457 in IFN- γ R1, recruitment and phosphorylation of Tyr701 in STAT1a, STAT1a dimerization, and nuclear translocation. The final step of the JAK/STAT pathway is the interaction between the STAT1a dimer and a GAS element in the promoter regions of IFN- γ -inducible genes to initiate the induction of this family of genes.

When cultured myoblasts were stimulated with exogenous IFN- γ, the proliferation of myoblasts and the fusion into myotubes were inhibited[178]. JAK1 and STAT1 are required for myoblast proliferation and also have a potent anti-differentiation effect. Intriguingly, the anti-differentiation effect is specific to STAT1 and is not mediated by STAT2, -3, -5A, or -5B. IFN-γ is known to have both positive and negative effects on myogenesis. While IFN-γ is required for efficient muscle repair, constitutive expression causes necrotizing myopathies[178].

JAK/STAT pathway there are seven STATs (STAT1, 2, 3, 4, 5A, 5B, and 6) and four JAKs (JAK1, 2, 3 and Tyk2). STAT1 has two splice variants; STAT1b, unlike STAT1a, lacks the terminal 38 amino acids and cannot restore IFN-γ responsiveness[178]. STATs are phosphorylated not only by JAK kinases that are associated with cytokine receptors but also by receptors with intrinsic tyrosine activity (for example, epidermal growth factor, platelet-derived growth factor, and colony-stimulating factor-1 receptors). JAK kinases do not seem to have specificity for a particular STAT substrate and the specificity of receptor tyrosine kinase activation of STATs is unclear.The complexity of the JAK/STAT pathway may explain why the activation of this pathway could activate other molecular pathways in the muscle cells.

Infiltration of leukocytes is a characteristic feature of acute inflammatory condition which is found in many secondary myopathies. A study on large selection of alpha/beta-

chemokines and their receptors in normal controls and in the inflammatory myopathies showed a general increase of specific chemokines and chemokine receptors[179]. A recent study by Vieira et al [180] showed that intraperitoneal injection of KC/CXCL1 and LIX/CXCL5 induces dose and time-dependent neutrophil recruitment and TNF-a production. Consistent with these published reports, our RNA-seq data show increased expression of many chemokine ligands and their receptors, especially, Cxcl5 which is up-regulated. These observations suggest that TNF-α and IFN- γ induces the expression of chemokines and their receptors, leading to acute inflammation and myopathy.

Our experiments demonstrate that TNF-α and IFN- γ induces the expression of IL-6 in myotubes (Table 13) suggesting that TNF-α and IFN- γ may also function through augmenting IL-6 expression to further accelerate inflammation and protein degradation in skeletal muscle. This cytokine is also called as 'myokine' because it is also expressed by skeletal muscle and its levels are elevated during muscle contraction[181,182]. Serum IL-6 levels are elevated in most experimental models of cachexia, and IL-6 is responsible at least in part for the muscle wasting seen in mice with colon-26 cancer cachexia as well as in Yomoto uterine cancer cachexia[181,182].

Stimulation of the IGF1-AKT-FOXO pathway in muscle causes hypertrophy and suppression of this pathway may trigger atrophy[57,64,183]. IGF-1-induced hypertrophy occurs via Akt; in all the cytokines treatment studied, mRNA for IGFBP-5, which enhances the effects of IGF-1[184], and the gene IGF1 fell dramatically, suggesting that activity of the Akt pathway is reduced in these muscle cells. It is noteworthy the up-regulation of the forkhead transcription factor Foxo increased in the synergistic state; this family of transcription factors is sequestered and inactivated in the cytoplasm by Akt phosphorylation[64]. Reduced Akt phosphorylation would leave Foxo in its under-phosphorylated, active form, which can induce programmed cell death and insulin resistance[57]. Insulin resistance is also a prominent feature of muscles in uremia, cancer cachexia, and fasting and should lead to enhanced proteolysis and reduced translation of new proteins [57].

Our analysis also revealed that cytokines inhibits the expression of Notch/WNT pathway (Table 17). Similar, reduction in Notch pathway was observed in TWEAK-treated myotubes and TWEAK-Tg mice. Notch/WNT pathway function in diverse developmental and cell maturation processes[185]. In a recent study, was demonstrated that in aged animals which show significant muscle wasting, the conversion of satellite cells from a myogenic to a

fibrogenic lineage occurs due to the activation of the canonical Notch/WNT signaling pathway[186]. It is important to note that the levels of proinflammatory cytokines are increased in skeletal muscle and in circulation during aging and in several chronic diseases. Besides its role in regulation of the activity of many other transcription factors, recent studies have shown that constitutively Notch-1 functions as a novel IkB-like molecule and regulates NF-kB mediated gene expression through a direct interaction with the NFkB1 (i.e. p50) subunit [185,186]. This interaction prevents NF-kB from binding to NF-kB recognition sites in DNA to regulate NF-kB-dependent gene expression[185,186].

Effetor pathways

The present findings provide further evidence that the accelerated proteolysis underlying muscle atrophy is due largely to activation of the Ubiquitin proteasome pathway. In fact, increases in mRNAs for poly Ubiquitin and several proteasome subunits in muscles and cells upon different atrophy conditions provide the first clue of a common set of transcriptional adaptations . This study confirms that mRNAs for poly Ubiquitin and multiple 26S proteasome subunits rise in atrophy increase. The Ubiquitin fusion UBA7 and UBD had been thought to function constitutively as a source of Ubiquitin monomers and serve as an additional source of Ubiquitin when overall proteolysis rises. Although transcription of several subunits of the 11S and 20S proteasome increase coordinately. Thus, expression of certain proteasome subunits may be subject to tighter transcriptional control than others and may be rate-limiting in assembly of the mature complex.

In addition to the acceleration of overall proteolysis, these cytokine induced atrophy involve a suppression of overall protein synthesis. However, even when protein synthesis is reduced, the atrophying muscles must maintain or even increase the expression of certain key proteins. Indeed, changes in mRNA for certain transcriptional regulators suggests both activation and repression of gene transcription. Several up-regulated mRNAs encode translation initiation factors that could indicate a reduction in translation in muscle. The strong induction of EIF4EBP1 and EIF2AK2, an inhibitor of translation of capped mRNA, should reduce overall rates of translation. Simultaneously, mRNA levels for EIF4E3 increase, which suggests a mechanism for enhancing translation of the subgroup of mRNAs with internal ribosome entry sites, which tend to be important in stressed cells. Together, these transcriptional changes indicate ways by which the levels of key proteins may be maintained when overall transcription and translation decrease.

We also observed up-regulation of an antioxidant enzyme, superoxide dismutase 1 (SOD). SOD is a well-known player of the anti-oxidative defense. The direct evidence of SOD in muscular atrophy was recently reported by Muller et al.[187], where they showed a dramatic increase in mitochondrial reactive oxygen species (ROS) in three conditions of muscular atrophy in animals lacking Sod1. In another study, mutations in Sod1gene (SOD1 G93A) selectively in skeletal muscle showed progressive muscle atrophy with concomitant reduction in muscle strength, alterations in contractile apparatus, and mitochondrial dysfunction[188].In this study they also analyzed the molecular pathways associated with muscle atrophy by Sod1 mutation and found that accumulation of oxidative stress initiated autophagy and thereby degradation of muscles. This suggests that skeletal muscle is the primary target of Sod1 mutation-mediated toxicity whereby oxidative stress triggers muscle atrophy. The up-regulation of this important antioxidant in response to cytokine treatment and the the enzyme NOS2 suggests a possible link between the regulations of oxidative stress and cytokine induced muscular atrophy. The production of reactive oxygen species has been proposed as a mechanism by which cytokines might damage muscle and regulate gene expression via activation of redox-sensitive transcription factors such as NF-B[177].Reactive oxygen species produced after burn injury have been proposed to contribute to the loss of muscle at distant sites. Clearly, the role of oxygen radicals in atrophy merits in-depth study.

In addition Bnip3, was up- regulated. Bnip3 interacts with Bcl-2 and can antagonize its pro-survival function[66,189]. In the ischemic heart, Bnip3 is induced by hypoxia and acidosis and triggers myocyte death. The finding that two proapoptotic genes are also atrogins suggests that both function in each process as part of a growth suppression program.

Finally our findings confirm the simplest model for atrophy in which the general acceleration of proteolysis and Ubiquitin conjugation results from increased expression of all or many Ubiquitin conjugating enzymes in muscle, but additionally expand the model for the up-regulation of autophagy, apoptosis and oxidative stress pathways which act in cooperatively in the protein breakdown and cell death.

Molecular targets

The interaction between myosin and actin is the molecular basis of muscle contraction and ATP hydrolyzed by myosin is the energy source for mechanical power output. Myosin heavy chain isoforms determine the contractile properties of the myosin molecule and are considered as molecular markers of the fiber type. So far nine myosin isoforms, each coded by a distinct gene, have been found to be expressed in striated muscles and incorporated in the thick filaments.Those genes have been found to be the major proteins that undergo proteolytic degradation in various atrophy conditions [38,44,190]. Our RNA-seq analysis show a down-regulation in MYH1,MYH2, MYH7 and MYH7b.Interestingly, we have also found that Citokines down-regulates the expression of desmin, myomesin and obscurin, structural constituent of sarcomeres[191].

The extracellular matrix in muscle is generally assumed to be stable. Nevertheless, a rapid decrease in mRNA occurred for many components of the extracellular matrix in cytokine induced atrophy. Previous studies have shown a loss of collagen proteins in disuse atrophy [192], and the marked reduction in mRNAs for several extracellular proteins suggests that reduced synthesis of the extracellular matrix is linked to loss of intracellular protein and presumably contractile load.

Cytokine regulates the expression of MicroRNAs (miRs) in skeletal muscle

The low-density miR array revealed that cytokines reduces the expression of a large number of miRs which coincidently is in directional correspondence with the up-regulation of majority of genes in our mRNA data with the selected stringent p-values and fold changes (Table 21). Differential expression of relatively fewer miRs when compared to the large number of differentially regulated genes in RNA-seq data also suggests the possibility of targeting more than one gene by each miRNA. Additionally, because miRNAs target genes can directly influence the expression of many other genes indirectly, many of the miRNAs differentially expressed could also be involved in the regulation of some non-target genes. Recently, a few muscle-specific miRs such as miR-1, miR-133a, miR-133b, and miR-206 (also called myomiRs) have been identified which are essential for muscle cell proliferation, differentiation, and maintenance[193].

Expression of miR-1 and miR-133a in embryonic stem cells and other non-muscle cell types showed that they promote the differentiation into the skeletal muscle lineage[193]. Unlike other myomiRs which are also expressed in cardiac tissues, miR-133b and miR-206 are

specifically expressed in skeletal muscle though their biological functions are yet to be established. Interestingly, our low density miRs array and independent demonstrate that Cytokines reduces the expression levels of miR-133a, miR-133b, and miR-206 in skeletal muscle cells (Figure 3A and Figure 4A). Furthermore, the level of at least miR-1 was also found to be significantly up-regulated (Figure 5A). Recent studies have demonstrated that myogenic transcription factors such as serum response factor (SRF), MEF2c, and MyoD control the expression of myomiRs in skeletal and cardiac muscles (reviewed in[193]). Our microarray and QRT-PCR assays in this study have also shown that cytokines inhibits the expression of MEF2c transcription factor in cultured myotubes (Figure 4C). MEF2C is particularly important for miR-1 and miR-133a and miR-1 further regulates MEF2C levels[194].

In addition to MyomiRs, citokines also down-regulated a few more miRNAs such as miR-27a, miR-199b, miR-107, and miR-23a (Fig. 5A). Though miRNAs have been explored extensively in recent years, the targets of many miRNAs are yet to be identified. For this purpose, we have utilized miRNA database (http://mirdb.org/miRDB/) to identify the putative targets of selected miRNAs. From the miRNA database, we identified that miR-27a and b targets ubiquitin-conjugating enzyme E2N with target score above 90. Ubiquitin-conjugating enzyme is an important component of ubiquitin-proteasome pathway, which causes muscle protein degradation in various atrophy conditions. From the miRNA database, we also observed that Citokines regulates miRNAs that are targeting proliferation and remodeling of muscles (miR-107), and genes involved in increasing cell growth and proliferation, and microtubule-associated proteins (miR-23a).

The Low-density miRNA arrays of Cytokine-treated C2C12 myotubes also showed up-regulation of a few select miRs. A recent study [120]showed that miR-146a targets Numb, which promotes satellite cell differen-tiation towards muscle cells and inhibition of miR-146a by antago-miR146a rescued the expression of Numb and facilitated the differentiation of C2C12 cells. miR-146a has a putative target TRAF6 ,TRAF6 belongs to E3 ubiquitin ligase family which induces the activation of multiple signaling proteins including Akt through formation of Lysine-63-linked poly-ubiquitin chains. The up-regulation of miR-146a suggests that one of the potential mechanisms by which TNF might be inducing loss of skeletal muscle mass is through down-regulation of Numb and TRAF6. It is also noteworthy that the expression of miR-146a is regulated through the activation of NF-kB [120].

TNF and IFN are two cytokines that share similar functions, it is of considerable importance that they affect common gene networks in skeletal muscle and coordinated activation of these pathways may be responsible for the loss of skeletal muscle mass and myopathy in a particular disease state. This finding is remarkable considering that muscle wasting are activated by different cytokines, but that triggers a common atrophic program. Furthermore, the existence of this very general atrophy-specific transcriptional program should be a powerful tool for detecting the earliest regulatory responses signaling these changes in the atrophying muscles.

7. CONCLUSIONS

The data presented in this study suggest that Cytokines treatments affects the expression of several genes and related miRNAs in skeletal muscle cells. These genes and microRNAs are involved in the regulation of various molecular pathways/processes including ubiquitin-proteasome pathway, extracellular matrix degradation, and muscle cell proliferation and differentiation. The study has also identified several important genes and miRNAs that are differentially expressed in skeletal muscle in response to Cytokines. Similar molecules might be involved in skeletal muscle wasting in response to cachexia.

8. BIBLIOGRAFIA

1. Miyazaki, M. & Esser, K. a. Cellular mechanisms regulating protein synthesis and skeletal muscle hypertrophy in animals. *Journal of applied physiology (Bethesda, Md. : 1985)* **106,** 1367–73 (2009).

2. Rennie, M. J., Wackerhage, H., Spangenburg, E. E. & Booth, F. W. Control of the size of the human muscle mass. *Annual review of physiology* **66,** 799–828 (2004).

3. Banerjee, A. & Guttridge, D. C. Mechanisms for maintaining muscle. *Current opinion in supportive and palliative care* **6,** 451–6 (2012).

4. Braun, T. & Gautel, M. Transcriptional mechanisms regulating skeletal muscle differentiation, growth and homeostasis. *Nature reviews. Molecular cell biology* **12,** 349–61 (2011).

5. Kandarian, S. C. & Jackman, R. W. Intracellular signaling during skeletal muscle atrophy. *Muscle & nerve* **33,** 155–65 (2006).

6. Lecker, S. H. *et al.* Multiple types of skeletal muscle atrophy involve a common program of changes in gene expression. *FASEB journal : official publication of the Federation of American Societies for Experimental Biology* **18,** 39–51 (2004).

7. Jackman, R. W. & Kandarian, S. C. The molecular basis of skeletal muscle atrophy. *American journal of physiology. Cell physiology* **287,** C834–43 (2004).

8. Glass, D. J. Skeletal muscle hypertrophy and atrophy signaling pathways. *The international journal of biochemistry & cell biology* **37,** 1974–84 (2005).

9. Bonaldo, P. & Sandri, M. Cellular and molecular mechanisms of muscle atrophy. *Disease models & mechanisms* **6,** 25–39 (2013).

10. Cao, P. R., Kim, H. J. & Lecker, S. H. Ubiquitin-protein ligases in muscle wasting. *The international journal of biochemistry & cell biology* **37,** 2088–97 (2005).

11. Bodine, S. C. *et al.* Identification of ubiquitin ligases required for skeletal muscle atrophy. *Science (New York, N.Y.)* **294,** 1704–8 (2001).

12. Yaron, A. *et al.* Identification of the receptor component of the IkappaBalpha-ubiquitin ligase. *Nature* **396,** 590–4 (1998).

13. Tisdale, M. J. Biology of cachexia. *Journal of the National Cancer Institute* **89,** 1763–73 (1997).

14. Tisdale, M. J. Cachexia in cancer patients. *Nature reviews cancer* **3,** 883–9 (2002).

15. Morley, J. E., Thomas, D. R. & Wilson, M. G. Cachexia: pathophysiology and clinical relevance. *The American journal of clinical nutrition* **83,** 735–43 (2006).

16. Donohoe, C. L., Ryan, A. M. & Reynolds, J. V. Cancer cachexia: mechanisms and clinical implications. *Gastroenterology research and practice* **2011,** 601434 (2011).

17. Evans, W. J. *et al.* Cachexia: a new definition. *Clinical nutrition (Edinburgh, Scotland)* **27,** 793–9 (2008).

18. Fearon, K. *et al.* Definition and classification of cancer cachexia: an international consensus. *The lancet oncology* **12,** 489–95 (2011).

19. Tisdale, M. J. Mechanisms of cancer cachexia. *Physiological reviews* **89,** 381–410 (2009).

20. Monitto, C. L. *et al.* Differential gene expression in a murine model of cancer cachexia. *American journal of physiology. Endocrinology and metabolism* **281,** E289–97 (2001).

21. Fearon, K. C. H., Glass, D. J. & Guttridge, D. C. Cancer cachexia: mediators, signaling, and metabolic pathways. *Cell metabolism* **16,** 153–66 (2012).

22. Tan, B. H. L. *et al.* P-selectin genotype is associated with the development of cancer cachexia. *EMBO molecular medicine* **4,** 462–71 (2012).

23. Deans, D. A. C. *et al.* Cancer cachexia is associated with the IL10 -1082 gene promoter polymorphism in patients with gastroesophageal malignancy. *The American journal of clinical nutrition* **89,** 1164–72 (2009).

24. Wigmore, S. J., Plester, C. E., Richardson, R. a & Fearon, K. C. Changes in nutritional status associated with unresectable pancreatic cancer. *British journal of cancer* **75,** 106–9 (1997).

25. Windsor, J. A. & Hill, G. L. Risk factors for postoperative pneumonia. The importance of protein depletion. *Annals of surgery* **208,** 209–14 (1988).

26. Dudgeon, W. D. *et al.* Counteracting muscle wasting in HIV-infected individuals. *HIV medicine* **7,** 299–310 (2006).

27. Fearon, K. C. The mechanisms and treatment of weight loss in cancer. *The Proceedings of the Nutrition Society* **51,** 251–65 (1992).

28. Sakuma, K. & Yamaguchi, A. Sarcopenia and cachexia: the adaptations of negative regulators of skeletal muscle mass. *Journal of cachexia, sarcopenia and muscle* **3,** 77–94 (2012).

29. Broussard, S. R. *et al.* IL-1beta impairs insulin-like growth factor i-induced differentiation and downstream activation signals of the insulin-like growth factor i receptor in myoblasts. *Journal of immunology (Baltimore, Md. : 1950)* **172,** 7713–20 (2004).

30. Miller, S. C., Ito, H., Blau, H. M. & Torti, F. M. Tumor necrosis factor inhibits human myogenesis in vitro. *Molecular and cellular biology* **8,** 2295–301 (1988).

31. Langen, R. C., Schols, a M., Kelders, M. C., Wouters, E. F. & Janssen-Heininger, Y. M. Inflammatory cytokines inhibit myogenic differentiation through activation of nuclear factor-kappaB. *FASEB journal : official publication of the Federation of American Societies for Experimental Biology* **15,** 1169–80 (2001).

32. Langen, R. C. J. *et al.* Tumor necrosis factor-alpha inhibits myogenic differentiation through MyoD protein destabilization. *FASEB journal : official publication of the Federation of American Societies for Experimental Biology* **18,** 227–37 (2004).

33. Li, Y. P., Schwartz, R. J., Waddell, I. D., Holloway, B. R. & Reid, M. B. Skeletal muscle myocytes undergo protein loss and reactive oxygen-mediated NF-kappaB activation in response to tumor necrosis factor alpha. *FASEB journal : official publication of the Federation of American Societies for Experimental Biology* **12,** 871–80 (1998).

34. Li, Y. P. & Reid, M. B. NF-kappaB mediates the protein loss induced by TNF-alpha in differentiated skeletal muscle myotubes. *American journal of physiology. Regulatory, integrative and comparative physiology* **279,** R1165–70 (2000).

35. Reid, M. B. & Li, Y. P. Tumor necrosis factor-alpha and muscle wasting: a cellular perspective. *Respiratory research* **2,** 269–72 (2001).

36. Haddad, F., Zaldivar, F., Cooper, D. M. & Adams, G. R. IL-6-induced skeletal muscle atrophy. *Journal of applied physiology (Bethesda, Md. : 1985)* **98,** 911–7 (2005).

37. Guttridge, D. C. NF-kappa B-Induced Loss of MyoD Messenger RNA: Possible Role in Muscle Decay and Cachexia. *Science* **289,** 2363–2366 (2000).

38. Acharyya, S. *et al.* Cancer cachexia is regulated by selective targeting of skeletal muscle gene products. *The Journal of clinical investigation* **114,** 370–8 (2004).

39. Srivastava, A. K. *et al.* Tumor necrosis factor-alpha augments matrix metalloproteinase-9 production in skeletal muscle cells through the activation of transforming growth factor-beta-activated kinase 1 (TAK1)-dependent signaling pathway. *The Journal of biological chemistry* **282,** 35113–24 (2007).

40. Tracey, K. J. & Cerami, a. Tumor necrosis factor, other cytokines and disease. *Annual review of cell biology* **9,** 317–43 (1993).

41. Tracey, K. J. *et al.* Cachectin/tumor necrosis factor induces cachexia, anemia, and inflammation. *The Journal of experimental medicine* **167,** 1211–27 (1988).

42. Glass, D. J. Signaling pathways perturbing muscle mass. *Current opinion in clinical nutrition and metabolic care* **13,** 225–9 (2010).

43. Guttridge, D. C. Signaling pathways weigh in on decisions to make or break skeletal muscle. *Current Opinion in Clinical Nutrition and Metabolic Care* **7,** 443–450 (2004).

44. Clarke, B. a *et al.* The E3 Ligase MuRF1 degrades myosin heavy chain protein in dexamethasone-treated skeletal muscle. *Cell metabolism* **6,** 376–85 (2007).

45. Cohen, S. *et al.* During muscle atrophy, thick, but not thin, filament components are degraded by MuRF1-dependent ubiquitylation. *The Journal of cell biology* **185,** 1083–95 (2009).

46. Mittal, A. *et al.* The TWEAK-Fn14 system is a critical regulator of denervation-induced skeletal muscle atrophy in mice. *The Journal of cell biology* **188,** 833–49 (2010).

47. Cai, D. *et al.* IKKbeta/NF-kappaB activation causes severe muscle wasting in mice. *Cell* **119,** 285–98 (2004).

48. Moore-Carrasco, R. *et al.* The AP-1/NF-kappaB double inhibitor SP100030 can revert muscle wasting during experimental cancer cachexia. *International journal of oncology* **30,** 1239–45 (2007).

49. Gomes, M. D., Lecker, S. H., Jagoe, R. T., Navon, A. & Goldberg, A. L. Atrogin-1, a muscle-specific F-box protein highly expressed during muscle atrophy. *Proceedings of the National Academy of Sciences of the United States of America* **98,** 14440–5 (2001).

50. Li, Y.-P. *et al.* TNF-alpha acts via p38 MAPK to stimulate expression of the ubiquitin ligase atrogin1/MAFbx in skeletal muscle. *FASEB journal : official publication of the Federation of American Societies for Experimental Biology* **19,** 362–70 (2005).

51. Zhang, G., Jin, B. & Li, Y.-P. C/EBPβ mediates tumour-induced ubiquitin ligase atrogin1/MAFbx upregulation and muscle wasting. *The EMBO journal* **30,** 4323–35 (2011).

52. Csibi, A., Leibovitch, M. P., Cornille, K., Tintignac, L. a & Leibovitch, S. a. MAFbx/Atrogin-1 controls the activity of the initiation factor eIF3-f in skeletal muscle atrophy by targeting multiple C-terminal lysines. *The Journal of biological chemistry* **284,** 4413–21 (2009).

53. Lagirand-Cantaloube, J. *et al.* The initiation factor eIF3-f is a major target for atrogin1/MAFbx function in skeletal muscle atrophy. *The EMBO journal* **27,** 1266–76 (2008).

54. Samuels, S. E. *et al.* Higher skeletal muscle protein synthesis and lower breakdown after chemotherapy in cachectic mice. *American journal of physiology. Regulatory, integrative and comparative physiology* **281,** R133–9 (2001).

55. Smith, K. L. & Tisdale, M. J. Increased protein degradation and decreased protein synthesis in skeletal muscle during cancer cachexia. *British journal of cancer* **67,** 680–5 (1993).

56. Singh, M. A. *et al.* Insulin-like growth factor I in skeletal muscle after weight-lifting exercise in frail elders. *The American journal of physiology* **277,** E135–43 (1999).

57. Rommel, C. *et al.* Mediation of IGF-1-induced skeletal myotube hypertrophy by PI(3)K/Akt/mTOR and PI(3)K/Akt/GSK3 pathways. *Nature cell biology* **3,** 1009–13 (2001).

58. Bentzinger, C. F. *et al.* Skeletal muscle-specific ablation of raptor, but not of rictor, causes metabolic changes and results in muscle dystrophy. *Cell metabolism* **8,** 411–24 (2008).

59. McGee, S. L., Mustard, K. J., Hardie, D. G. & Baar, K. Normal hypertrophy accompanied by phosphoryation and activation of AMP-activated protein kinase alpha1 following overload in LKB1 knockout mice. *The Journal of physiology* **586,** 1731–41 (2008).

60. Mammucari, C. *et al.* FoxO3 controls autophagy in skeletal muscle in vivo. *Cell metabolism* **6,** 458–71 (2007).

61. Mieulet, V. *et al.* S6 kinase inactivation impairs growth and translational target phosphorylation in muscle cells maintaining proper regulation of protein turnover. *American journal of physiology. Cell physiology* **293,** C712–22 (2007).

62. Zhao, J. *et al.* FoxO3 coordinately activates protein degradation by the autophagic/lysosomal and proteasomal pathways in atrophying muscle cells. *Cell metabolism* **6,** 472–83 (2007).

63. Sandri, M. *et al.* Foxo transcription factors induce the atrophy-related ubiquitin ligase atrogin-1 and cause skeletal muscle atrophy. *Cell* **117,** 399–412 (2004).

64. Stitt, T. N. *et al.* The IGF-1/PI3K/Akt pathway prevents expression of muscle atrophy-induced ubiquitin ligases by inhibiting FOXO transcription factors. *Molecular cell* **14,** 395–403 (2004).

65. Kamei, Y. *et al.* Skeletal muscle FOXO1 (FKHR) transgenic mice have less skeletal muscle mass, down-regulated Type I (slow twitch/red muscle) fiber genes, and impaired glycemic control. *The Journal of biological chemistry* **279,** 41114–23 (2004).

66. Reed, S. a, Sandesara, P. B., Senf, S. M. & Judge, A. R. Inhibition of FoxO transcriptional activity prevents muscle fiber atrophy during cachexia and induces hypertrophy. *FASEB journal : official publication of the Federation of American Societies for Experimental Biology* **26,** 987–1000 (2012).

67. Lum, J. J., DeBerardinis, R. J. & Thompson, C. B. Autophagy in metazoans: cell survival in the land of plenty. *Nature reviews. Molecular cell biology* **6,** 439–48 (2005).

68. Sandri, M. *et al.* PGC-1alpha protects skeletal muscle from atrophy by suppressing FoxO3 action and atrophy-specific gene transcription. *Proceedings of the National Academy of Sciences of the United States of America* **103,** 16260–5 (2006).

69. Lin, J., Wu, H., Tarr, P. T., Zhang, C. & Wu, Z. Transcriptional co-activator PGC-1 a drives the formation of slow-twitch muscle fibres. **418,** 797–801 (2002).

70. Baar, K. *et al.* Adaptations of skeletal muscle to exercise: rapid increase in the transcriptional coactivator PGC-1. *FASEB journal : official publication of the Federation of American Societies for Experimental Biology* **16,** 1879–86 (2002).

71. Arany, Z. *et al.* Gene expression-based screening identifies microtubule inhibitors as inducers of PGC-1alpha and oxidative phosphorylation. *Proceedings of the National Academy of Sciences of the United States of America* **105,** 4721–6 (2008).

72. Mannoor, K., Liao, J. & Jiang, F. Small nucleolar RNAs in cancer. *Biochimica et biophysica acta* **1826,** 121–8 (2012).

73. Ghildiyal, M. & Zamore, P. D. Small silencing RNAs: an expanding universe. *Nature reviews. Genetics* **10,** 94–108 (2009).

74. Dey, B. K., Mueller, A. C. & Dutta, A. Non-micro-short RNAs: the new kids on the block. *Molecular biology of the cell* **23,** 4664–7 (2012).

75. Esteller, M. Non-coding RNAs in human disease. *Nature reviews. Genetics* **12,** 861–74 (2011).

76. Lee, R. C., Feinbaum, R. L. & Ambros, V. The C. elegans heterochronic gene lin-4 encodes small RNAs with antisense complementarity to lin-14. *Cell* **75,** 843–54 (1993).

77. Pasquinelli, a E. *et al.* Conservation of the sequence and temporal expression of let-7 heterochronic regulatory RNA. *Nature* **408,** 86–9 (2000).

78. Ventura, A. *et al.* Targeted deletion reveals essential and overlapping functions of the miR-17 through 92 family of miRNA clusters. *Cell* **132,** 875–86 (2008).

79. Lee, Y., Jeon, K., Lee, J.-T., Kim, S. & Kim, V. N. MicroRNA maturation: stepwise processing and subcellular localization. *The EMBO journal* **21,** 4663–70 (2002).

80. Kim, V. N., Han, J. & Siomi, M. C. Biogenesis of small RNAs in animals. *Nature reviews. Molecular cell biology* **10,** 126–39 (2009).

81. Olena, A. F. & Patton, J. G. Genomic organization of microRNAs. *Journal of cellular physiology* **222,** 540–5 (2010).

82. Yang, J.-S. & Lai, E. C. Alternative miRNA biogenesis pathways and the interpretation of core miRNA pathway mutants. *Molecular cell* **43,** 892–903 (2011).

83. Landthaler, M., Yalcin, A. & Tuschl, T. The human DiGeorge syndrome critical region gene 8 and Its D. melanogaster homolog are required for miRNA biogenesis. *Current biology : CB* **14,** 2162–7 (2004).

84. Gregory, R. I. *et al.* The Microprocessor complex mediates the genesis of microRNAs. *Nature* **432,** 235–40 (2004).

85. Han, J. *et al.* The Drosha-DGCR8 complex in primary microRNA processing. *Genes & development* **18,** 3016–27 (2004).

86. Denli, A. M., Tops, B. B. J., Plasterk, R. H. a, Ketting, R. F. & Hannon, G. J. Processing of primary microRNAs by the Microprocessor complex. *Nature* **432,** 231–5 (2004).

87. Zeng, Y. & Cullen, B. R. Efficient processing of primary microRNA hairpins by Drosha requires flanking nonstructured RNA sequences. *The Journal of biological chemistry* **280,** 27595–603 (2005).

88. Han, J. *et al.* Molecular basis for the recognition of primary microRNAs by the Drosha-DGCR8 complex. *Cell* **125,** 887–901 (2006).

89. Yi, R., Qin, Y., Macara, I. G. & Cullen, B. R. Exportin-5 mediates the nuclear export of pre-microRNAs and short hairpin RNAs. *Genes & development* **17,** 3011–6 (2003).

90. Bohnsack, M. T., Czaplinski, K. & Go, D. Exportin 5 is a RanGTP-dependent dsRNA-binding protein that mediates nuclear export of pre-miRNAs. *Rna* **10,** 185–191 (2004).

91. Lund, E., Güttinger, S., Calado, A., Dahlberg, J. E. & Kutay, U. Nuclear export of microRNA precursors. *Science (New York, N.Y.)* **303,** 95–8 (2004).

92. Schwarz, D. S. *et al.* Asymmetry in the assembly of the RNAi enzyme complex. *Cell* **115,** 199–208 (2003).

93. Salzman, D. W., Shubert-coleman, J. & Furneaux, H. P68 RNA helicase unwinds the human let-7 microRNA precursor duplex and is required for let-7-directed silencing of gene expression. *The Journal of biological chemistry* **282,** 32773–9 (2007).

94. Westholm, J. O. & Lai, E. C. Mirtrons: microRNA biogenesis via splicing. *Biochimie* **93,** 1897–904 (2011).

95. Berezikov, E., Chung, W.-J., Willis, J., Cuppen, E. & Lai, E. C. Mammalian mirtron genes. *Molecular cell* **28,** 328–36 (2007).

96. Kawamata, T. & Tomari, Y. Making RISC. *Trends in biochemical sciences* **35,** 368–76 (2010).

97. Krol, J., Loedige, I. & Filipowicz, W. The widespread regulation of microRNA biogenesis, function and decay. *Nature reviews. Genetics* **11,** 597–610 (2010).

98. Esquela-Kerscher, A. & Slack, F. J. Oncomirs - microRNAs with a role in cancer. *Nature reviews. Cancer* **6,** 259–69 (2006).

99. Bartel, D. P. MicroRNAs: genomics, biogenesis, mechanism, and function. *Cell* **116,** 281–97 (2004).

100. Guo, H., Ingolia, N. T., Weissman, J. S. & Bartel, D. P. Mammalian microRNAs predominantly act to decrease target mRNA levels. *Nature* **466,** 835–40 (2010).

101. Bartel, D. P. MicroRNAs: target recognition and regulatory functions. *Cell* **136,** 215–33 (2009).

102. Van Rooij, E. *et al.* A family of microRNAs encoded by myosin genes governs myosin expression and muscle performance. *Developmental cell* **17,** 662–73 (2009).

103. Chen, J.-F., Callis, T. E. & Wang, D.-Z. microRNAs and muscle disorders. *Journal of cell science* **122,** 13–20 (2009).

104. Güller, I., Russell, A. P. & Isabelle, G. MicroRNAs in skeletal muscle: their role and regulation in development, disease and function. *The Journal of physiology* **588,** 4075–87 (2010).

105. Davies, K. E. & Nowak, K. J. Molecular mechanisms of muscular dystrophies: old and new players. *Nature reviews. Molecular cell biology* **7,** 762–73 (2006).

106. Eisenberg, I. *et al.* Distinctive patterns of microRNA expression in primary muscular disorders. *Proceedings of the National Academy of Sciences of the United States of America* **104,** 17016–21 (2007).

107. McCarthy, J. J. & Esser, K. a. MicroRNA-1 and microRNA-133a expression are decreased during skeletal muscle hypertrophy. *Journal of applied physiology (Bethesda, Md. : 1985)* **102,** 306–13 (2007).

108. McCarthy, J. J., Esser, K. A. & Andrade, F. H. MicroRNA-206 is overexpressed in the diaphragm but not the hindlimb muscle of mdx mouse. *American journal of physiology. Cell physiology* **293,** C451–7 (2007).

109. McCarthy, J. J., Esser, K. A., Peterson, C. a & Dupont-Versteegden, E. E. Evidence of MyomiR network regulation of beta-myosin heavy chain gene expression during skeletal muscle atrophy. *Physiological genomics* **39,** 219–26 (2009).

110. Wang, H. *et al.* NF-kappaB-YY1-miR-29 regulatory circuitry in skeletal myogenesis and rhabdomyosarcoma. *Cancer cell* **14,** 369–81 (2008).

111. Clop, A. *et al.* A mutation creating a potential illegitimate microRNA target site in the myostatin gene affects muscularity in sheep. *Nature genetics* **38,** 813–8 (2006).

112. Lee, S.-J. Regulation of muscle mass by myostatin. *Annual review of cell and developmental biology* **20,** 61–86 (2004).

113. Tobin, J. F. & Celeste, A. J. Myostatin, a negative regulator of muscle mass: implications for muscle degenerative diseases. *Current opinion in pharmacology* **5,** 328–32 (2005).

114. Bhatnagar, S. *et al.* Tumor necrosis factor-α regulates distinct molecular pathways and gene networks in cultured skeletal muscle cells. *PloS one* **5,** e13262 (2010).

115. Greco, S. *et al.* Common micro-RNA signature in skeletal muscle damage and regeneration induced by Duchenne muscular dystrophy and acute ischemia. *FASEB journal : official publication of the Federation of American Societies for Experimental Biology* **23,** 3335–46 (2009).

116. Stevenson, E. J., Giresi, P. G., Koncarevic, A. & Kandarian, S. C. Global analysis of gene expression patterns during disuse atrophy in rat skeletal muscle. *The Journal of physiology* **551,** 33–48 (2003).

117. Giresi, P. G. *et al.* Identification of a molecular signature of sarcopenia. *Physiological genomics* **21,** 253–63 (2005).

118. Stevenson, E. J., Koncarevic, A., Giresi, P. G., Jackman, R. W. & Kandarian, S. C. Transcriptional profile of a myotube starvation model of atrophy. *Journal of applied physiology (Bethesda, Md. : 1985)* **98,** 1396–406 (2005).

119. Di Marco, S. *et al.* NF-kappa B-mediated MyoD decay during muscle wasting requires nitric oxide synthase mRNA stabilization, HuR protein, and nitric oxide release. *Molecular and cellular biology* **25,** 6533–45 (2005).

120. Panguluri, S. K. *et al.* Genomic profiling of messenger RNAs and microRNAs reveals potential mechanisms of TWEAK-induced skeletal muscle wasting in mice. *PloS one* **5,** e8760 (2010).

121. Kitano, H. Computational systems biology. *Nature* **420,** 206–10 (2002).

122. Oltvai, Z. N. & Barabási, A.-L. Systems biology. Life's complexity pyramid. *Science (New York, N.Y.)* **298,** 763–4 (2002).

123. Bray, D. Molecular networks: the top-down view. *Science (New York, N.Y.)* **301,** 1864–5 (2003).

124. Murali, T. M. & Rivera, C. G. Network legos: building blocks of cellular wiring diagrams. *Journal of computational biology : a journal of computational molecular cell biology* **15,** 829–44 (2008).

125. Hartwell, L. H., Hopfield, J. J., Leibler, S. & Murray, a W. From molecular to modular cell biology. *Nature* **402,** C47–52 (1999).

126. Hasty, J., McMillen, D. & Collins, J. J. Engineered gene circuits. *Nature* **420,** 224–30 (2002).

127. Veenstra-Vanderweele, J., Christian, S. L. & Cook, E. H. Autism as a paradigmatic complex genetic disorder. *Annual review of genomics and human genetics* **5,** 379–405 (2004).

128. Schadt, E. E. Molecular networks as sensors and drivers of common human diseases. *Nature* **461,** 218–23 (2009).

129. Palsson, B. & Zengler, K. The challenges of integrating multi-omic data sets. *Nature chemical biology* **6,** 787–9 (2010).

130. Schwanhäusser, B. *et al.* Global quantification of mammalian gene expression control. *Nature* **473,** 337–42 (2011).

131. Akavia, U. D. *et al.* An integrated approach to uncover drivers of cancer. *Cell* **143,** 1005–17 (2010).

132. Bailly-Bechet, M. *et al.* Finding undetected protein associations in cell signaling by belief propagation. *Proceedings of the National Academy of Sciences of the United States of America* **108,** 882–7 (2011).

133. Dittrich, M. T., Klau, G. W., Rosenwald, A., Dandekar, T. & Müller, T. Identifying functional modules in protein-protein interaction networks: an integrated exact approach. *Bioinformatics (Oxford, England)* **24,** i223–31 (2008).

134. Friedman, N. Inferring cellular networks using probabilistic graphical models. *Science (New York, N.Y.)* **303,** 799–805 (2004).

135. Huang, S.-S. C. & Fraenkel, E. Integrating proteomic, transcriptional, and interactome data reveals hidden components of signaling and regulatory networks. *Science signaling* **2,** ra40 (2009).

136. Kim, Y.-A., Wuchty, S. & Przytycka, T. M. Identifying causal genes and dysregulated pathways in complex diseases. *PLoS computational biology* **7,** e1001095 (2011).

137. Lan, A., Smoly, I. Y., Rapaport, G., Lindquist, S. & Fraenkel, E. ResponseNet : revealing signaling and regulatory networks linking genetic and transcriptomic screening data. **39,** 424–429 (2011).

138. Missiuro, P. V. *et al.* Information flow analysis of interactome networks. *PLoS computational biology* **5,** e1000350 (2009).

139. Ourfali, O., Shlomi, T., Ideker, T., Ruppin, E. & Sharan, R. SPINE: a framework for signaling-regulatory pathway inference from cause-effect experiments. *Bioinformatics (Oxford, England)* **23,** i359–66 (2007).

140. Suthram, S., Beyer, A., Karp, R. M., Eldar, Y. & Ideker, T. eQED: an efficient method for interpreting eQTL associations using protein networks. *Molecular systems biology* **4,** 162 (2008).

141. Tu, Z. *et al.* Integrating siRNA and protein-protein interaction data to identify an expanded insulin signaling network. *Genome research* **19,** 1057–67 (2009).

142. Vanunu, O., Magger, O., Ruppin, E., Shlomi, T. & Sharan, R. Associating genes and protein complexes with disease via network propagation. *PLoS computational biology* **6,** e1000641 (2010).

143. Yeang, C.-H., Ideker, T. & Jaakkola, T. Physical network models. *Journal of computational biology : a journal of computational molecular cell biology* **11,** 243–62 (2004).

144. Yeger-Lotem, E. *et al.* Bridging high-throughput genetic and transcriptional data reveals cellular responses to alpha-synuclein toxicity. *Nature genetics* **41,** 316–23 (2009).

145. Fleige, S. & Pfaffl, M. W. RNA integrity and the effect on the real-time qRT-PCR performance. *Molecular aspects of medicine* **27,** 126–39 (2006).

146. Becker, C., Riedmaier, I., Pfaffl, M. W. & Hammerle-Fickinger, a. mRNA and microRNA quality control for RT-qPCR analysis. *Methods (San Diego, Calif.)* **50,** 237–43 (2010).

147. Bustin, S. a *et al.* The MIQE guidelines: minimum information for publication of quantitative real-time PCR experiments. *Clinical chemistry* **55,** 611–22 (2009).

148. Pfaffl, M. W. A new mathematical model for relative quantification in real-time RT-PCR. *Nucleic acids research* **29,** e45 (2001).

149. Pfaffl, M. W., Horgan, G. W. & Dempfle, L. Relative expression software tool (REST) for group-wise comparison and statistical analysis of relative expression results in real-time PCR. *Nucleic acids research* **30,** e36 (2002).

150. Ruijter, J. M. *et al.* Amplification efficiency: linking baseline and bias in the analysis of quantitative PCR data. *Nucleic acids research* **37,** e45 (2009).

151. Chen, C. *et al.* Real-time quantification of microRNAs by stem-loop RT-PCR. *Nucleic acids research* **33,** e179 (2005).

152. Mestdagh, P. *et al.* High-throughput stem-loop RT-qPCR miRNA expression profiling using minute amounts of input RNA. *Nucleic acids research* **36,** e143 (2008).

153. Lefever, S. *et al.* RDML: structured language and reporting guidelines for real-time quantitative PCR data. *Nucleic acids research* **37,** 2065–9 (2009).

154. Livak, K. J. & Schmittgen, T. D. Analysis of relative gene expression data using real-time quantitative PCR and the 2(-Delta Delta C(T)) Method. *Methods (San Diego, Calif.)* **25,** 402–8 (2001).

155. Dvinge, H. & Bertone, P. HTqPCR: high-throughput analysis and visualization of quantitative real-time PCR data in R. *Bioinformatics (Oxford, England)* **25,** 3325–6 (2009).

156. Trapnell, C. *et al.* Differential gene and transcript expression analysis of RNA-seq experiments with TopHat and Cufflinks. *Nature protocols* **7,** 562–78 (2012).

157. Anders, S. & Huber, W. Differential expression analysis for sequence count data. *Genome biology* **11,** R106 (2010).

158. Cloots, L. & Marchal, K. Network-based functional modeling of genomics, transcriptomics and metabolism in bacteria. *Current opinion in microbiology* **14,** 599–607 (2011).

159. Keshava Prasad, T. S. *et al.* Human Protein Reference Database--2009 update. *Nucleic acids research* **37,** D767–72 (2009).

160. Mathivanan, S. *et al.* An evaluation of human protein-protein interaction data in the public domain. *BMC bioinformatics* **7 Suppl 5,** S19 (2006).

161. Croft, D. *et al.* Reactome: a database of reactions, pathways and biological processes. *Nucleic acids research* **39,** D691–7 (2011).

162. Gerstein, M. B. *et al.* Architecture of the human regulatory network derived from ENCODE data. *Nature* **489,** 91–100 (2012).

163. Tuncbag, N., McCallum, S., Huang, S.-S. C. & Fraenkel, E. SteinerNet: a web server for integrating "omic" data to discover hidden components of response pathways. *Nucleic acids research* **40,** W505–9 (2012).

164. Wang, X. miRDB: a microRNA target prediction and functional annotation database with a wiki interface. *RNA (New York, N.Y.)* **14,** 1012–7 (2008).

165. Garcia, D. M. *et al.* Weak seed-pairing stability and high target-site abundance decrease the proficiency of lsy-6 and other microRNAs. *Nature structural & molecular biology* **18,** 1139–46 (2011).

166. Maragkakis, M. *et al.* DIANA-microT web server: elucidating microRNA functions through target prediction. *Nucleic acids research* **37,** W273–6 (2009).

167. Krek, A. *et al.* Combinatorial microRNA target predictions. *Nature genetics* **37,** 495–500 (2005).

168. Hsu, S.-D. *et al.* miRTarBase: a database curates experimentally validated microRNA-target interactions. *Nucleic acids research* **39,** D163–9 (2011).

169. Maere, S., Heymans, K. & Kuiper, M. BiNGO: a Cytoscape plugin to assess overrepresentation of gene ontology categories in biological networks. *Bioinformatics (Oxford, England)* **21,** 3448–9 (2005).

170. Bindea, G. *et al.* ClueGO: a Cytoscape plug-in to decipher functionally grouped gene ontology and pathway annotation networks. *Bioinformatics (Oxford, England)* **25,** 1091–3 (2009).

171. Cline, M. S. *et al.* Integration of biological networks and gene expression data using Cytoscape. *Nature protocols* **2,** 2366–82 (2007).

172. Acharyya, S. *et al.* Dystrophin glycoprotein complex dysfunction: a regulatory link between muscular dystrophy and cancer cachexia. *Cancer cell* **8,** 421–32 (2005).

173. Wold, B. & Myers, R. M. Sequence census methods for functional genomics. **5,** 19–21 (2008).

174. Mestdagh, P. *et al.* A novel and universal method for microRNA RT-qPCR data normalization. *Genome biology* **10,** R64 (2009).

175. Fanzani, A., Conraads, V. M., Penna, F. & Martinet, W. Molecular and cellular mechanisms of skeletal muscle atrophy: an update. *Journal of cachexia, sarcopenia and muscle* **3,** 163–79 (2012).

176. Hunter, R. B. & Kandarian, S. C. Disruption of either the Nfkb1 or the Bcl3 gene inhibits skeletal muscle atrophy. *The Journal of clinical investigation* **114,** 1504–11 (2004).

177. Napetschnig, J. & Wu, H. Molecular basis of NF-κB signaling. *Annual review of biophysics* **42,** 443–68 (2013).

178. Londhe, P. & Davie, J. K. Gamma interferon modulates myogenesis through the major histocompatibility complex class II transactivator, CIITA. *Molecular and cellular biology* **31,** 2854–66 (2011).

179. De Paepe, B., Creus, K. K. & De Bleecker, J. L. Chemokine profile of different inflammatory myopathies reflects humoral versus cytotoxic immune responses. *Annals of the New York Academy of Sciences* **1109,** 441–53 (2007).

180. Vieira, S. M. *et al.* A crucial role for TNF-alpha in mediating neutrophil influx induced by endogenously generated or exogenous chemokines, KC/CXCL1 and LIX/CXCL5. *British journal of pharmacology* **158,** 779–89 (2009).

181. Bonetto, A. *et al.* STAT3 activation in skeletal muscle links muscle wasting and the acute phase response in cancer cachexia. *PloS one* **6,** e22538 (2011).

182. Bonetto, A. *et al.* JAK/STAT3 pathway inhibition blocks skeletal muscle wasting downstream of IL-6 and in experimental cancer cachexia. *American journal of physiology. Endocrinology and metabolism* **303,** E410–21 (2012).

183. Dehoux, M. *et al.* IGF-I does not prevent myotube atrophy caused by proinflammatory cytokines despite activation of Akt/Foxo and GSK-3beta pathways and inhibition of atrogin-1 mRNA. *American journal of physiology. Endocrinology and metabolism* **292,** E145–50 (2007).

184. Cirilo, P. D. R. *et al.* An integrative genomic and transcriptomic analysis reveals potential targets associated with cell proliferation in uterine leiomyomas. *PloS one* **8,** e57901 (2013).

185. Cisternas, P., Henriquez, J. P., Brandan, E. & Inestrosa, N. C. Wnt Signaling in Skeletal Muscle Dynamics: Myogenesis, Neuromuscular Synapse and Fibrosis. *Molecular neurobiology* (2013). doi:10.1007/s12035-013-8540-5

186. Arthur, S. T. & Cooley, I. D. The effect of physiological stimuli on sarcopenia; impact of Notch and Wnt signaling on impaired aged skeletal muscle repair. *International journal of biological sciences* **8,** 731–60 (2012).

187. Muller, F. L. *et al.* Denervation-induced skeletal muscle atrophy is associated with increased mitochondrial ROS production. *American journal of physiology. Regulatory, integrative and comparative physiology* **293,** R1159–68 (2007).

188. Dobrowolny, G. *et al.* Skeletal muscle is a primary target of SOD1G93A-mediated toxicity. *Cell metabolism* **8,** 425–36 (2008).

189. Chang, N. C. *et al.* Bcl-2-associated autophagy regulator Naf-1 required for maintenance of skeletal muscle. *Human molecular genetics* **21,** 2277–87 (2012).

190. Li, H., Malhotra, S. & Kumar, A. Nuclear factor-kappa B signaling in skeletal muscle atrophy. *Journal of molecular medicine (Berlin, Germany)* **86,** 1113–26 (2008).

191. Randazzo, D. *et al.* Obscurin is required for ankyrinB-dependent dystrophin localization and sarcolemma integrity. *The Journal of cell biology* **200,** 523–36 (2013).

192. Grumati, P., Coletto, L., Sandri, M. & Bonaldo, P. Autophagy induction rescues muscular dystrophy. *Autophagy* **7,** 426–8 (2011).

193. Rooij, E. Van, Liu, N., Olson, E. N. & van Rooij, E. MicroRNAs flex their muscles. *Trends in genetics : TIG* **24,** 159–66 (2008).

194. Cesana, M. *et al.* A long noncoding RNA controls muscle differentiation by functioning as a competing endogenous RNA. *Cell* **147,** 358–69 (2011).

9. Supplementary Information

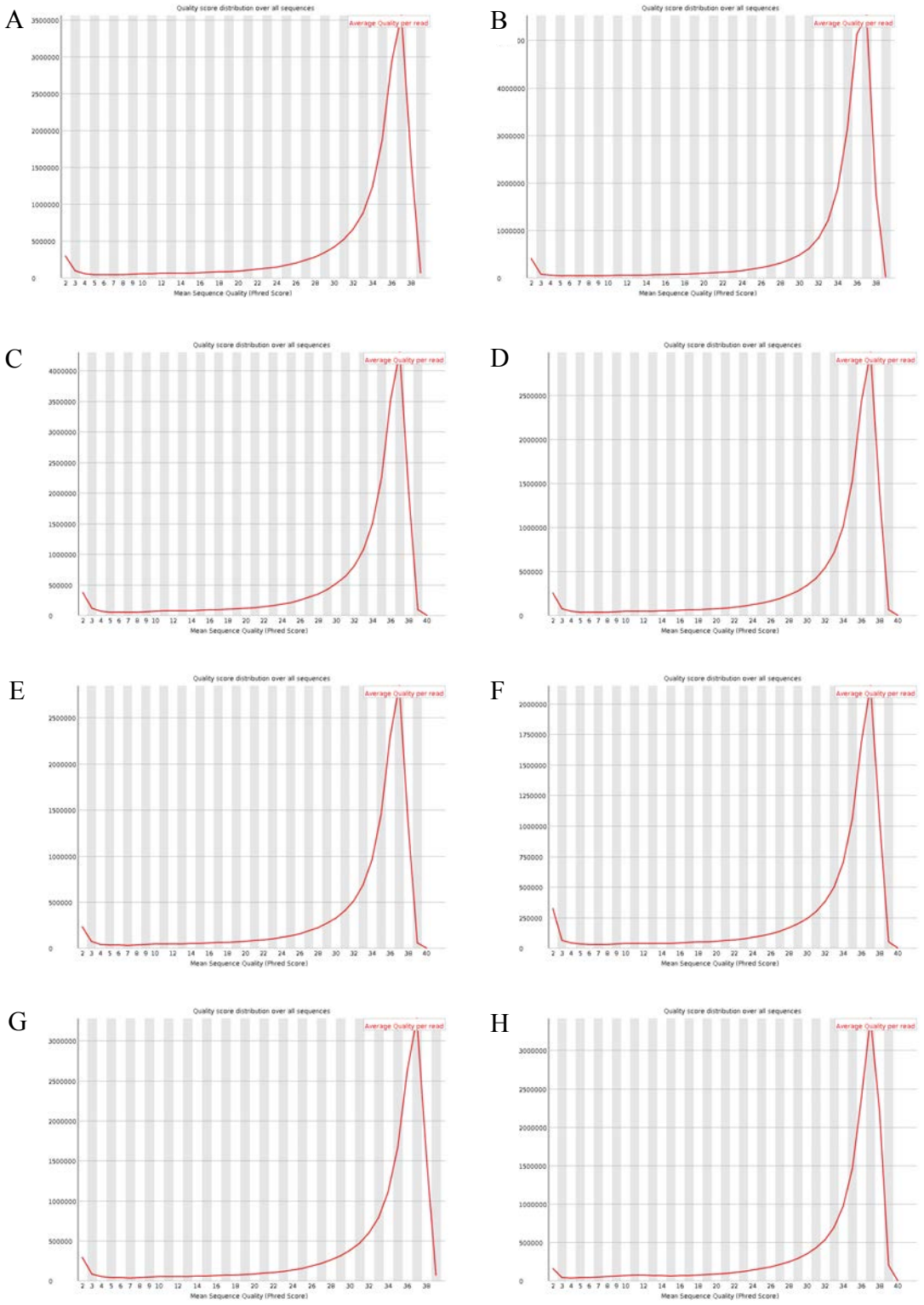

S1. Quality score distribution over all read sequences. A and B, are the control control myotubes; C and D, are the libraries for the TNF-α treated myotubes; E and F, are the libraries for the IFN-γ treated myotubes and G and H are the libraries for the TNF-α + IFN-γ treated myotubes.

J Cachexia Sarcopenia Muscle (2012) 3:281–301
DOI 10.1007/s13539-012-0088-0

ABSTRACTS

Abstracts of the Cancer Cachexia Conference, Boston, USA, 21–23 September 2012

Time course of atrogenes MurF1 and MAFbx mRNA expression during skeletal muscle atrophy in C2C12 cells

Geysson Javier Fernandez[1], Sandro Jose Conde[2], Celia Regina Nogueira[2], Patrícia Pintor dos Reis[3], Maeli Dal Pai[1], Robson Francisco Carvalho[1]

[1]*Department of Morphology, IBB, UNESP, Botucatu, SP, Brazil,* [2]*Department of Clinical Medicine, São Paulo State University-UNESP, Botucatu, SP, Brazil* [3] *Dept. of Surgery and Orthopedics, FMB, São Paulo State University–UNESP, Botucatu, SP, Brazil*

Skeletal muscle atrophy is a common event in many chronic systemic conditions or diseases such a sepsis, chronic heart failure, chronic obstructive pulmonary disease, chronic kidney disease, diabetes, AIDS and cancer. These conditions may be accompanied by a complex metabolic syndrome characterized by muscle wasting, known as cachexia. Molecular pathways responsible for cachexia are not completely understood, however, pro-inflammatory cytokines such as Tumor Necrosis Factor (TNF)-α and Interferon (INF)-γ have a key role in molecular pathways related to loss of muscle mass and function. Complex mechanisms controlling gene expression in muscle atrophy may include genes with a common mode of regulation with deregulated transcript levels over the time course. We performed a time-series expression analysis of four genes in differentiated C2C12 muscle cells; in these cells, atrophy was induced by treatment with TNF-α (10 ng/ml) and IFN-γ (100 U/ml) at different times (0 h, 6 h, 12 h, 18 h, 24 h, and 48 h). The dynamic gene expression of MyHC IIa, MyoD, MuRF1, and MAFbx was measured by Reverse Transcription-Quantitative Real-Time PCR (RT-qPCR). Our results demonstrated that TNF-α/IFN-γ treatment decreases MyHC IIa and MyoD gene expression (98 % and 78 %, respectively) from 0 h to 24 h. However, MyoD mRNA decay is faster (90 %) compared to MyHC IIa decay (50 %) at 6 h. In addition, atrogenes MuRF1 and MAFbx show a 2-fold up regulation peak at 18 h. Our data support the hypothesis that altered gene regulation loops occurs within the first 18 h and suggest a common regulatory program for E3 ubiquitin ligases MurF1 and MAFbx genes. Results from our study will contribute to the dynamic description and regulation of gene expression involved in skeletal muscle atrophy induced by cytokines.

S2. Abstract published

S3. Abstract Acepted

MOLECULAR MECHANISMS OF MUSCLE GROWTH AND WASTING IN HEALTH AND DISEASE

Centro Stefano Franscini, Monte Verità, Ascona, Switzerland

15-20 September, 2013

Reconstruction of molecular networks involved in cytokine-induced myotubes atrophy by integrating microRNA and mRNA expression profiling

G. J. G Fernandez [a, d], P. P. dos Reis [b], L. L. Coutinho [c], C. R. Nogueira [b], C. Fierro [d], A. Sanchez [d], K. Marchal [d], M. Dal Pai [a] and **R. F. Carvalho** [a].

[a] *Institute of Biosciences, Sao Paulo State University - UNESP, Brazil*
[b] *School of Medicine, Sao Paulo State University - UNESP, Brazil*
[c] *Luiz de Queiroz College of Agriculture, São Paulo University - USP, Brazil*
[d] *Faculty of Science, Ghent University, Belgium*

rcarvalho@ibb.unesp.br

Cachexia is a wasting condition tightly associated with chronic illnesses including, but not limited to, cancer, AIDS, chronic obstructive pulmonary disease (COPD), heart and renal failure, diabetes, and inflammatory bowel disease. The syndrome is characterized by depletion of skeletal muscle mass, leading to pronounced weight loss that severely impacts patient morbidity and mortality. Although the molecular basis of cachexia remains largely unresolved, pro-inflammatory cytokines such as tumor necrosis factor (TNF)-α and interferon gamma (IFN)-γ have been identified as key mediators and expanded the knowledge of molecular pathways in the development of muscular abnormalities resulting in loss of muscle mass and function. Multiple lines of evidence indicate that small RNAs that recognize and regulate mRNA target genes, such as microRNAs (miRNAs), are important regulators of numerous critical functions in muscle wasting conditions. However, defining the place and function of miRNAs in complex regulatory networks is not straightforward. Systems approaches, like the inference of a module network from expression data, can help to achieve this goal in atrophying muscle cells. We performed an integrative analysis using miRNA and mRNA expression profile in C2C12 myotubes to identify pathways and mechanisms of action of TNF-α and INF-γ in muscle atrophy. Integrated bioinformatics analysis showed that the most significantly deregulated genes ($p<0,001$) comprised genes associated with cancer, inflammatory response, fibrosis, and cytoskeletal function. The prioritizing analysis indicated a strong association between miRNAs and deregulated modules in the network including the microRNAs mmu-miR-107, mmu-miR-153, mmu-miR20b, and mmu-miR182. Additionally, we show that several miRNAs are predicted as statistically significant regulators for various modules of tightly co-expressed genes. Our results show a robust molecular network analysis of expression data that provides novel insights of miRNA function in muscle atrophy. Such a computational approach, integrating miRNA and mRNA expression data, is useful for the identification of deregulated miRNA-mRNA networks, leading to further studies on the functional characterization of miRNA-modulated pathways in muscle wasting.

Acknowledgements: São Paulo Research Foundation, FAPESP, Brazil (RFC, grant number 2012/13961-6)